BARI-TH/788-26

Effective Matter Flavor Conversion Mediated by Pseudo-Sterile States as the Possible Origin of Neutrino Oscillation Anomalies

Sabya Sachi Chatterjee[1,*] and Antonio Palazzo[2,3,†]

[1] *Institut für Astroteilchenphysik, Karlsruher Institut für Technologie (KIT), Hermann-von-Helmholtz-Platz 1, 76344 Eggenstein-Leopoldshafen, Germany*
[2] *Dipartimento Interateneo di Fisica "Michelangelo Merlin," Via Amendola 173, 70126 Bari, Italy*
[3] *Istituto Nazionale di Fisica Nucleare, Sezione di Bari, Via Orabona 4, 70126 Bari, Italy*

Neutrino oscillation experiments present anomalous results across a vast range of baselines and energies. Here we show that a 3+1 scenario in which sterile neutrinos feel a novel matter potential V_s proportional to background density of ordinary or (asymmetric) dark matter is able to explain several anomalies. In the limit of low-energies $E \lesssim 1$ TeV the model behaves as an effective 3-flavor NSI-like scheme among active flavors and eliminates the tension between the two LBL experiments NOvA and T2K provided that the potential is negative and the two sterile mixing angles θ_{14} and θ_{24} are non-zero. Solar neutrino data further constrain the strength of the potential and impose the bound $|U_{e4}|^2 \simeq \sin^2\theta_{14} \lesssim 0.04$, while LBL and low-energy atmospheric data establish the hierarchical pattern $|U_{\mu4}|^2 \ll |U_{e4}|^2$ and $|U_{\tau4}|^2 \ll |U_{e4}|^2$. A further indication in favor of a non-zero negative potential comes from the anomalous excess of ν_e-like events observed in Super-Kamiokande multi-GeV atmospheric neutrinos, which, in the new scenario can be explained by a modification of the 3-flavor resonance at energies of a few GeV. In the high-energy regime ($E \gtrsim 1$ TeV) the new framework reveals its genuine 4-flavor nature and can produce a resonant behavior at $E \simeq 10$ TeV as hinted at by IceCube which, for the preferred negative values of the potential, occurs in the neutrino channel. The resonance presents unconventional features, reflecting the complex structure of the amplification phenomenon. Specifically, we identify an irreducible three-level dynamics generating a new resonance in the (ν_e, ν_μ) sector intertwined with two conventional resonances in the (ν_e, ν_s) and (ν_μ, ν_s) subsystems. The novel amplification mechanism manifests with the emergence of effective mixing angles in matter (θ_{12}^m or θ_{13}^m) involving active neutrinos unrelated to their vacuum counterparts and can be operative even in the absence of conventional resonances. In order to be phenomenologically relevant the scenario requires values of $f = V_s/|V_{NC}| \sim -20$, $\Delta m^2_{41} \sim 60$ eV^2 (both roughly uncertain by a factor of two), $|U_{e4}|^2 \simeq \sin^2\theta_{14} \simeq 0.01 - 0.03$ and $|U_{\mu4}|^2 \simeq \sin^2\theta_{24} \simeq 10^{-4} - 10^{-3}$. Such a very small size of $|U_{\mu4}|^2$ eliminates the tension between IceCube and the other (all negative) ν_μ disappearance searches. The third mixing angle can have a sizable impact even for tiny values as small as $|U_{\tau4}|^2 \simeq \sin^2\theta_{34} \sim 3\times10^{-4}$. The model can play a substantial role in the Reactor anomaly and partially explain the Gallium one. More crucially, it can be directly probed by KATRIN, which is very sensitive to the electron-sterile neutrino admixture in the region of high Δm^2_{41}.

I. INTRODUCTION

The question of the anomalies in the neutrino sector is becoming increasingly intricate. Together with the long-standing results of LSND [1], the Reactor [2], Gallium [3–9] and Neutrino-4 [10] anomalies and the MiniBooNE excess [11],[1] new anomalous results are gradually emerging and consolidating. This is the case of IceCube [13, 14], which hints at a resonant-like behavior in atmospheric muon neutrinos for energies of ~ 10 TeV. In addition, an apparently unrelated tension between the two long-baseline (LBL) experiments NOvA [15] and T2K [16] has recently apperared [17–19]. Finally, here we evidence that there is a possibly anomalous excess of electron-like events in the atmospheric neutrino data collected by Super-Kamiokande [20], which in our opinion deserves attention. According to these latest developments, the anomalous results involve a vast range of energies and distances. Hence, in our view, a more complex picture is emerging, in which the "traditional" short-baseline (SBL) anomalies represent only one piece of a broader mosaic. In addition, the new discrepancies involving LBL, low-energy and high-energy atmospheric neutrinos, strongly suggest a key role of matter effects in the anomalies.

The so-called 3+1 scenario, entailing one sterile neutrino in addition to the three active species, has been thoroughly explored as a possible solution of the anomalies with prominent attention to those recorded in SBL experiments (for

*Electronic address: sabya.chatterjee@kit.edu
†Electronic address: palazzo@ba.infn.it

[1] The anomalous excess of electron neutrinos recorded by MiniBooNE has been recently challenged by the negative results of a dedicate search of MicroBooNE [12].

a recent review see [21, 22]). However, it has been gradually recognized that this simple scheme is not able to address simultaneously all the SBL anomalies and it can only explain a limited subset of them. Adding further light sterile degrees of freedom (the so-called 3+N schemes) does not help. Perhaps, the most important drawback of these scenarios is their inability to explain simultaneously the positive signal of electron neutrino appearance and the joint disappearance searches of electron neutrinos (with positive outcome) and muon neutrinos (with negative outcome) [23–25]. Additionally, a tension between the IceCube high-energy results and the other muon neutrino disappearance searches is consolidating and has been recently quantified to lie around the 3σ level [26]. Also, very recently the 3+1 scheme has been challenged by a dedicated analysis of MicroBooNE [27]. Finally, in the background, it remains the question of the incompatibility of such "vanilla" sterile neutrinos with cosmology (see for example [28–30]). In an effort to overcome these drawbacks, it has been gradually accepted that sterile neutrinos, if still deemed relevant for the anomalies, should possess additional exotic properties. This is not implausible and in retrospect it seems quite natural given that we are scrutinizing completely unknown fundamental particles. Examples of ideas going in this direction are given by the recent hypothesis of the non-unitary 3+1 scheme [31], the invisible sterile neutrino decay [25, 32, 33] or decoherence [33] as a mean to alleviate the appearance-disapearance tension, the decay in visible products [34–38] to explain the LSND and MiniBooNE excesses, and the so-called secret interactions [39–50], put forward to reconcile terrestrial neutrino data with cosmology.

Here we consider a 3+1 scenario which entails a new matter potential felt by the sterile neutrinos, already investigated in various contexts related to neutrino oscillations [51–62], but without reaching a concrete conclusion on its role in the anomalies.[2] We will refer to such a kind of neutrinos as *pseudo-sterile neutrinos* to emphasize that these states, albeit being singlets under the Standard Model gauge group, can have other kinds of interactions in addition to the gravitational one.[3] We will show that the pseudo-sterile states can concretely help to explain several anomalies. The key point of this scenario, unrecognized in the previous literature, is that these exotic states can act as mediators of new unconventional matter flavor conversion phenomena among the active flavors, which under appropriate conditions can be even resonantly amplified. We will explore the rich phenomenology implied by this scenario having in mind two goals. First, we will ensure that the new scenario respects the constraints coming from the entire neutrino oscillation phenomenology. Second, we will show how it can provide a satisfying explanation of several anomalies, without being affected by the internal tensions plaguing the ordinary 3+1 scheme.

We will demonstrate that in the limit of relatively low energies ($E \lesssim 1$ TeV) the sterile state ν_s can be integrated out from the dynamics, and the model behaves as an effective 3-flavor NSI-like scheme among active flavors. This behavior allows us to explain the tension between the two LBL experiments NOvA and T2K provided that the new potential is negative[4] and the two sterile mixing angles θ_{14} and θ_{24} are non-zero. With a dedicated analytical and numerical study we will show that solar neutrino data further constrain the strength of the new potential and impose the bound $|U_{e4}|^2 \simeq \sin^2\theta_{14} \lesssim 0.04$. In addition, we will see that LBL and low-energy atmospheric data establish the hierarchical pattern $|U_{\mu4}|^2 \ll |U_{e4}|^2$ and $|U_{\tau4}|^2 \ll |U_{e4}|^2$. This information will guide us to identify the benchmark parameters of the model which seem able to help in resolving other experimental anomalies. In particular, remaining in the low-energy regime, we will show that in addition to the LBL discrepancy, the model can explain an anomalous excess of ν_e-like events recorded in multi-GeV atmospheric data in Super-Kamiokande. This is possible because the NSI-like couplings lead to a substantial modification of the standard 3-flavor resonant behavior occurring in the atmospheric neutrino flavor conversion at energies of a few GeV.

At high energies $E \gtrsim 1$ TeV, the fourth state ν_s cannot be integrated out and the new framework reveals its genuine 4-flavor nature producing a resonant behavior at $E \simeq 10$ TeV as hinted at by IceCube which, for the preferred negative values of the potential, occurs in the neutrino channel. The possibility of the realization of a resonance in high-energy neutrinos is not new and indeed it is expected in the ordinary 3+1 scheme. However, we will demonstrate that in the new scenario the resonant amplification mechanism becomes much more complex and presents unconventional features. More precisely, the model predicts new resonances in the active $(\nu_e, \nu_\mu, \nu_\tau)$ sector, which are mediated by the fourth pseudo-sterile state ν_s through amplified NSI-like effects. We enucleate an irreducible three-level dynamics in which a new resonance in the active sector, for example the (ν_e, ν_μ) sub-system, is intertwined with two conventional resonances in the (ν_e, ν_s) and (ν_μ, ν_s) sub-systems, giving rise to a triple-avoided crossing phenomenon. This three-level behavior manifests with the emergence of large matter mixing angles and mass-squared differences in the active sector unrelated to their (irrelevant) vacuum counterparts. While three-level systems are widely studied in other fields of physics (photonics, quantum optics and quantum information among the others), they are basically unexplored in the neutrino field. This circumstance has deep roots in the structure of the

[2] Interestingly, such a scenario has been recently considered in [63] as a possible explanation of the tension between KM3NeT and IceCube concerning the high-energy 220 PeV event recorded in KM3NeT.

[3] Pseudo comes from Greek ψευδής (pseudēs) meaning "false".

[4] Here we tacitly refer to neutrinos. For antineutrinos the potential has the opposite sign.

3-flavor Hamiltonian in which the two mass-squared differences (solar and atmospheric) are hierarchically separated and the potential has a particularly simple form, leading to two distinct resonances [64]. Therefore, the pseudo-sterile neutrino scenario, in addition to its prominent purpose of providing a possible interpretation of the experimental anomalies, offers the opportunity to study and hopefully observe the rich dynamics of three-level systems in neutrino oscillations. In order to work and being of phenomenological interest, the scenario under investigation requires values of $f = V_s/|V_{NC}| \simeq -20$, $\Delta m^2_{41} \simeq 60$ eV^2 (both roughly uncertain by a factor of two), $|U_{e4}|^2 \simeq \sin^2\theta_{14} \simeq 0.01 - 0.03$ and $|U_{\mu 4}|^2 \simeq \sin^2\theta_{24} \simeq 10^{-4} - 10^{-3}$. Notably, such small values of $\sin^2\theta_{24}$ eliminate the tension of IceCube with the stringent bounds deriving from the negative searches of ν_μ disappearance performed by MINOS/MINOS+ [65] and NOvA [66]. Beyond this, the model predicts several additional experimental signatures. Most importantly, for the non-negligible value of $|U_{e4}|^2 \simeq \sin^2\theta_{14} \sim 0.01 - 0.03$, it should show up with a distinctive kink in the β-decay energy spectrum measured by KATRIN, which is very sensitive to the electron neutrino mixing at high indicated values of Δm^2_{41}.

The paper is structured as follows. In Sec. II we introduce the 3+1 scheme with the new matter potential. In Sec. III we demonstrate how this framework at low energies can be approximated for small values of the new mixing angles and elucidate the formal similarity of the ordinary NSI Hamiltonian involving the active neutrinos. In Sec. IV we show that the tension between NOvA and T2K can be resolved within the new framework. In Sec. V we perform an analytical and numerical study of the new model in the context of solar neutrino flavor conversions showing their role in constraining its parameters. We consider the two cases in which the new matter potential is proportional to the electron (or proton) number density and to neutron number density. We show that only in the first case, a degenerate solution is present in the upper (dubbed as "dark") octant of the solar mixing ange θ_{12}. In Sec. VI, guided by NOvA and T2K findings, the solar neutrino results and the existing bounds/hints on NSI from low energy atmospheric neutrino experiments, we identify the benchmark parameters of the model of phenomenological interest. In Sec. VII we describe the modifications induced by the new matter potential on the standard 3-flavor resonance occurring in atmospheric neutrinos at energies of few GeV, showing that they can explain the excess of ν_e-like events observed in Super-Kamiokande. Also, we assess the status of the neutrino mass ordering (NMO) determination in the new framework. In Sec. VIII we show that for the benchmark parameters of the model an unconventional resonant behavior is expected around 10 TeV in IceCube, qualitatively different from the one realized in the ordinary 3+1 scheme. We clarify the framework behind the conventional resonances and explain the basic features of the new resonances aided by a numerical study of the behavior of the eigenvalues and mixing angles (eigenvectors) in matter. We point out the irreducible three-level origin of the new resonant phenomenon. For completeness, in Sec. IX we illustrate the dark-octant (with reference to the solar mixing angle θ_{12}) degenerate solution existing for the case of a matter potential proportional to electron or proton number density, demonstrating that it can be distinguished from the ordinary lower-octant solution by analyzing the properties of the high-energy 10 TeV resonance. In Sec. X we briefly discuss the possibility that the new potential may be related to the interaction of the pseudo-sterile neutrinos with a background of asymmetric dark matter. In Sec. XI we discuss the possible origin of the new matter potential, the nature (Dirac vs Majorana) of the pseudo-sterile neutrinos and the phenomenological implications of the proposed scenario. Finally, we trace our conclusions in Sec. XII.

II. THE MODEL

In the presence of a sterile neutrino, the mixing between the flavor $(\nu_e, \nu_\mu, \nu_\tau, \nu_s)$ and the mass eigenstates $(\nu_1, \nu_2, \nu_3, \nu_4)$ is parametrized by a 4×4 unitary matrix[5]

$$U = \tilde{R}_{34} R_{24} \tilde{R}_{14} R_{23} \tilde{R}_{13} R_{12}\,, \tag{1}$$

where, R_{ij} ($\tilde{R}_{ij}$) represents a real (complex) 4×4 rotation of a mixing angle θ_{ij} which contains the 2×2 submatrix

$$R^{2\times 2}_{ij} = \begin{pmatrix} c_{ij} & s_{ij} \\ -s_{ij} & c_{ij} \end{pmatrix}, \quad \tilde{R}^{2\times 2}_{ij} = \begin{pmatrix} c_{ij} & \tilde{s}_{ij} \\ -\tilde{s}^*_{ij} & c_{ij} \end{pmatrix}, \tag{2}$$

in the (i, j) sub-block, having defined

$$c_{ij} \equiv \cos\theta_{ij}, \qquad s_{ij} \equiv \sin\theta_{ij}, \qquad \tilde{s}_{ij} \equiv s_{ij} e^{-i\delta_{ij}}. \tag{3}$$

[5] We recall that in the 3-flavor framework one introduces three mass eigenstates ν_i with masses m_i $(i = 1, 2, 3)$, three mixing angles $\theta_{12}, \theta_{13}, \theta_{13}$, and one CP-phase $\delta_{\rm CP}$. In this work we will indicate $\delta_{\rm CP} \equiv \delta_{13}$ both in the 3-flavor framework and in the 3+1 scheme. The neutrino mass ordering (NMO) is said to be normal (inverted) if $m_3 > m_{1,2}$ $(m_3 < m_{1,2})$. We will abbreviate normal (inverted) ordering as NO (IO).

Some useful properties of the matrix in Eq. (1) can be evidenced as follows: i) The 3-flavor PMNS matrix is recovered if one sets $\theta_{14} = \theta_{24} = \theta_{34} = 0$. ii) For small values of the mixing angles θ_{13}, θ_{14}, and θ_{24}, we have $|U_{e3}|^2 \simeq s_{13}^2$, $|U_{e4}|^2 = s_{14}^2$, $|U_{\mu 4}|^2 \simeq s_{24}^2$, and $|U_{\tau 4}|^2 \simeq s_{34}^2$, with a simple connection between the matrix elements and the mixing angles. iii) The leftmost positioning of the matrix $\tilde{R}_{34}$ guarantees that the $\nu_\mu \to \nu_e$ probability in vacuum is independent of θ_{34} and of the associated CP phase δ_{34} (see [67]).

The presence of a new sterile neutrino potential modifies the Hamiltonian of neutrino propagation in matter, which in the flavor basis becomes

$$H = U\,K\,U^\dagger + V\,, \tag{4}$$

where, $K = \mathrm{diag}\,(0, k_{21}, k_{31}, k_{41})$ denotes the diagonal matrix containing the wave numbers $k_{ij} = (m_i^2 - m_j^2)/2E$, while V represents the diagonal matrix encoding the matter effects defined as

$$V = \mathrm{diag}\,(V_{CC}, 0, 0, V_S - V_{NC})\,, \tag{5}$$

where

$$V_{CC} = \sqrt{2} G_F N_e\,, \tag{6}$$

is the standard charged current (CC) potential, N_e being the electron number density of the background matter, and

$$V_{NC} = -\frac{1}{2}\sqrt{2} G_F N_n\,, \tag{7}$$

is the standard neutral current (NC) potential, N_n being the neutron number density. The additional term V_S is the new sterile potential which, for definiteness, we measure in units of the standard NC potential as

$$V_S = -f \times V_{NC} \tag{8}$$

by introducing the rescaling parameter f. With this definition, the new potential has the same sign of f, since V_{NC} is negative. For the sake of convenience, we introduce the auxiliary parameter

$$\bar{f} = r(1+f) \tag{9}$$

where $r = |V_{NC}|/|V_{CC}|$, which in the Earth is constant and approximately $r = 0.5$, while in Sun it depends on the radial position $x = R/R_{sun}$, where R_{sun} is the Sun radius. Using this notation the matrix representing the matter potential simply reads

$$V = V_{CC} \times \mathrm{diag}\left(1, 0, 0, \bar{f}\right)\,. \tag{10}$$

We see that $\bar{f}$ allows us to gauge the potential felt by sterile neutrinos in units of the charged-current potential V_{CC}. We note that $\bar{f} = r$ in the standard model case (being $f = 0$), while for the big values of f, which will be phenomenologically relevant, the approximation $\bar{f} \simeq rf$ holds. When considering the evolution of antineutrinos, in addition to the replacement $U \to U^*$, one has to change the sign of the potentials V_{CC}, V_{NC} and V_S, which is equivalent to change the sign of V_{CC} in Eq. (10).

Here, an important remark is in order. Equation (8) assumes that the new matter potential is proportional to the neutron number density. While we will adopt this choice as a benchmark throughout our work, it should be stressed that the nature of the interaction of the sterile neutrinos is unknown and it can involve electrons, protons and neutrons. For the propagation in the Earth the particular choice of the fermion is irrelevant since the number densities of the three particles are approximately equal $N_e = N_p \simeq N_n$, being the Earth an iso-scalar medium. Differently, for solar neutrinos we still have $N_e = N_p$ to ensure neutrality, while N_n is suppressed by a factor which depends on the radial position $x = R/R_{sun}$. In particular, the neutron number density close to the center of the sun, which is relevant for adiabatic flavor conversions, is approximately a factor of two smaller than N_e. Therefore, in the treatment of solar neutrinos this aspect must be taken into account if one considers a matter potential different from our benchmark choice. In case of interaction with fermions different from neutrons (electrons or protons), the new potential should be rescaled consistently with the adopted choice (see Sec. V for further clarifications).

III. SMALL-MIXING NSI-LIKE APPROXIMATION IN LBL AND ATMOSPHERIC NEUTRINOS

Let us now consider the impact of the new potential for the phenomenology of LBL experiments such as NOvA and T2K. The treatment is valid also for atmospheric neutrinos for energies which are much lower than the resonance energy, which as we will see in Sec. VIII, lies around 10 TeV. Before treating the matter effects, we consider the kinematical ones by giving a look to the appearance probability in vacuum. As first pointed out [67], the $\nu_\mu \to \nu_e$ probability can be approximated as the sum of three terms,

$$P_{\mu e}^{4\nu} \simeq P^{\rm ATM} + P_{\rm I}^{\rm INT} + P_{\rm II}^{\rm INT}\,, \tag{11}$$

where,

$$\begin{aligned} P^{\rm ATM} &\simeq 4 s_{23}^2 s_{13}^2 \sin^2\Delta, &(12)\\ P_{\rm I}^{\rm INT} &\simeq 8 s_{13} s_{12} c_{12} s_{23} c_{23} (\alpha\Delta)\sin\Delta\cos(\Delta+\delta_{13}), &(13)\\ P_{\rm II}^{\rm INT} &\simeq 4 s_{14} s_{24} s_{13} s_{23} \sin\Delta\sin(\Delta+\delta_{13}-\delta_{14})\,, &(14)\end{aligned}$$

where $\Delta \equiv \Delta m^2_{31} L/4E$ is the atmospheric oscillating factor, L and E being the neutrino baseline and energy, respectively. We have also defined the ratio of the solar over the atmospheric mass-squared splitting $\alpha \equiv \Delta m^2_{21}/\Delta m^2_{31} \simeq 0.03$. The term $P^{\rm ATM}$ represents the leading order standard three neutrino term which is related to the oscillations driven by the atmospheric mass-squared splitting. The other two terms, namely $P_{\rm I}^{\rm INT}$ and $P_{\rm II}^{\rm INT}$ represent two interference terms and each one of them is generated by the interference of two independent frequencies. In particular, the term $P_{\rm I}^{\rm INT}$ arises from the interference between the solar and atmospheric frequencies, whereas the term $P_{\rm II}^{\rm INT}$, a genuine 4-flavor effect, arises from the interference between the atmospheric and the new frequency introduced by the fourth mass eigenstate. Note that these terms survive the averaging process of the fast oscillations induced by the large eV^2-scale value of Δm^2_{41}. For the small values of the mixing angles that we will find phenomenologically relevant in the next sections ($s^2_{14} \simeq 0.02$ and $s^2_{24} \simeq 10^{-3}$), the amplitude of the new interference term is 2.5×10^{-3}, almost one order of magnitude smaller than that of the standard interference effect which lies around 10^{-2}. Therefore, the new interference term has negligible impact in LBL experiments and in atmospheric neutrinos as we have explicitly checked. An analogous derivation can be done for the disappearance probability of muon neutrinos $P_{\mu\mu}$ (see [68]), which shows that the corrections to the 3–flavor case are proportional to the product of $s_{14}s_{24}s_{13}$ and thus below 10^{-3}. Hence, the kinematical/vacuum effects induced by the sterile neutrinos are negligible, and we must be concerned only with the perturbations induced in the oscillations probabilities by the matter effects.

Let's consider the matter effects explicitly. As shown in [67] (see the appendix), in order to simplify the treatment of matter effects in LBL setups, it is useful to introduce the new basis

$$\bar\nu = \bar U^\dagger \nu\,, \tag{15}$$

where, $\bar U = \tilde R_{34} R_{24} \tilde R_{14}$, is the part of the mixing matrix defined in Eq. (1) that contains only the rotations involving the fourth neutrino mass eigenstate. The mixing matrix U is split as follows $U = \bar U U_{3\nu}$, where $U_{3\nu}$ is the 4×4 matrix which contains the standard 3-flavor mixing matrix in the (1,2,3) sub-block. In the new basis, the Hamiltonian takes the form

$$\bar H = \bar H^{\rm vac} + \bar H^{\rm mat} = U_{3\nu} K U_{3\nu}^\dagger + \bar U^\dagger V \bar U\,, \tag{16}$$

where the first term describes the oscillations in vacuum, and the second one represents a non-standard dynamical term. Since the wavenumber k_{41} is much bigger than k_{21} and $|k_{31}|$, we can reduce the dynamics to that of an effective 3-flavor system. In fact, from Eq. (16) one can see that the (4,4) entry of $\bar H$ is much larger than all the other entries and the fourth eigenvalue of $\bar H$ is much larger than the other three ones. As a consequence, the eigenstate $\bar\nu_s$ evolves independently of the others. Extracting from $\bar H$ the submatrix with indices $(1,2,3)$, one obtains the effective 3×3 Hamiltonian

$$\bar H_{3\nu} = \bar H^{\rm vac}_{3\nu} + \bar H^{\rm mat}_{3\nu}, \tag{17}$$

which governs the evolution of the rotated eigenstates $(\bar\nu_e, \bar\nu_\mu, \bar\nu_\tau)$. It should be noted that labeling the rotated states with the flavor index makes sense, since for very small mixing angles they are very close to the original flavor eigenstates. In order to calculate the oscillation probabilities, it is useful to intoduce the evolution operator, which, in the new basis, takes the expression

$$\bar S \equiv e^{-i\bar H L} \approx \begin{pmatrix} e^{-i\bar H_{3\nu} L} & \mathbf{0} \\ \mathbf{0} & e^{-ik_{41}L}\end{pmatrix}\,, \tag{18}$$

and is related to the evolution operator in the flavor basis via the unitary transformation

$$S = \bar U \bar S \bar U^\dagger\,. \tag{19}$$

Considering the block-diagonal form of $\bar{S}$ and the identities $\bar{U}_{e2} = \bar{U}_{e3} = \bar{U}_{\mu 3} = 0$, one has for the relevant transition amplitudes (see [67, 69])

$$\begin{aligned} S_{e\mu} &= \bar{U}_{e1}\bar{S}_{ee}\bar{U}^*_{\mu 1} + \bar{U}_{e1}\bar{S}_{e\mu}\bar{U}^*_{\mu 2} + \bar{U}_{e4}\bar{S}_{ss}\bar{U}^*_{\mu 4}\,, && (20)\\ S_{\mu\mu} &= \bar{U}_{\mu 1}\bar{S}_{ee}\bar{U}^*_{\mu 1} + \bar{U}_{\mu 1}\bar{S}_{e\mu}\bar{U}^*_{\mu 2} + \bar{U}_{\mu 2}\bar{S}_{\mu e}\bar{U}^*_{\mu 1} + \bar{U}_{\mu 2}\bar{S}_{\mu\mu}\bar{U}^*_{\mu 2} + \bar{U}_{\mu 4}\bar{S}_{ss}\bar{U}^*_{\mu 4}\,. && (21)\end{aligned}$$

Since $\bar{S}_{ss} = e^{-ik_{14}L}$ oscillates very fast, the associated terms are averaged out by the finite energy resolution of the detector. Considering the explicit expressions of the elements of the matrix $\bar{U}$, and expanding in the small values of the mixing angles, one has for the oscillation probabilities the approximate expressions

$$\begin{aligned} P^{4\nu}_{\mu e} \equiv |S_{e\mu}|^2 &\simeq (1 - s^2_{14} - s^2_{24})\bar{P}^{3\nu}_{\mu e} - 2s_{14}s_{24}\mathrm{Re}(e^{-i\delta_{14}}\bar{S}_{ee}\bar{S}^*_{e\mu})\,, && (22)\\ P^{4\nu}_{\mu\mu} \equiv |S_{\mu\mu}|^2 &\simeq (1 - 2s^2_{24})\bar{P}^{3\nu}_{\mu\mu} - 2s_{14}s_{24}\mathrm{Re}(e^{-i\delta_{14}}\bar{S}_{\mu\mu}\bar{S}^*_{e\mu} + e^{i\delta_{14}}\bar{S}_{\mu\mu}\bar{S}^*_{\mu e})\,, \end{aligned}$$

where $\bar{P}^{3\nu}_{\mu e} \equiv |\bar{S}_{e\mu}|^2$ and $\bar{P}^{3\nu}_{\mu\mu} \equiv |\bar{S}_{\mu\mu}|^2$. Therefore, the 4-flavor problem is reduced to a more familiar 3-flavor one, being the probabilities expressed in terms of the amplitudes $\bar{S}_{ee}$, $\bar{S}_{e\mu}$, $\bar{S}_{\mu e}$ and $\bar{S}_{\mu\mu}$ of the 3-flavor system governed by the effective Hamiltonian $\bar{H}_{3\nu}$ in Eq. (17). More specifically, we see that the 4-flavor probabilities are the sum of two contributions, the first one being the 3-flavor probability (with rotated Hamiltionian $\bar{H}_{3\nu}$) with a prefactor close to unity, and a term deriving from the interference of the sterile frequency with the atmospheric and solar ones. As first noted in [67] such an interference, maybe counterintuitively, survives the process of averaging the oscillations. It is easy to check (see [67]) that in the vacuum limit one obtains the probability expression given in Eqs. (12-14), and in particular the 4-flavor interference term in Eq. (14). If the active-sterile mixing angles are very small like in our case, in which we will consider $s^2_{14} \simeq 0.02$ and $s^2_{24} \simeq 10^{-3}$, and also taking into account that[6] $|\bar{S}_{e\mu}| \ll 1$, one can neglect the interference terms and arrive at the approximate expressions

$$\begin{aligned} P^{4\nu}_{\mu e} &\simeq \bar{P}^{3\nu}_{\mu e} && (23)\\ P^{4\nu}_{\mu\mu} &\simeq \bar{P}^{3\nu}_{\mu\mu}\,. \end{aligned}$$

Therefore, the 4-flavor probabilities with the original Hamiltonian in Eq. (4) can be approximated by the 3-flavor probabilities with the effective Hamiltonian $\bar{H}_{3\nu}$. While these expressions cannot be used for precision calculations (in fact we use full 4-flavor evolution in our codes), they can be very insightful to grasp the behavior of the 4-flavor probabilities in the limit of very small mixing angles. In fact, using a result found in [67] and making the appropriate modifications needed to incorporate the new potential, the matter part of the effective Hamiltonian in Eq. (17), for small values of the mixing angles, can be approximated by

$$\bar{H}^{\mathrm{mat}}_{3\nu} \approx V_{\mathrm{CC}} \begin{bmatrix} 1+\bar{f}_\oplus s^2_{14} & \bar{f}_\oplus \tilde{s}_{14}s_{24} & \bar{f}_\oplus \tilde{s}_{14}\tilde{s}^*_{34} \\ \dagger & \bar{f}_\oplus s^2_{24} & \bar{f}_\oplus s_{24}\tilde{s}^*_{34} \\ \dagger & \dagger & \bar{f}_\oplus s^2_{34} \end{bmatrix}, \quad (24)$$

where we have denoted $\bar{f}_\oplus = r_\oplus(1+f) \simeq 0.5(1+f)$. The Hamiltonian in Eq. (24) returns the standard 3-flavor matter effect when one sets $\theta_{14} = \theta_{24} = \theta_{34} = 0$. On the other hand for the case $f = 0$ it reproduces the 3+1 scheme. Now, one can notice that this matter Hamiltonian, apart from the term equal to unity in the $(1,1)$ entry, represents a perturbation matrix which is formally equivalent to the one which regulates the usual non-standard interactions (NSI), and can be written as

$$\bar{H}^{\mathrm{NSI}}_{3\nu} \approx V_{\mathrm{CC}} \begin{bmatrix} \varepsilon^\oplus_{ee} & \varepsilon^\oplus_{e\mu} & \varepsilon^\oplus_{e\tau} \\ \dagger & \varepsilon^\oplus_{\mu\mu} & \varepsilon^\oplus_{\mu\tau} \\ \dagger & \dagger & \varepsilon^\oplus_{\tau\tau} \end{bmatrix}. \quad (25)$$

It is important to observe that these couplings do not describe interactions which involve directly the active neutrinos, since the interaction intervenes only mediated by their mixing with the fourth mass eigenstate and by the new potential. Also, we note that in the NSI-like Hamiltonian in Eqs. (25) there are not nine independent parameters as in a generic hermitian matrix but only six,[7] since there are three mixing angles $\theta_{14}, \theta_{24}, \theta_{34}$, two CP-phases δ_{14} and δ_{34}, and the

---

[6] In normal conditions $|\bar{S}_{e\mu}| \propto s_{13}$, but in the presence of the 1-3 resonance it can be bigger. We have checked that even in this case, for the small values of the sterile mixing angles considered in the present work, the relations in the Eqs. (23) provide a good estimate of the oscillation probabilities.

[7] In neutrino oscillations a diagonal matrix proportional to the identity can be always added/subtracted, so the number of independent parameters decreases by one unit.

rescaling parameter $\bar{f}_\oplus$.[8] It should be also stressed that $\bar{f}_\oplus$ is an overall multiplicative factor that, apart from its sign, can be reabsorbed in the couplings by recasting the NSI-like hamiltonian in the form

$$\bar{H}_{3\nu}^{\rm NSI} \approx ({\rm sgn}\, \bar{f}_\oplus) V_{\rm CC} \begin{bmatrix} |\varepsilon_{ee}^\oplus| & \sqrt{|\varepsilon_{ee}^\oplus||\varepsilon_{\mu\mu}^\oplus|}e^{i\phi_{e\mu}} & \sqrt{|\varepsilon_{ee}^\oplus||\varepsilon_{\tau\tau}^\oplus|}e^{i\phi_{e\tau}} \\ \dagger & |\varepsilon_{\mu\mu}^\oplus| & \sqrt{|\varepsilon_{\mu\mu}^\oplus||\varepsilon_{\tau\tau}^\oplus|}e^{i\phi_{\mu\tau}} \\ \dagger & \dagger & |\varepsilon_{\tau\tau}^\oplus| \end{bmatrix}, \tag{26}$$

which depends on the three independent diagonal amplitudes $|\varepsilon_{\alpha\alpha}^\oplus|$ ($\alpha = e, \mu, \tau$) and three CP-phases $\phi_{e\mu} \equiv -\delta_{14}$, $\phi_{\mu\tau} \equiv \delta_{34}$, the third one being a linear combination of the first two ones $\phi_{e\tau} = \phi_{e\mu} + \phi_{\mu\tau} = \delta_{34} - \delta_{14}$. This observation allows us to derive three important consequences. First, the Hamiltonian depends on five effective parameters instead of six. Second, there is a complete degeneracy among the rescaling parameter $\bar{f}_\oplus$ and the products of the mixing angles $s_{i4}s_{j4}$ with ($i = 1, 2, 3$) appearing in the (i, j) position of the matrix. In order to break such a degeneracy, one will need other kind of systems, different from LBL and low-energy neutrinos, like for example, SBL setups, solar neutrinos and the resonant behavior like that occurring in IceCube high-energy neutrinos, which present a different analytical dependency on the model parameters. Third, despite this complete degeneracy, the system (in our case LBL and atmospheric oscillations) is sensitive to the sign of $\bar{f}_\oplus$. We will see that this last property will be crucial for our findings concerning NOvA and T2K.

We underline that the sterile NSI-like Hamiltonian in Eqs. (24) and (26) has a very distinctive pattern and constitutes one of the main signatures of the model under consideration, which could be the target of future LBL experiments such as DUNE, Hyper-Kamiokande and ESSνSB. In the absence of the new potential of sterile neutrinos one has $\bar{f}_\oplus = r_\oplus \simeq 0.5$ and all the couplings in Eq. (24) are very small, being of the second order in powers of the s_{ij}. In this limit, one recovers the ordinary 3+1 scenario in which matter effects have almost no relevance.[9] However, things are expected to qualitatively change when the rescaling factor $\bar{f}_\oplus$ is allowed to assume large $O(10)$ values, in which case some of the NSI-like couplings will have a non-negligible impact.

IV. RESOLUTION OF THE TENSION BETWEEN NOvA AND T2K

As we underlined in [18], the two long-baseline accelerator experiments NOvA and T2K represent the ideal setup where to seek non-standard matter effects in neutrino propagation due to their different and complementary configurations. In particular, the two experiments work at different peak energies (2 GeV for NOvA and 0.6 GeV for T2K) because of the different baselines (810 km for NOvA and 295 km for T2K). As a consequence, in NOvA matter effects are approximately three/four times larger with respect to T2K. In this situation, one can use T2K as a quasi-vacuum experiment which is capable of measuring the CP-phase δ_{13} almost independently of the presence of NSI. On the other hand, NOvA can exploit this external information to acquire sensitivity to the NSI couplings. The interplay between NOvA and T2K presents similarities with the synergy of solar neutrinos with the KamLAND experiment. In fact, the irrefutable proof of the existence of matter effects in solar neutrino flavor conversion could be obtained only by exploiting the external information provided by KamLAND, which fixes the oscillation parameters (in particular Δm_{21}^2) independently of matter effects [71].

NOvA and T2K since 2020 display a persisting discrepancy in the ν_e appearance channel, which shows up in three ways when the data are interpreted in the standard 3-flavor scheme.[10] First, in the normal neutrino mass ordering the estimates of the CP-phase δ_{13} provided by the two experiments are in disagreement, being in tension with a statistical significance of $\sim 2\sigma$, as recently reevaluated in [19]. While T2K [16] prefers values of $\delta_{13} \simeq 1.5\pi$, NOvA [15] points towards $\delta_{13} \simeq \pi$. Second, while each of the two experiments taken separately prefers the NO, their combination prefer the IO. Third, their joint preference for IO is in contrast with all the remaining world neutrino oscillation data, which prefer NO [72–76]. In [18] (see also [17]) we pointed out that all these three discrepancies could be

---

[8] This parameter counting can be understood also by observing that the NSI-like Hamiltonian can be constructed with the real scalar $\bar{f}$ and the complex vector $u^T = (\tilde{s}_{14}, s_{24}, \tilde{s}_{34})$ being $H_{3\nu}^{\rm NSI} = \bar{f} u u^\dagger$. This also implies that the matrix is rank-deficient being of rank 1, having only one linearly independent column (or row).

[9] The role of the ordinary 3+1 scheme as a possible solution of the NOvA and T2K tension has been considered in [70], where it has been shown that it is not able to explain the discrepancy assuming for the mixing angles θ_{14} and θ_{24} the values preferred by the global fits performed in the 3+1 scheme. For the choice of the mixing angles which will be relevant for the present work, we have checked that the 3+1 fit to NOvA and T2K is almost indistinguishable from that obtained in the 3-flavor scheme.

[10] An alternative way to interpret the observed discrepancy, which is conceptually more correct when adopting a non-standard scenario, is to consider it as an internal tension of the theoretical 3-flavor framework, which is not flexible enough to provide a satisfying fit of the experimental data.

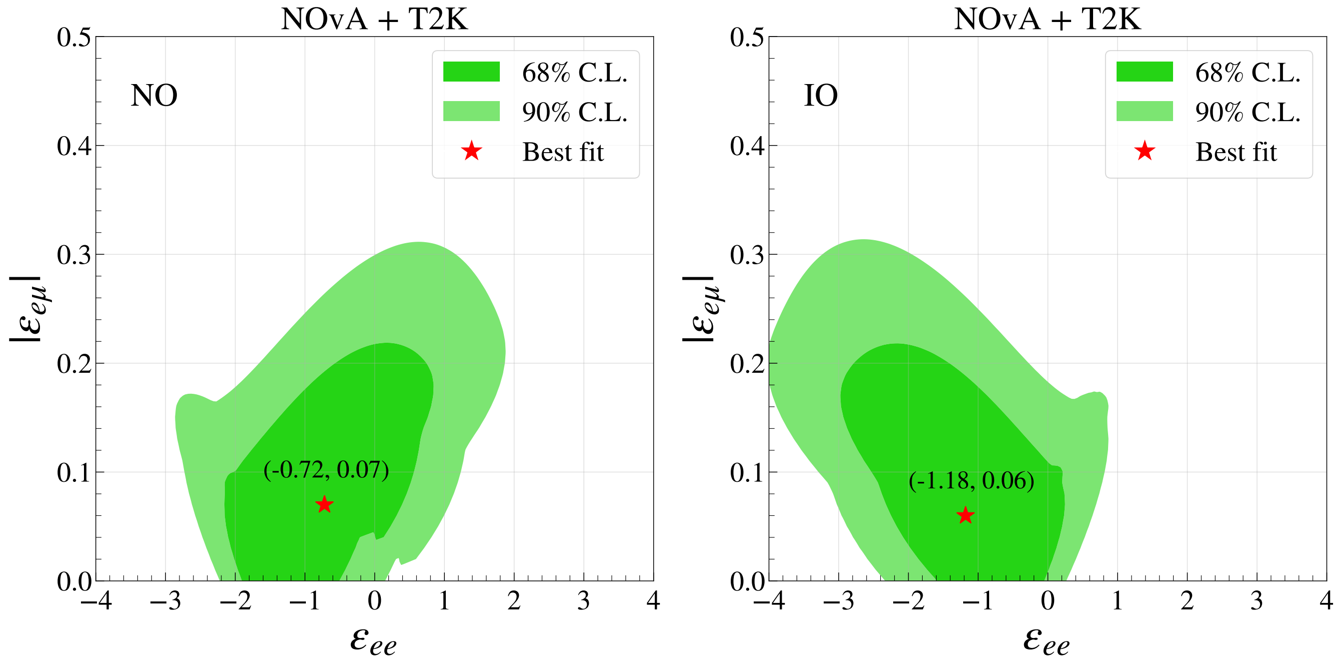

FIG. 1: Allowed regions for the two NSI couplings ε_{ee} and $|\varepsilon_{e\mu}|$ determined by the combined analysis of NOvA and T2K. The left (right) panel refers to NO (IO). The contours correspond to the 68% and 90% C.L. for 2 d.o.f..

solved by hypothesizing the existence of NSI. More specifically, we found a $\sim 2\sigma$ level preference for non-zero complex neutral-current NSI of the flavor changing type involving the $e-\mu$ or the $e-\tau$ sectors with couplings $|\varepsilon^{\oplus}_{e\mu}| \sim |\varepsilon^{\oplus}_{e\tau}| \sim 0.1$.

In the present work, as a preliminary step, we generalize the NSI analysis of NOvA and T2K by taking into account two NSI couplings simultaneously. More specifically, we consider the off-diagonal complex coupling $\varepsilon^{\oplus}_{e\mu}$ (already considered alone in our previous work) and the diagonal coupling $\varepsilon^{\oplus}_{ee}$ (not considered in our previous work). We have done a similar analysis (whose results will be not shown for brevity) by replacing $\varepsilon^{\oplus}_{e\mu}$ with $\varepsilon^{\oplus}_{e\tau}$. Thanks to the formal analogy expounded in the previous section, the results of the NSI analysis will allow us to gain insight when interpreting the findings concerning the 3+1 scenario with the novel matter potential. In addition, this analysis will allow us to compare the hint of non-zero NSI coming from NOvA and T2K with the bounds/hints deriving from low energy atmospheric neutrino experiments. For the analysis, we have made use of the same datasets for NOvA [15] and T2K [16] experiments used in [19]. We have fully accounted for both the disappearance and appearance channels for each experiment. We use the GLoBES software package [77, 78] along with an additional public tool [79] designed to implement non-standard interactions. We marginalized over θ_{13} using a 2.4% 1 sigma prior, with a central value of $\sin^2\theta_{13} = 0.0223$, as determined by the global analysis [74]. The solar parameters Δm^2_{21} and $\sin^2\theta_{12}$ are taken at their best fit values found in the updated global fit [72].[11]

Figure 1 displays the results of this analysis for NO (IO) in the left (right) panel, where the CP phase $\phi_{e\mu}$ is marginalized. In addition, we marginalize the standard parameters θ_{13}, δ_{13}, θ_{23} and Δm^2_{31}. We see that in both orderings there is a preference for non-zero NSI couplings, which is more pronounced for the case of NO. Specifically, in NO the case of no NSI is disfavored with $\Delta\chi^2 \simeq 4.1$, while in IO, it is disfavored at $\Delta\chi^2 \simeq 2.6$. In both plots we observe a pronounced correlation between $\varepsilon^{\oplus}_{ee}$ and $|\varepsilon^{\oplus}_{e\mu}|$. We also observe that the plots corresponding to NO and IO are symmetrical with respect to the replacement $\varepsilon^{\oplus}_{ee} \to -2-\varepsilon^{\oplus}_{ee}$. Also we have checked that for such a transformation the marginalization process provides the replacement $\phi_{e\mu} \to 2\pi - \phi_{e\mu}$ i.e. $\varepsilon^{\oplus}_{e\mu} \to \varepsilon^{\oplus *}_{e\mu}$. This behavior is expected due to a well known degeneracy property of the neutrino flavor evolution (see [81]). We notice that while the preferred values of the off-diagonal coupling lie around 0.05, the diagonal coupling $|\varepsilon^{\oplus}_{ee}|$ can assume large $O(1)$ negative values. To this regard, one should note that in both NMO, the case $\varepsilon^{\oplus}_{ee} = -1$ (for $\varepsilon^{\oplus}_{e\mu} = 0$), corresponds to the complete absence of matter effects (standard and non-standard), i.e. to propagation in vacuum. Graphically, this would correspond to

[11] When considering the so called Dark-LMA solution [80], in NOvA and in T2K we fix $\sin^2\theta_{12}$ at the octant symmetric value with respect to the value obtained for the ordinary LMA solution.

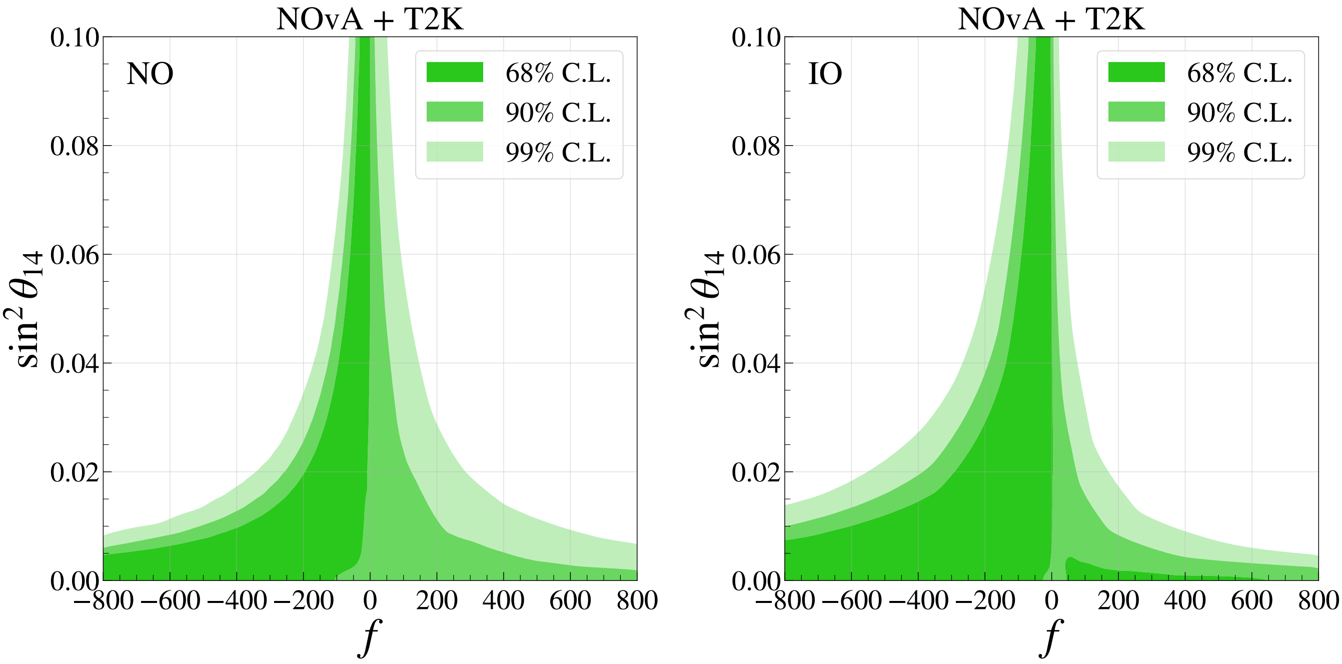

FIG. 2: The left (right) panel represents the allowed regions for NO (IO) at the 68%, 90% and 99% C.L. for 2 d.o.f. by the combination of NOvA and T2K in the plane spanned by the two parameters $[f, s^2_{14}]$. We have marginalized over the CP phase δ_{14} and imposed the prior $|fs^2_{24}| < 0.1$ at 90% C.L. to take into account the bound on $|\varepsilon_{\mu\mu}|$ deriving from atmospheric neutrino experiments.

coinciding biprobability plots for the two cases of NO and IO for both experiments NOvA and T2K, which, as it is well known, get separated due to (standard) matter effects. Hence, it is very interesting to note that the two LBL experiments jointly prefer the vacuum case, and that this weird circumstance can be seen as a further declination of their mutual tension.

Let's now consider the 3+1 scenario with the novel potential. Figure 2 presents the constraints in the plane spanned by the two parameters f and s^2_{14} obtained by the combined analysis of NOvA and T2K, having marginalized away the new CP phase δ_{14}. The left (right) panel refers to NO (IO). The allowed regions are drawn at the 68%, 90% and 99% C.L. in 2 d.o.f.. Concerning the 3-flavor parameters, we have fixed $\Delta m^2_{21} = 7.48 \times 10^{-5}\,\mathrm{eV}^2$, $\sin^2\theta_{12} = 0.308$, $\sin^2\theta_{13} = 0.0223$, and marginalized over θ_{23} and δ_{13}. In these plots we have assumed $s^2_{34} = 0$, thus automatically setting to zero the NSI-like couplings involving the τ neutrino ($\varepsilon^{\oplus}_{e\tau} = \varepsilon^{\oplus}_{\mu\tau} = \varepsilon^{\oplus}_{\tau\tau} = 0$). In addition, we have imposed the prior $|\bar{f}_{\oplus} s^2_{24}| < 0.05$ (equivalent to $|fs^2_{24}| < 0.1$) at 90% C.L. justified by the stringent bound on the $\varepsilon_{\mu\mu}$-like copling deriving from atmospheric neutrino experiments (see below). Under these working assumptions the 3+1 model with the new potential becomes easily comparable with the NSI scheme analyzed above, which can be used to gain insight in the numerical results.

From these two plots we learn that in NO (IO) the 3-flavor scheme (corresponding to $f = 0$ and $s^2_{14} = 0$) is disfavored at more than the 90% C.L (68% C.L). Specifically we find $\Delta\chi^2 \simeq 4.3$ in NO and $\Delta\chi^2 \simeq 2.5$ in IO. The allowed regions exhibit an inverted funnel-like structure, which can be explained thanks to the NSI analogy, by observing that NOvA and T2K are mostly sensitive to the coupling $\varepsilon^{\oplus}_{ee} = \bar{f}_{\oplus} s^2_{14}$, and therefore they can limit only the product of the two parameters f and s^2_{14}. The asymmetry of the allowed regions, which indicates a preference for negative values of f, is related to the fact that the combination of NOvA and T2K prefers a negative value of the $\varepsilon^{\oplus}_{ee}$. Also the preference for a negative real part of the complex NSI coupling $\varepsilon^{\oplus}_{e\mu} = \bar{f}_{\oplus} \tilde{s}_{14} s_{24}$ goes in the same direction. In summary, our combined analysis of NOvA and T2K shows that the LBL data provide an indication in favor of the 3+1 scheme with the novel potential over the 3-flavor scheme with a preference for negative values of the potential. In addition, the data tell us that the indication is stronger in the NO case with respect to the IO.

In order to illustrate that such an improved fit is related to the capability of the model of resolving the tension between the two experiments, we present in Figure 3 the regions allowed for the two parameters δ_{13} and $\sin^2\theta_{23}$ for the case of NO. The left plot represents the standard 3-favor fit, where a clear tension emerges in the determination of the CP phase δ_{13}. The right plot refers to the 3+1 scheme with enhanced potential. In this case we have fixed $s^2_{14} = 0.02$, all the other parameters being constrained exactly as in Fig. 2. For this value of s^2_{14}, we find the best fit values $\bar{f}_{\oplus} = -21.0$ (or equivalently $f = -43.0$) and $\delta_{14} = 1.7\pi$. In the new 3+1 framework there is a high level of

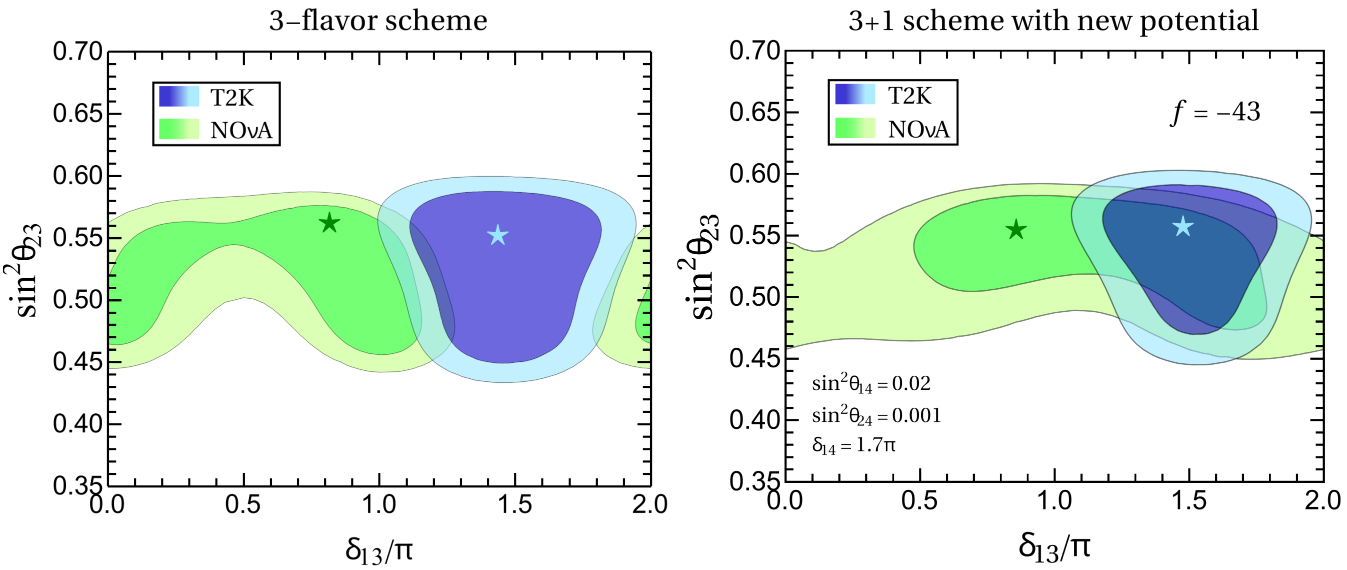

FIG. 3: Allowed regions by NOvA and T2K for normal ordering. The left panel represents the 3-flavor framework, while the right panel refers to the 3+1 scheme with the new potential. The contours correspond to the 68% and 90% C.L. for 2 d.o.f.

overlap of the allowed regions for values of δ_{13} close to 1.5π, showing that the new model is very effective in reducing the tension between the two experiments. We can observe that the T2K regions are basically unchanged as expected because of the low sensitivity to matter effects. Differently, the NOvA regions appreciably change because of its pronounced sensitivity to matter effects. These findings are in agreement with our analytical discussion and evidence the vacuum-matter synergy of the two experiments.

It is interesting and useful to compare the indication in favor of non-zero NSI coming from NOvA and T2K with the bounds/hints provided by the low-energy atmospheric neutrino experiments. For this purpose, we list such bounds in Table I also providing their combination performed assuming gaussian (asymmetric where appropriate) uncertainties, which may serve as a benchmark. From this table we can observe that only IceCube provides an interval for the diagonal coupling $\varepsilon^{\oplus}_{ee} - \varepsilon^{\oplus}_{\mu\mu}$, which interesting weakly favors non-zero negative values like NOvA in T2K. In IceCube the case $\varepsilon^{\oplus}_{ee} = -1$ (no matter effects) is disfavored at $\Delta\chi^2 \simeq 7.0$, demonstrating an interesting sensitivity to this coupling. Concerning the off-diagonal parameters $\varepsilon^{\oplus}_{e\mu}$ and $\varepsilon^{\oplus}_{e\tau}$, we note that the atmospheric experiments provide a sensitivity for couplings of magnitude ~ 0.05, and in some cases there are feeble hints in favor of a non-zero value. On the third off-diagonal coupling $\varepsilon^{\oplus}_{\mu\tau}$ the same experiments provide the very stringent bound $\sim 3.3 \times 10^{-3}$. Finally, for the diagonal coupling $|\varepsilon^{\oplus}_{\mu\mu} - \varepsilon^{\oplus}_{\tau\tau}|$ there is an upper bound around 0.02. Such a bound justifies the prior $|fs^2_{24}| < 0.1$ used in the analysis of NOvA and T2K, since in the limit $\theta_{34} = 0$ we have considered, one has $\varepsilon^{\oplus}_{\tau\tau} = \bar{f}_{\oplus} s^2_{34} = 0$, and the equality $\varepsilon^{\oplus}_{\mu\mu} - \varepsilon^{\oplus}_{\tau\tau} = \varepsilon^{\oplus}_{\mu\mu}$ holds.

V. CONSTRAINTS FROM SOLAR NEUTRINO DATA

Solar neutrinos have played a pivotal role in establishing the existence of matter effects as predicted by Wolfenstein [82]. This is due to the high electron number density in the central region of the Sun, where neutrinos are produced in nuclear fusion reactions. In fact, solar neutrino data, with the solid anchor of the quasi-vacuum measurements performed with KamLAND, where matter effects are much smaller, provided the first irrefutable evidence for the coherent forward scattering of electron neutrinos mediated by charged currents [71]. Therefore, one naturally expects that solar neutrinos should play an important role in constraining the scenario we are studying. For this reason we provide an analytical and numerical study of the solar neutrino conversion in the model under investigation.

The treatment of the matter effects relevant for solar neutrinos in the ordinary 3+1 scheme has been performed in [87] (see also [88]), to which we refer the reader for more details (see the Appendixes). Here, we report the basic results with the appropriate modifications necessary to include the new matter potential. It is convenient to introduce the new basis

$$\bar{\nu} = A^T \nu \,, \tag{27}$$

TABLE I: Best estimates with 1 σ error of the listed NSI couplings. The intervals/bounds refer to the 90% C.L. for 1 d.o.f.

Experiment	$\varepsilon^{\oplus}_{ee} - \varepsilon^{\oplus}_{\mu\mu}$	$\varepsilon^{\oplus}_{\tau\tau} - \varepsilon^{\oplus}_{\mu\mu}$	$\lvert\varepsilon^{\oplus}_{e\mu}\rvert$	$\lvert\varepsilon^{\oplus}_{e\tau}\rvert$	$\lvert\varepsilon^{\oplus}_{\mu\tau}\rvert$
ANTARES [83]	–	$-0.032^{+0.015}_{-0.025} \cup 0.032^{+0.035}_{-0.015}$	–	–	< 0.0045
IceCube [84]	$[-2.26, -1.27] \cup [-0.74, 0.32]$	0.002 ± 0.025	$0.072^{+0.038}_{-0.069}$	$0.060^{+0.08}$	< 0.0232
KM3NeT/ORCA [85]	–	0.00 ± 0.01	$0.03^{+0.02}_{-0.03}$	$0.04^{+0.02}_{-0.04}$	< 0.0055
SuperKamiokande [86]	–	$[-0.049, 0.049]$	–	–	< 0.011
Combination	$[-2.26, -1.27] \cup [-0.74, 0.32]$	$[-0.018, 0.019]$	$0.038^{+0.018}_{-0.028}$	$0.041^{+0.019}_{-0.040}$	< 0.0033

where we have defined the matrix A as

$$A = \tilde{R}_{34} R_{24} \tilde{R}_{14} R_{23} \tilde{R}_{13} \equiv U R_{12}^T \,. \tag{28}$$

In this new basis the Hamiltonian assumes the form

$$\bar{H} = \bar{H}^{\rm vac} + \bar{H}^{\rm mat} = R_{12} K R_{12}^T + A^T V A \,, \tag{29}$$

and, in the hierarchical limit $\Delta m^2_{21} \ll \Delta m^2_{31} \ll \Delta m^2_{41}$, the dynamics can be reduced to an effective 2-flavor one with Hamiltonian

$$\bar{H}_{2\nu} = \bar{H}^{\rm vac}_{2\nu} + \bar{H}^{\rm mat}_{2\nu} \,, \tag{30}$$

where the matter term, using the expressions of the elements of the matrix A, can be written in the form

$$\bar{H}^{\rm mat}_{2\nu} = V_{CC}(x) \begin{pmatrix} \gamma^2 + \bar{f}_\odot \, |\alpha|^2 & \bar{f}_\odot \, \alpha\beta \\ \bar{f}_\odot \, (\alpha\beta)^* & \bar{f}_\odot \, |\beta|^2 \end{pmatrix} \,, \tag{31}$$

where the parameter $\bar{f}_\odot = r_\odot(x)(1+f)$ depends on the radial position $x = R/R_{sun}$ (R_{sun} being the Sun radius), through $r_\odot(x)$, which assumes the maximal value $r^{max}_\odot \simeq 0.25$ at the center of the Sun. The constant parameters (α, β, γ) are given by[12]

$$\alpha = c_{13} c_{24} c_{34} \tilde{s}_{14} - \tilde{s}_{13} \left(c_{34} s_{23} s_{24} + c_{23} \tilde{s}_{34} \right) , \tag{32}$$

$$\beta = c_{23} c_{34} s_{24} - s_{23} \tilde{s}^*_{34} \,, \tag{33}$$

$$\gamma = c_{14} c_{13} \,. \tag{34}$$

The matrix in Eq. (31) can be written, modulo an irrelevant diagonal factor, as a NSI-like Hamiltonian

$$\bar{H}^{\rm mat}_{3\nu} \approx V_{\rm CC} \begin{bmatrix} \gamma^2 + \varepsilon^{\odot}_{ee} & \varepsilon^{\odot}_{ex} \\ \dagger & 0 \end{bmatrix} \,, \tag{35}$$

with

$$\varepsilon^{\odot}_{ee} = \bar{f}_\odot (|\alpha|^2 - |\beta|^2) \,, \tag{36}$$

$$\varepsilon^{\odot}_{ex} = \bar{f}_\odot \alpha\beta \,. \tag{37}$$

We see that in the case $f = 0$ one has $\bar{f}_\odot = r_\odot$ and the ordinary 3+1 scheme is recovered (see the appendix A in [87]). At the second order in the small values of s^2_{i4} $(i = 1, 2, 3)$ we have the approximate expressions

$$\varepsilon^{\odot}_{ee} \simeq \bar{f}_\odot s^2_{14} \,, \tag{38}$$

$$\varepsilon^{\odot}_{ex} \simeq \bar{f}_\odot \tilde{s}_{14} (c_{23} s_{24} - s_{23} \tilde{s}^*_{34}) \,. \tag{39}$$

[12] Note that in [87] a different parametrization of the mixing matrix was used and the parameters (α, β, γ) do not depend on the mixing angle θ_{23}. Here consistently we adopt the parametrization introduced in Eq. (1). Similar results were achieved in [89] considering a different scenario where sterile neutrinos are supposed to interact with dark matter particles accreted by the Sun and confined in its central region.

In this limit the expressions of the NSI-like couplings are similar to those found in the treatment of LBL experiments in Eq. (24), with $\varepsilon_{ex}^{\odot}$ being a linear combination of $\varepsilon_{e\mu}^{\odot}$ and $\varepsilon_{e\tau}^{\odot}$. Note, however, that the size of the couplings is different because $\bar{f}_{\odot} \neq \bar{f}_{\oplus}$. In particular in the central region of the Sun, which is relevant for solar neutrinos, we have $r_{\odot} \simeq 0.25 \simeq 0.5 r_{\oplus}$ and $\bar{f}_{\odot} \simeq 0.5 \bar{f}_{\oplus}$. Therefore, the amplitude of the solar NSI-like couplings is approximately one half of that acting in the Earth. The matrix $\bar{H}_{2\nu}$ in Eq. (30) can be exactly diagonalized by a 2×2 rotation R_{12}^m which defines the mixing angle in matter θ_{12}^m and the full 4-flavor Hamiltonian in the flavor basis in Eq. (4) is diagonalized by the matrix $U^m = AR_{12}^m$. For adiabatic propagation of solar neutrinos the transition probabilities only depend upon their production and detection points. Neglecting Earth-induced matter effects one has the general expressions for the conversion probabilities

$$P_{e\alpha} = \sum_{i=1}^{4} |U_{\alpha i}|^2 |U_{ei}^m|^2 \quad (\alpha = e, \mu, \tau, s)\,, \tag{40}$$

where the U_{ei}^m's denote the mixing matrix elements involving the electron neutrino in the production point. One can find that the mixing angle θ_{12}^m is given by

$$\cos 2\theta_{12}^m = \frac{\cos 2\theta_{12} - v(\gamma^2 + \varepsilon_{ee}^{\odot})}{\sqrt{|\sin 2\theta_{12} + 2v\varepsilon_{ex}^{\odot}|^2 + [\cos 2\theta_{12} - v(\gamma^2 + \varepsilon_{ee}^{\odot})]^2}}\,, \tag{41}$$

where $v = V_{CC}/k_{21} = 2V_{CC}E/\Delta m_{21}^2$. The 4-flavor survival probability can be expressed as

$$P_{ee} = c_{14}^4 c_{13}^4 \bar{P}_{ee}^{2\nu} + c_{14}^4 s_{13}^4 + s_{14}^4\,, \tag{42}$$

where

$$\bar{P}_{ee}^{2\nu} = \frac{1}{2}\left(1 + \cos 2\theta_{12} \cos 2\theta_{12}^m\right) \tag{43}$$

is the well known expression of the 2-flavor survival probability in the adiabatic regime [90]. The expression of P_{es} is less straightforward. In the limit of small mixing angles it depends on second order combinations $s_{i4}s_{j4}$ $(i,j = 1,2,3)$ and presents a dependency on the CP-phases δ_{14} and δ_{34}. In the analytical treatment above we have assumed that the propagation of neutrinos is adiabatic. We have checked that this approximation is valid exploiting the analytical criterion described in [87].[13] The Earth-regeneration effects are expected to modify the picture above and have been included as described in [87].

In the left panel of Fig. 4, we show the probability for the 3-flavor and the ordinary 3+1 framework. The solid curve represents the best fit 3-flavor scheme, while the dotted curve refers to the ordinary 3+1 scheme with $s_{14}^2 = 0.02$. In this scheme, the dynamical couplings in the Hamiltonian Eq. (31) are negligible, and the other sterile mixing angles are irrelevant. The only effect of the sterile neutrinos is the kinematical one, and consists in an energy independent suppression induced by the non-zero value of s_{14}^2, which can be quantified as $c_{14}^4 \simeq 1 - 2s_{14}^2$. It is clear that if one increases s_{14}^2 the suppression becomes too large to be tolerated by the data. In fact, it is precisely this behavior that allows one to set an upper bound on the admixture of the electron neutrino with the fourth mass eigenstate, as first deduced in [87, 91]. The existing analyses [91–93] set a 90% C.L. upper limit on s_{14}^2 lying in the interval $[0.02 - 0.04]$. The bound we obtain in the 3+1 scheme (see below the case $f = 0$) is in agreement with that obtained by one of us in the analysis performed in [87, 91], where a very similar data set was used.

In the right panel of Fig. 4, we show a few representative profiles of the electron neutrino survival probability in the 3+1 scheme with the new potential. We assume interaction with neutrons. All curves refers to the same value of the standard parameters $\Delta m_{21}^2 = 7.48 \times 10^{-5}\,\mathrm{eV}^2$, $\sin^2\theta_{12} = 0.308$ and $\sin^2\theta_{13} = 0.0223$. The different curves represent the probability for different values of f as listed in the legend. The black profile corresponds to the case $f = 0$, coinciding with the ordinary 3+1 scheme. The colored profiles refer to four cases in which $f \neq 0$ and are chosen to be relatively large in order to magnify the visibility of the effect. The parameters related to the sterile sector are

[13] Violation from adiabaticity can occur if along the neutrino trajectory inside the Sun there is a point $x = R/R_{\odot}$ where he difference between the two energy eigenstates in matter approaches zero. As shown in [87], this occurs if the two conditions: i) $v(x)(\gamma^2 + \varepsilon_{ee}^{\odot}) = \cos 2\theta_{12}$ and ii) $|2v(x)\varepsilon_{ex}^{\odot} + \sin 2\theta_{12}| = 0$ hold simultaneously. The second condition can be verified only if $\varepsilon_{ex}^{\odot}$ is real and negative (i.e. $f < 0$), and if $|\varepsilon_{ex}^{\odot}|$ is very large. In the limit case $\theta_{34} = 0$ we will consider in the analysis, one has $|\varepsilon_{ex}^{\odot} \simeq f_{\odot} c_{23} \tilde{s}_{14} s_{24}|$. In addition, justified by the atmospheric neutrino data we will consider only small values of the product $f_{\odot} s_{24}^2$ and this ensures that the off-diagonal coupling $|\varepsilon_{ex}^{\odot}|$ is always small enough to guaranty adiabaticity in the allowed regions.

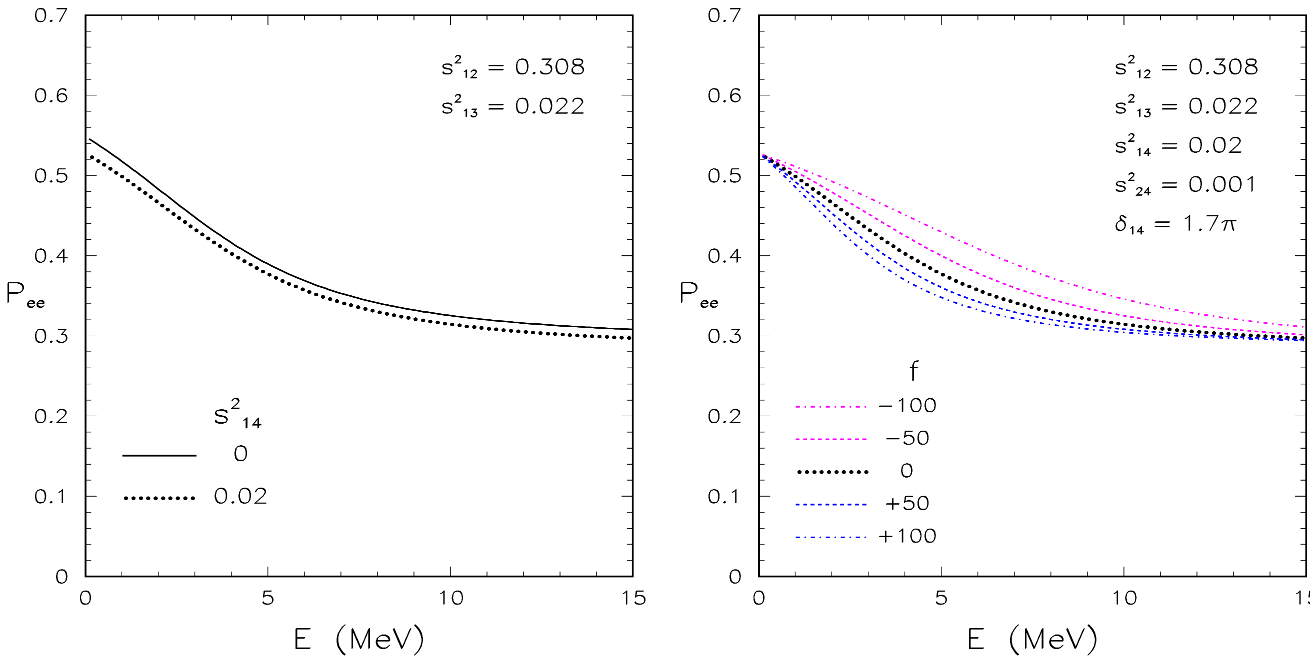

FIG. 4: Daytime survival probability of solar neutrinos averaged over the ^{8}B neutrinos production region. The left panel shows the impact of the non-zero value of $s^2_{14} = 0.02$ with respect to the 3-flavor case in the ordinary 3+1 scheme. The right panel confronts the ordinary 3+1 scheme with the 3+1 scenario with the new potential for four choices of the parameter f. In both panels we fix $\Delta m^2_{21} = 7.48 \times 10^{-5}\,\mathrm{eV}^2$ as determined by KamLAND and JUNO.

fixed at the values $s^2_{14} = 0.02$, $s^2_{24} = 10^{-3}$ and $\delta_{14} = 1.7\pi$. We see that in the four cases in which $f \neq 0$ there are energy dependent modifications of the probability with respect to the normal 3+1 scheme. For positive (negative) values of f the survival probability in the presence of the new potential is lower (higher) compared with the case $f = 0$ and this occurs at all energies. Also, we note that the modifications of the profile of the probability are more (less) pronounced for negative (positive) values of f.

In order to better evaluate the impact of the new sterile matter potential scenario in solar neutrino oscillations, we have performed a numerical analysis of solar neutrino data including the radiochemical experiments Homestake for Chlorine [94] and GALLEX+GNO and SAGE for Gallium [5, 7], the three-phase data [95] from the Sudbury Neutrino Observatory (SNO), the Super-Kamiokande data from 1496-day phase I (energy and zenith spectrum) [96] and 2970-day phase IV (day and night energy spectrum) [96], and the low energy Borexino data [97–99]. We adopt the recent solar model denoted MB22m in [100]. We have included the first JUNO results imposing a prior on the solar mixing angle using the estimate determined in the official analysis of the JUNO Collaboration [101]. To this purpose, we note that JUNO, probing vacuum oscillations, cannot distinguish between the two octants of the solar mixing angle θ_{12}, and one obtains a mirror (dubbed "dark") solution [80] with the replacement $\theta_{12} \to \pi/2 - \theta_{12}$. While this is irrelevant within the standard 3-flavor framework, where solar neutrinos fix θ_{12} in the first octant thanks to matter effects, it becomes relevant in our new scenario in which solar neutrinos in general cannot fix the θ_{12} octant because the model entails the possibility of large NSI-like couplings, in particular $\varepsilon^{\odot}_{ee} = -2$. In this case, due to a well known degeneracy theorem the octant of θ_{12} cannot be distinguished. We will see that this conclusion holds only in the case of a potential proportional to the electron or proton number density. In the case of a potential proportional to the neutron number density things are different because the NSI couplings in the Sun and in the Earth scale differently. In such a case the inclusion of Earth matter effects breaks the degeneracy distinguishing the ordinary LMA solution from the dark-LMA solution, strongly disfavoring the second one. For completeness and illustrative purposes we consider both cases in which the potential is proportional to the electron/proton and to neutron number density. In the first case we define the new potential as $V_S = f'\,V_{CC}$ introducing the parameter f' used only in the present section. In the second case we define $V_S = -f\,V_{NC}$ as in the rest of the paper.

Fig. 5 displays in the three upper (lower) panels the regions allowed in the plane spanned by the two parameters f' (f) and θ_{14}. The left panels represent the regions allowed by solar neutrinos which are identical for the two neutrino mass orderings (NO/IO). The central panels represent the regions allowed by the two LBL experiments NOvA and T2K, while the right panels show the combination of solar with LBL experiments. The LBL experiments are sensitive to the NMO and we have adopted the NO choice for all the panels. In order to determine the solar neutrino regions

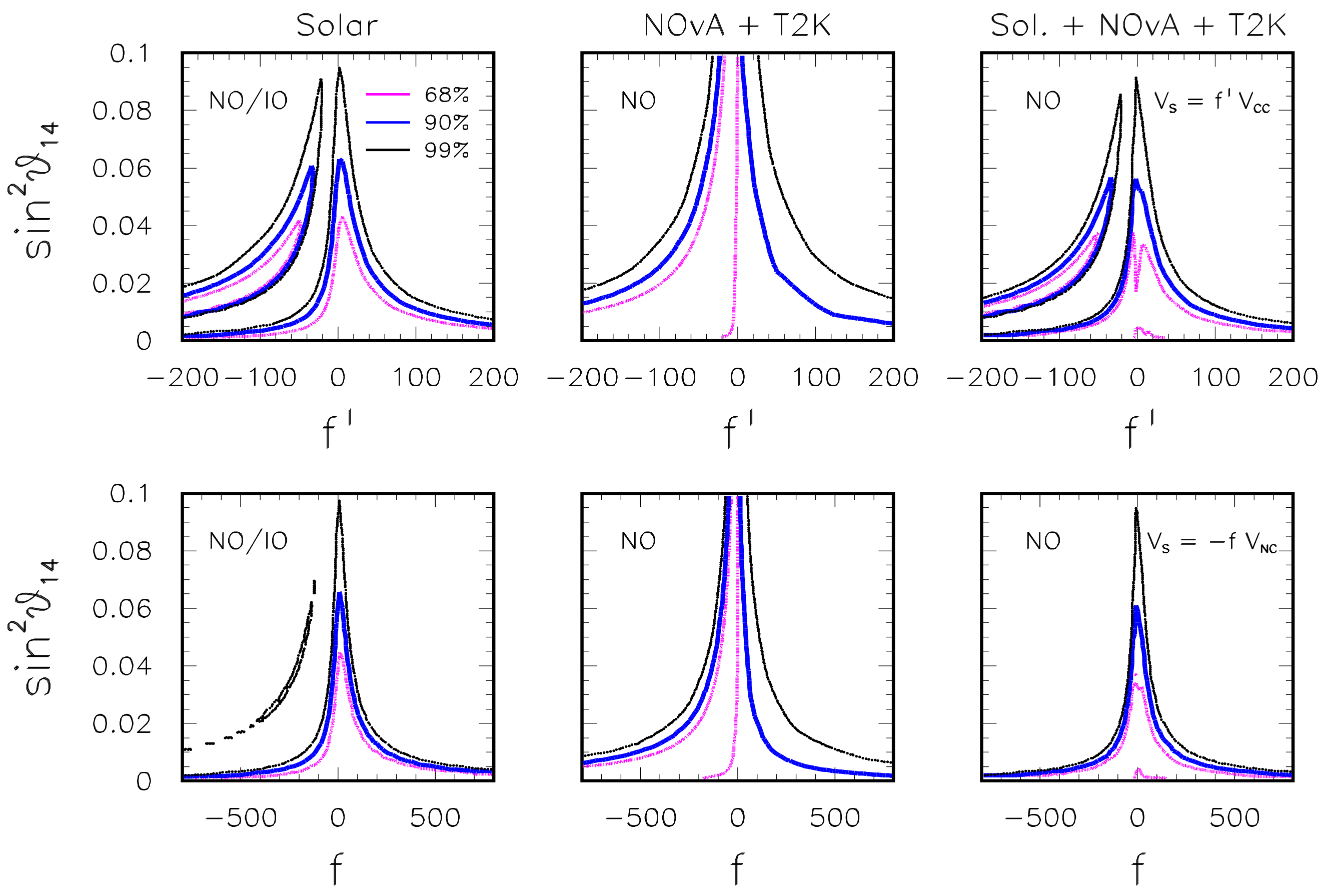

FIG. 5: Allowed regions of the two displayed parameters assuming interaction with electron/protons $V_s = f' V_{CC}$ (upper panels) and with neutrons $V_s = -f V_{NC}$ (lower panels), as obtained from the solar neutrinos (left panels), LBL experiments NOvA and T2K (central panels) and their combination (right panels). The allowed regions in the left panels are independent of the NMO, while those represented in the central and right panels refer to NO. The contours are obtained fixing $s^2_{34} = 0$, imposing the prior $f s^2_{24} < 0.1$, and marginalizing over δ_{14}. Concerning the 3-flavor parameters we have fixed $\Delta m^2_{21} = 7.48 \times 10^{-5}\,\mathrm{eV}^2$, $\sin^2\theta_{13} = 0.0223$, and marginalized over θ_{12}, θ_{23} and δ_{13}.

in the left panels, we have applied exactly the same procedure adopted for NOvA and T2K by assuming $s^2_{34} = 0$ and imposing the prior $|f' s^2_{24}| < 0.1$ at 90% C.L., that as we stress again, is justified by the stringent bound on the $\varepsilon_{\mu\mu}$-like coupling from atmospheric neutrino experiments (see Sec.VI). Focusing on the left-upper panel referring to a potential proportional to the electron/proton number density, we see that the allowed regions are composed by two separate branches. The right branch, approximately centered on $f' = 0$, corresponds to (marginalized values of) $s^2_{12} < 0.5$ (lying in the ordinary LMA solution), while the left branch is obtained for $s^2_{12} > 0.5$ (lying in the so-called dark-LMA solution [80]). The borders of the allowed regions follow approximately iso-contours of constant $\varepsilon^{\odot}_{ee} = f' s^2_{14}$. By inspection of the contours, we derive that this coupling is limited at the 90% C.L. in the two intervals $[-0.3, 0.8]$ and $[-2.7, 1.7]$. These ranges are in agreement with those derived in NSI analyses (see [102]). The dark branch is approximately centered on $\varepsilon^{\odot}_{ee} = f' s^2_{14} \simeq -2$, as expected. The χ^2 minima of the two branches are basically degenerate, as expected on the basis of the so-called generalized mass-ordering degeneracy [81]. The value $\varepsilon^{\odot}_{ee} = -1$ is excluded at a very high confidence level (more than 10 standard deviations), reflecting the strong rejection of solar neutrino data of a mere vacuum-like flavor conversion, in agreement with the early study [71]. We observe that solar neutrinos provide an upper bound on s^2_{14}, which is allowed to reach the maximal value for $f' \simeq 0$ or along the iso-contour corresponding to $\varepsilon^{\odot}_{ee} \simeq -2$. It is now very interesting to investigate what is the result of the combined analysis of the solar neutrino sector data with the two LBL experiments NOvA and T2K. The upper-central panel reports the regions allowed by NOvA and T2K for the NO case. Note that these regions are different with respect to those obtained for a potential proportional to V_{NC} (shown in the lower-central panel), because in the Earth V_{CC} and V_{NC} used in the definition of the new potential differ by a factor of two (being $|V_{CC}| = 2|V_{NC}|$). The contours for the two kinds of potential are related by a simple rescaling of a factor of two. In any case the standard 3-flavor scheme corresponding to the origin of the axes ($f' = 0$, $s^2_{14} = 0$) is disfavored at $\Delta\chi^2 \simeq 4.3$. In the right upper-panel, we see that in the combined fit there are still two degenerate branches as expected. Also, we see that a slight preference for a non-zero value of f' persists around the 90% C.L. with $\Delta\chi^2 \simeq 2.7$.

Let's now consider the three lower panels in Fig. 5, corresponding to a new potential proportional to the neutron number density. In the left-lower panel we see that only the ordinary LMA branch survives, while the dark-LMA branch is excluded almost at the 99% C.L. The degeneracy is broken due to the fact that in the Sun the effective coupling with neutrons of the new potential is different with respect to the Earth, being approximately two times smaller. In particular, the dark branch approximately centered on $\varepsilon^{\odot}_{ee} = \bar{f}_{\odot} s^2_{14} \simeq -2$, corresponds to the larger coupling in the Earth $\varepsilon^{\oplus}_{ee} = \bar{f}_{\oplus} s^2_{14} \simeq -4$, which leads to an enhanced regeneration effects in the Earth and a consequent higher day-night asymmetry in tension with data at approximately $\Delta\chi^2 \simeq 4$. We have checked that JUNO constraints indirectly contribute to further disfavor the dark-LMA by $\Delta\chi^2 \simeq 4$ by rendering the solar neutrino data less flexible in tolerating the different NSI-like couplings in the Sun and the Earth. The lower-central panel reports the regions allowed by NOvA and T2K (already shown in the left panel of Fig. 2). The lower-right panel displays the combination of LBL with solar neutrino data. We can observe that the LBL data further disfavor the dark-LMA solution, which is excluded at more than 99% C.L. This can be understood, as already observed above, because the NSI-like couplings in the Earth probed by LBL neutrinos are a factor of two larger than those probed by solar neutrinos in the Sun. The 3-flavor case, coinciding with the origin of the axes is disfavored at more than the 90% C.L. with $\Delta\chi^2 \simeq 2.7$.

It is very interesting to observe that the size of the Earth matter effects in the LBL experiments NOvA and T2K is similar to that experienced by solar neutrinos traversing the Earth. This can be seen by looking at the dimensionless parameter $v = 2V_{CC}/k = 2V_{CC}E/\Delta m^2$, where E is the neutrino energy ($E \simeq 10$ MeV for solar and $E \simeq 1$ GeV for LBL neutrinos) and Δm^2 is the relevant mass-squared difference (Δm^2_{21} for solar and Δm^2_{31} for LBL neutrinos). Assuming for solar neutrinos propagating in the Earth its average density ($\rho_{\rm ave} = 5.5\,{\rm g/cm^3}$) and for LBL neutrinos the density of the crust ($\rho_{\rm crust} = 2.7\,{\rm g/cm^3}$), one has $v_{\rm sol}/v_{\rm LBL} = 0.6\,(E/10\,{\rm MeV})(E/{\rm GeV})$. Hence, it is not surprising to find that NOvA and T2K disfavor the LMA-dark solution similarly to the day-night effects experienced by solar neutrinos in the case of a potential proportional to the neutron number density. While Fig. 5 refers to the case of NO, we find similar results in IO, where the dark-LMA branch is still disfavored at more than the 99% C.L. in the combination of solar and LBL neutrinos. In conclusion, we observe that in the combination of solar with LBL data a slight indication at 90% C.L ($\Delta\chi^2 \simeq 2.7$) persists in favor of non-zero f (or f').[14] We can observe that by selecting a value of $s^2_{14} \simeq 0.01 - 0.03$ of some relevance for the short-baseline anomalies, the combination of solar with LBL data is compatible with values of f in the range $[-60, 120]$ (f' in the range $[-30, 60]$). These results will be of guide in the next section in identifying a benchmark set of parameters towards which to address our attention.

VI. IDENTIFICATION OF THE BENCHMARK PARAMETERS

Now, on the basis of all the indication/bounds at our disposal and of the insight gained in the structure of the model, we try to acquire further information on its parameters. In the previous section we have seen that NOvA and T2K, together with IceCube indicate a preference for a non-zero negative value of $\varepsilon^{\oplus}_{ee}$ and a non-zero $|\varepsilon^{\oplus}_{e\mu}|$. In addition, LBL, IceCube DeepCore and KM3NeT/ORCA tend to weakly prefer a non-zero value of the complex coupling $\varepsilon^{\oplus}_{e\mu}$. We now observe, that in our model with the extra matter potential, in order to construct a non-zero value of these two NSI-like couplings one needs a non-zero value of all the three parameters f, s_{14} and s_{24}. Then, by construction the other diagonal coupling $\varepsilon^{\oplus}_{\mu\mu}$ is automatically non-zero as well. The preference of a negative $\varepsilon^{\oplus}_{ee}$ translates into a preference for $f < 0$ with respect to $f > 0$. Concerning the $\mu - \mu$ diagonal coupling, the limits are much stringent. In fact, the atmospheric data provide for the combination ($\varepsilon^{\oplus}_{\mu\mu} - \varepsilon^{\oplus}_{\tau\tau}$), the 90% range [-0.022, 0.019] (see Table I). Therefore, the amplitude of the NSI-like coupling $|\varepsilon^{\oplus}_{\mu\mu}| = |\bar{f}_{\oplus}| s^2_{24}$ must be at least one order of magnitude smaller[15] than that of $|\varepsilon^{\oplus}_{ee}| = |\bar{f}_{\oplus}| s^2_{14}$. This leads us to consider $s^2_{24} \ll s^2_{14}$, with s^2_{24} being one order of magnitude smaller than s^2_{14}. Taking into account all the existing constraints we are led to the following benchmark values for the NSI-like couplings entering the Hamiltonian, which are compatible at 1σ level with the existing combined bounds listed in the last row of Table I and with the solar neutrino constraints, respecting at the same time the relations among the three

[14] We find that the preferred value of s^2_{14} is very sensitive to the gallium cross section. By increasing or decreasing by 5% such a cross section we obtain a smaller/larger best fit. In literature there are several evaluations of the cross section driven by the Gallium anomaly. Therefore, the exact best fit value of s^2_{14} is quite uncertain.

[15] In principle the bounds on the difference $\varepsilon^{\oplus}_{\mu\mu} - \varepsilon^{\oplus}_{\tau\tau}$ would allow big values for the single couplings which cancel out in the linear combination. However, we will see that the IceCube resonance will require very small values of both mixing angles $s^2_{24} \sim s^2_{34} \ll 10^{-2}$. Therefore, this possibility is excluded.

parameters (f, s^2_{14}, s^2_{14}) imposed by our model

$$\varepsilon^{\oplus}_{ee} \simeq \bar{f}_{\oplus} s^2_{14} = -0.2\,, \tag{44}$$
$$\varepsilon^{\oplus}_{e\mu} \simeq \bar{f}_{\oplus} s_{14} s_{24} e^{-i\delta_{14}} = -0.045\,, \tag{45}$$
$$\varepsilon^{\oplus}_{\mu\mu} \simeq \bar{f}_{\oplus} s^2_{24} = -0.01\,. \tag{46}$$

We have fixed the CP-phase $\delta_{14} = 0$, which is allowed within the 68% C.L. in the NOvA and T2K analysis.[16] We stress once again that, as it is clear from the Eqs. (45-46), the LBL neutrinos and low-energy atmospheric data give information only on the product of $\bar{f}_{\oplus}$ with s^2_{i4} or $s_{i4}s_{j4}$ with $(i,j) = 1, 2$. Therefore, although they allow us to identify the hierarchical pattern $s^2_{14} \gg s^2_{24}$, in order to fix the values of the mixing angles, one needs to know at least one of them or the value of f. Since f, based on the data considered until now is completely unknown, we proceed by fixing one of the two mixing angles, in particular s^2_{14}. Quite interestingly, we will see that the IceCube resonance at $E \simeq 10$ TeV, in conjunction with the limits determined by KATRIN, will provide us a preferred interval for f compatible with that determined below.

The choice of fixing θ_{14} is motivated by the strong evidences of disappearance of electron neutrinos provided by the Reactor and Gallium anomalies as well as Neutrino-4, which naturally lead to assume a non-negligible value of s^2_{14}. However, in doing this choice we must take into account all the available upper bounds on this parameter, and in particular the strongest ones, which come from KATRIN and from solar neutrino data. Based on the numerical analysis of solar neutrinos presented in Sec. V and on the constraints from KATRIN [103], we take $s^2_{14} = 0.02$ as a benchmark value, which is compatible at 90% C.L. with f in the range [-50, 50] according to the combined analysis of LBL and solar neutrino data. With this choice Eqs. (44) provides a benchmark value of $f = -20$ (corresponding to $\bar{f}_{\oplus} \simeq -10$). We choose a negative value of f since NOvA and T2K show a clear preference for such values. In the next section, we will see that also Super-Kamiokande atmospheric neutrino data point towards a negative potential. We also note that, once the benchmark values for s^2_{14} and f have been chosen, from Eqs. (44)-(46), a benchmark value of the second sterile mixing angle is fixed to be $s^2_{24} \simeq 10^{-3}$ being the ratio $s^2_{14}/s^2_{24} \simeq 20$. We underline that, even after fixing $s^2_{14} = 0.02$, the uncertainty on the estimates of the NSI couplings will translate into an uncertainty on s^2_{24}. The estimate of $\varepsilon^{\oplus}_{\mu\mu}$ in the range $[-0.018, 0.019]$ makes it compatible with zero. So, the actual value of s^2_{24}, albeit necessarily non-zero by construction due to the structure of the model, may be substantially smaller than the benchmark value $s^2_{24} \simeq 10^{-3}$. It is interesting to note that the indicated very small values of s^2_{24} eliminate altogether the tension even with the most stringent bounds deriving from the negative searches of muon neutrino disappearance performed by MINOS/MINOS+ [65] and NOvA [66], which put a 90% upper limit $s^2_{24} \lesssim 0.01$ for eV^2 mass-squared differences.[17]

For the $\varepsilon^{\oplus}_{e\tau}$ coupling, we can reason similarly to $\varepsilon^{\oplus}_{e\mu}$. The indication for a non-zero $\varepsilon^{\oplus}_{e\tau}$ from NOvA and T2K leads to consider a non-zero s_{34}. This automatically switches on the other two couplings $\varepsilon^{\oplus}_{\mu\tau} = \bar{f}_{\oplus}\tilde{s}_{24}s^*_{34}$ and $\varepsilon^{\oplus}_{\tau\tau} = \bar{f}_{\oplus}s^2_{34}$. The limits on the combination $\varepsilon^{\oplus}_{\mu\mu} - \varepsilon^{\oplus}_{\tau\tau}$ lead us to assume a non-zero very small value for s^2_{34} similarly to s^2_{24}. The low-energy atmospheric data put a very stringent bound on this NSI coupling[18] $|\varepsilon^{\oplus}_{\mu\tau}| \lesssim 3.3 \times 10^{-3}$. Hence, once the benchmark value $f = -20$ is fixed, the product of $s_{24}s_{34}$ is constrained to be smaller than $\lesssim 3 \times 10^{-4}$. One can have both mixing angles of similar size $s^2_{24} \simeq s^2_{34} \simeq 10^{-4}$, or different size with the larger one being not bigger than 10^{-3} (and consequently the smaller one being not lower than 10^{-5}) in order to respect the upper bound on $|\varepsilon^{\oplus}_{\mu\mu} - \varepsilon^{\oplus}_{\tau\tau}|$. In summary, we see that the current limits on the NSI lead us to identify the hierarchical pattern $s^2_{14} \gg s^2_{24}$ and $s^2_{14} \gg s^2_{34}$, while the ratio s^2_{34}/s^2_{24} lie in the interval $[0.1, 10]$. As it will be clear from Sec. VIII, one of the most important purposes of our work is to show that the new 3+1 model is able to produce in IceCube the high-energy resonance in the $\mu-\mu$ channel. Similarly to the standard 3+1 scheme the leading mixing angle regulating such a resonance is s^2_{24}. For this reason, for simplicity, we consider the benchmark case $s^2_{34} = 0$, commenting later

[16] This choice will simplify the numerical simulations performed in the following sections concerning the IceCube resonance at ~ 10 TeV. We will underline the situations in which the CP-phase δ_{14} can play an important role as in the case of the 1-3 resonance occurring in multi-GeV atmospheric neutrinos measured by Super-Kamiokande (see Sec. VII).

[17] We have explicitly checked that in MINOS and NOvA the muon neutrino survival probability $P_{\mu\mu}$ in the presence of the new matter potential is basically indistinguishable from the 3-flavor case. This can be understood because the NSI-like couplings $\varepsilon^{\oplus}_{\mu\mu}$ and $\varepsilon^{\oplus}_{\mu\tau}$, which have more impact on such a channel, are negligibly small in our scenario. Also, we have verified that the transition probability $P_{\mu s}$ of muon neutrinos into sterile neutrinos is very small being proportional to $s^2_{24} = 0.001$. Therefore, the scenario is unobservable in the present dual-baseline searches performed using ν_μ charged-current and neutral-currents as in MINOS/MINOS+ and NOvA.

[18] We point out that there exists an independent bound $|\varepsilon^{\oplus}_{\mu\tau}| \lesssim 4 \times 10^{-3}$ derived from IceCube [104], which interestingly indicates a $\sim 90\%$ C.L. preference for the non-zero coupling $|\varepsilon^{\oplus}_{\mu\tau}| \simeq 2.9 \times 10^{-3}$, which would imply an estimate of a non-zero s^2_{34}. However, this indication is derived by using a neutrino sample with very high energies, included those involved in the resonant-like behavior, a region where our NSI-like treatment does not hold. For this reason we do not consider this indication.

TABLE II: Benchmark values of parameters and their approximate allowed ranges. Note that $|f|$ and Δm^2_{41} are fully positively correlated since their ratio must be approximately constant.

Parameter	f	$\Delta m^2_{41}/\mathrm{eV}^2$	$s^2_{14}/10^{-2}$	$s^2_{24}/10^{-3}$	$s^2_{34}/10^{-3}$	δ_{13}/π	δ_{14}/π	δ_{34}/π
Benchmark value	-20	60	2	1	0	1.5	1.7	–
Preferred range	[-40, -10]	[30, 120]	[1, 3]	[0.5, 2]	$\lesssim 1$	[1.1, 1.8]	[0, 0.3] $\cup$ [1.2, 2.0]	[0, 2]

on the impact of non-zero s^2_{34}. For clarity we summarize the benchmark values of the model parameters and their approximate allowed ranges in the first row of Table II. The range of the parameters will be further clarified when discussing the high-energy resonance relevant for IceCube in Sec. VIII. In particular, we will see that the value of Δm^2_{41} is strictly related to that of $|f|$.

VII. IMPACT ON THE 3-FLAVOR ATMOSPHERIC NEUTRINO RESONANCES AT FEW GEV

A. Explaining the excess of electron-like events in Super-Kamiokande

We have shown the new sterile potential induces NSI-like couplings in low-energy atmospheric neutrinos. Consequently, one may expect a modification of the standard 3-flavor MSW and parametric resonances, which occur at few GeV. Although these resonances are difficult to observe, a first indication is coming from atmospheric neutrinos. In fact, the preference for NO found in Super-Kamiokande, as stressed in [20], is imputable to an excess of ν_e-like events (without an excess of $\bar{\nu}_e$-like events) in the multi-GeV and multi-ring samples and their concurrent up-down asymmetry (see Figs. 6, 8 and 15), which can naturally be traced to the resonantly enhanced muon-to-electron flavor conversion, occurring in the neutrino (anti-neutrino) channel in NO (IO). Looking at the plots, the excess is bigger than expected in the 3-flavor framework, and this plausibly leads to a statistical significance of the indication in favor of NO ($\Delta\chi^2 \simeq 6$), which is sensibly larger than the expected sensitivity ($\Delta\chi^2 \simeq 2$, see Fig. 16). Concerning IceCube DeepCore, the official analysis [105] does not provide information on the NMO preference. However, the preliminary study [106] using a 9.28-years data sample, indicates a preference for NO at $\Delta\chi^2 \simeq 4.4$. In such a study it is emphasized that the origin of the preference can be traced to an excess of cascades events related to electron neutrinos (see Fig. 6.4), which as in Super-Kamiokande are expected to be produced by the MSW resonant-like behavior for neutrino energies $E \simeq$ 3-7 GeV. Also in this case, the indication has a statistical significance sensibly larger than the expected sensitivity (see Fig. 8.2), which is below $\sim 1.2\sigma$.

While the excess of electron-like events is compatible with a statistical over fluctuation, it may constitute a manifestation of active-sterile neutrino oscillations with the novel potential. Here, we demonstrate that the proposed scenario can indeed lead to an enhanced excess of ν_e-like events at few GeV. In order to illustrate this point, we show in Fig. 6 the plots of the transition probability $P(\nu_\mu \to \nu_e)$ in the neutrino channel. The upper (lower) panels refer to the negative (positive) valued new potential with $|f| = 20$. The left panels refer to a mantle-crossing trajectory while the right ones refer to a core-crossing trajectory. In the first case, one expects a MSW resonance at ~ 6 GeV, while in the second case three parametric enhancements are predicted (see for example [107]). The black profile corresponds to the 3-flavor scheme, in which case we have fixed the parameters at the best fit values of the global analysis [74], with the exception of δ_{13}, which we have fixed at the best fit value obtained from our joint fit of NOvA and T2K in the presence of the new matter potential, which is basically the same for both NMO ($\delta_{13} \simeq 1.5\pi$). The colored profiles are obtained for the benchmark parameters of the model with the novel potential, $|f| = 20$, $\Delta m^2_{41} = 60$ eV^2, $s^2_{14} = 0.02$, $s^2_{24} = 10^{-3}$. The different colors correspond to four different choices of the CP-phase δ_{14} indicated in the legend. Focusing on the 6 GeV MSW resonance occurring for mantle crossing (left panels), we can observe that all properties of the resonance (peak energy, height, width and tail) are markedly modified in the presence of the new physics. However, the effects are radically different for negative with respect to positive values of the potential. In the upper-left plot, corresponding to $f = -20$, we see that the peak energy appreciably moves toward larger energies with a shift $\Delta E \simeq +1.5$ GeV. The peak height strongly depends on the value of the CP-phase δ_{14}. In all cases, the width is approximately the double compared to the 3-flavor scheme and the tail extends to much higher energies. This means that, for the same peak height, in the presence of the new (negative) potential, the resonance would lead to at least as twice the number of events compared with the 3-flavor case. Given the linear grow with the energy of the involved cross sections, the number of events can be even substantially larger. In the left-lower plot, we can notice that in the case with positive potential ($f = +20$), the resonance is shifted toward lower energies ($\Delta E \simeq -1$ GeV), and has smaller width. These findings, clearly indicate that the new scenario goes in the direction indicated by data only for a negative valued potential. The modifications of the parametric enhancements shown in the right panels are less trivial and a numerical analysis is needed to properly evaluate the impact of the new effects. However, due to the lower

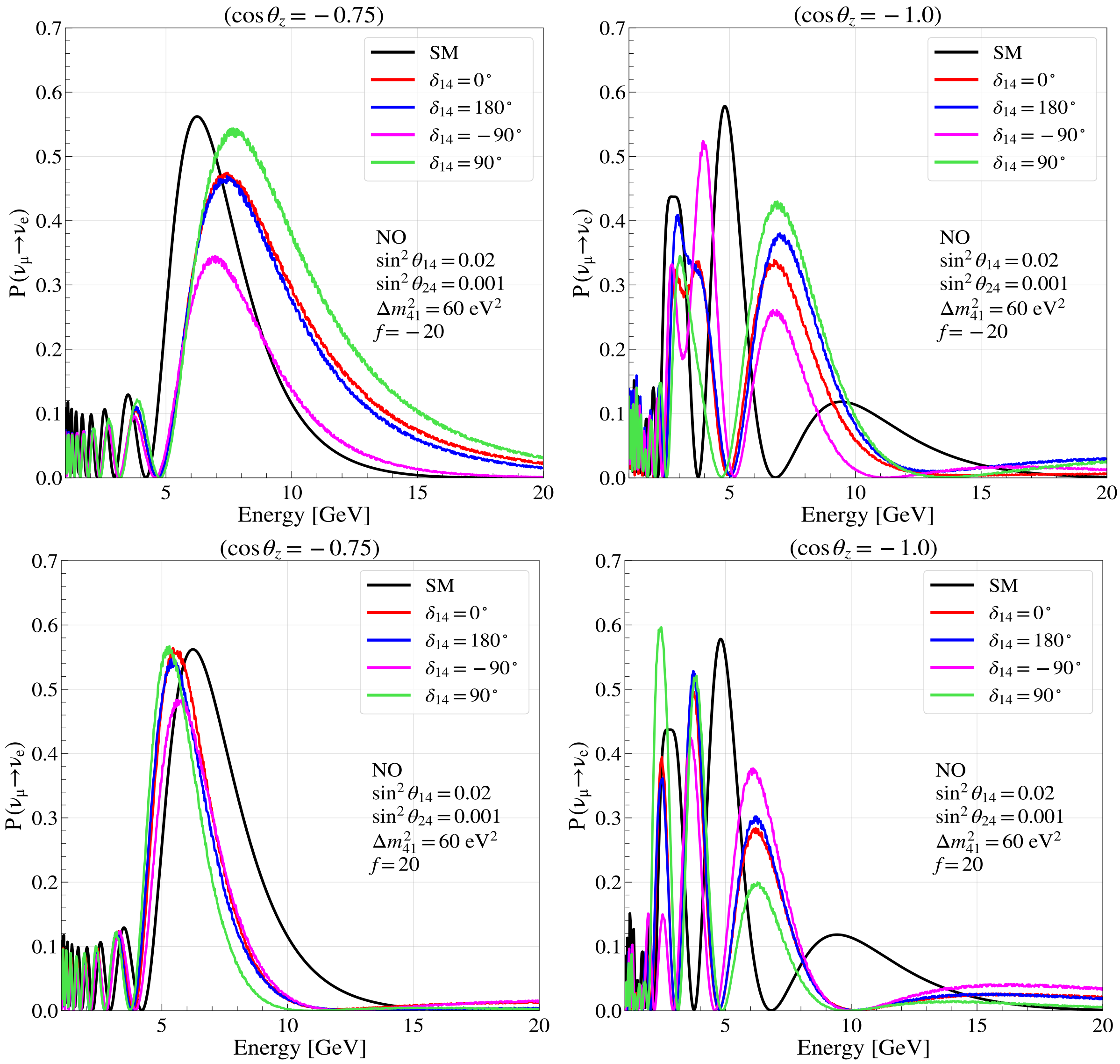

FIG. 6: The plots represent the electron neutrino appearance probability for energies around a few GeV, where the MSW and parametric resonances occur. The upper (lower) panels refer to a negative (positive) value of the parameter f regulating the strength of the new potential. The left panels illustrate a mantle-crossing trajectory with $\cos\theta_z = -0.75$, in which case a MSW resonance is expected. The right panels correspond to a core-crossing trajectory with $\cos\theta_z = -1.0$, in which case three parametric enhancements occur. The black profile depicts the 3-flavor case. The colored curves represent the 3+1 model with the new matter potential with parameters $f = \pm 20$, $\Delta m^2_{41} = 60$ eV^2, $s^2_{14} = 0.02$, $s^2_{24} = 0.001$, $s^2_{34} = 0$. The CP-phase δ_{14} assumes the four values indicated in the legend.

energy and lower area under the curve they should be less important in the overall excess. We note that these findings on the resonance at few GeV are in striking agreement with the independent indication provided by NOvA and T2K, which prefer a negative potential. We deem that the excess of electron-like events observed in Super-Kamiokande and IcecCube DeepCore may be easily explained by the scenario under consideration. Our educated guess is that Super-Kamiokande and IceCube DeepCore could provide an indication in favor of the new model with a statistical level comparable to that of the indication in favor of NO.

B. Impact on the status of the current indication on the neutrino mass ordering

The modification of the few GeV resonances naturally rises the issue of the robustness of the indication in favor of NO provided by global neutrino analyses in the 3+1 framework with pseudo-sterile neutrinos. To understand this point, one must carefully consider the origin of the current preference for NO in the 3-flavor scheme. The global fits incorporate several datasets, which overall in the combination lead to the indication in favor of the NO. There are three distinct sources which provide the aforementioned indication. First, there is the $\nu_\mu \to \nu_e$ appearance channel of NOvA and T2K. In the 3-flavor scheme the two LBL experiments jointly provide a weak indication in favor of IO. In our analysis, we find that in the new scenario there is weak indication in favor of NO (as also observed in analyses with ordinary NSI [18, 19]). In any case the hint from this source is currently very weak. Second, there is a well known interplay between the LBL $\nu_\mu \to \nu_\mu$ disappearance channel and reactor neutrinos (currently dominated by Daya Bay and expected to be dominated by JUNO in the near future). In fact, the joint estimates of the atmospheric mass-squared splitting Δm^2_{31} from these two classes of experiments, provide a $\Delta\chi^2 \simeq 2.0$ in favor of the NO [74] (see also [75, 76]).[19] We have explicitly checked that the estimate of Δm^2_{31} by NOvA and T2K is stable and independent on the new matter potential. This can be easily understood because the NSI-like $\varepsilon_{\mu\mu}$ and $\varepsilon_{\mu\tau}$ couplings, which have more impact on the muon neutrino survival probability that is sensitive to Δm^2_{31}, are negligibly small in our scenario. Similarly, Daya Bay and other reactor experiments have basically no sensitivity to matter effects and also their estimate of Δm^2_{31} is unaffected. As a consequence the interplay between LBL and Reactor experiments remains intact in the presence of pseudo-sterile neutrinos, and their (small) indication in favor of NO is unaltered. This is very important for the future searches. In fact, in case of confirmation of the new 3+1 scenario here considered, the interplay of LBL experiments with JUNO, which is expected to soon release relevant data, would provide a clean signature on the NMO. The third, currently dominant, piece of information on the NMO is potentially more problematic, because, as we have discussed in the subsection above, it comes from the SK atmospheric neutrino data [20], which show a preference for NO with $\Delta\chi^2 \simeq 6$, which is strictly related to the few GeV resonant enhancements. Based on our findings, the NO seems to be favored also in the presence of pseudo-sterile neutrinos, because only in NO one can explain the observed excess of ν_e-like events. One should expect and increased statistical level of the indication in favor of NO since the new scenario offers a better fit of the experimental data. Hence, we can conclude, with the important caveat given below, that the status of the indication in favor of NO in current global analyses is robust and the indication would be even enhanced by LBL (which jointly prefer NO in the new scheme) and by Super-Kamiokande.

In the discussion above, we have tacitly assumed that the solar lower octant ($\sin^2\theta_{12} < 0.5$) solution is that chosen by Nature. However, we have seen that in the case in which the new potential is proportional to the electron or proton number density, a degenerate solution exists for the dark octant ($\sin^2\theta_{12} > 0.5$). In the presence of such a degenerate solution, one cannot distinguish between NO and IO. This happens because the 3-flavor scheme suffers from the so-called generalized mass ordering degeneracy [81]. It implies that in the dark-octant solution ($\sin^2\theta_{12} \simeq 0.7$), all the existing experiments sensitive to the NMO prefer the alternate case (IO) with respect to the one (NO) preferred for the lower-octant solution ($\sin^2\theta_{12} \simeq 0.3$). In particular, also JUNO, in the presence of the octant degeneracy is completely blind to the NMO [108], and its combination to the disappearance channel of LBL experiments is also ineffective in this respect. Therefore, if the existence of the dark-solution is taken into account (as it should be in the senario entailing pseudo-sterile neutrinos with a matter potential proportional to the electron or proton number density), the NMO is completely undetermined by current data. However, we will see that the high energy (~ 10 TeV) atmospheric data offer a tool able to break the degeneracy because they are sensitive to a 4-flavor resonance which presents different features in the two (otherwise) degenerate solutions.

VIII. NEW RESONANT CONVERSION PHENOMENA IN HIGH-ENERGY ATMOSPHERIC NEUTRINOS

It is well known that neutrino flavor transitions in matter can give rise to resonant-like amplification. This distinctive behavior was first predicted in the context of solar neutrinos [109, 110]. Within the 3-flavor framework, it is extremely difficult to observe the resonant phenomenon in terrestrial experiments, albeit some hints are coming from multi-GeV atmospheric neutrinos, as we have discussed in the previous section. The situation is radically different when an extra light sterile neutrino species comes into play. In fact, in the 3+1 scheme, as first evidenced in [111], high-energy ($E \simeq$ TeV) atmospheric neutrinos can undergo matter enhanced conversion. As pointed out in [112], neutrino telescopes

---

[19] A recent exploratory analysis [73] of JUNO data in conjunction with NOvA and T2K provides an enhanced indication at $\Delta\chi^2 \simeq 5$ in favor of NO.

have the unique potential to detect such a resonant behavior. More precisely, matter effects can result in the near complete disappearance of TeV-scale muon anti-neutrinos traveling through the Earth for a sterile neutrino with eV^2-scale mass-squared difference (see [113–124] for further studies on this topic). The experimental search for the resonant signature has been pioneered by the IceCube Collaboration with high-energy analyses exploiting neutrinos from 500 GeV to 100 TeV. Starting from the eight-years data analysis [125], the collaboration has found a hint in favor of sterile neutrinos within the ordinary 3+1 scheme, which has been subsequently confirmed and consolidated in the eleven-years data analyses [13, 14, 126]. This indication seems to come from the observation of a resonant-like behavior occurring at energies of $\sim$ 10 TeV. In the analysis [13], performed under the assumption of $\theta_{34} = 0$, the best fit point is obtained for $\Delta m^2_{41} \sim 3.5$ eV^2 and $s^2_{24} = 0.04$. Such a best fit point is rather stable if θ_{34} is allowed to assume a non-zero value compatible with the existing bounds, as shown in [14]. Here, we will show that in the pseudo-sterile neutrino scenario the picture of the resonant phenomena involving high-energy neutrinos becomes much more complex. In particular, we will see that together with the ordinary resonances involving a pair of active-sterile states (ν_α, ν_s) $(\alpha = e, \mu, \tau)$ one can have new resonances in the active (ν_α, ν_β) $(\alpha, \beta = e, \mu, \tau)$ sub-systems, mediated by the pseudo-sterile states. We will see that such new resonances are dynamically and algebraically different with respect to the conventional ones.

A. Qualitative aspects of the conventional resonances and the bare level crossing diagram

As a first step in our study of the resonant behavior we clarify the framework behind the conventional resonances usually considered in the literature. This will allow us to better appreciate the unconventional features of the new amplification phenomena implied by the new matter potential, which will be addressed in the following subsections. A resonant behavior can take place if the matter potential is comparable to the wavenumber $k_{41} = \Delta m^2_{41}/2E$ associated to the active-sterile oscillation frequency. For an eV-scale sterile neutrino and matter density $\rho = 5.0$ g/cm^3 in the Earth, one gets the reference neutrino energy of $\sim$ 10 TeV as follows

$$\frac{|V_{NC}|}{k_{41}} \;=\; 0.74 \left(\frac{\Delta m^2_{41}}{3.5\ \mathrm{eV}^2}\right)^{-1} \left(\frac{\rho}{5.0\,\mathrm{g/cm}^3}\right) \left(\frac{E}{10\ \mathrm{TeV}}\right) , \tag{47}$$

where we have used as a benchmark the best fit value $\Delta m^2_{41} = 3.5$ eV^2 found in the IceCube analysis [13]. This value is roughly uncertain by a factor of two as derived from the 90% C.L. contours. Qualitatively, one expects that if $|V_{NC}|$ is multiplied by a large factor f, the resonance energy will remain unaltered provided that Δm^2_{41} is rescaled by the same factor (taking its absolute value). In addition, one must note that the sign of the rescaling factor f would determine the channel of the resonance. One expects the resonance in the neutrino (antineutrino) channel for $V_s < 0$ $(V_s > 0)$.

It is useful to define the "bare" Hamiltonian setting to zero all the six mixing angles, thus considering $U = \mathbb{1}$ in the original Hamiltonian in Eq. (4), obtaining

$$H^{\mathrm{bare}}_{4\nu} = K + V = \frac{1}{2E}\begin{bmatrix} 0 & 0 & 0 & 0 \\ 0 & \Delta m^2_{21} & 0 & 0 \\ 0 & 0 & \Delta m^2_{31} & 0 \\ 0 & 0 & 0 & \Delta m^2_{41} \end{bmatrix} + \begin{bmatrix} V_{\mathrm{CC}} & 0 & 0 & 0 \\ 0 & 0 & 0 & 0 \\ 0 & 0 & 0 & 0 \\ 0 & 0 & 0 & \bar{f} V_{CC} \end{bmatrix} , \tag{48}$$

which is diagonal. The matrix $2EH^{\mathrm{bare}}_{4\nu}$ has the (2,2) and (3,3) entries constant, while the (1,1) and (4,4) entries present a linear dependency on the energy. The behavior of the eigenvalues of $2EH^{\mathrm{bare}}_{4\nu}$, which we will denote with λ^{B}_i $(i = 1, 2, 3, 4)$, can be represented in a diagram recently introduced in [124] to analyze the high–energy resonance in the ordinary 3+1 scheme. While in [124] the diagram is called with the name "surface level crossing diagram", here we prefer to call it "bare level crossing diagram", in contrast with the ordinary level crossing diagram obtained when the mixing angles are taken into account in the full or "dressed" Hamiltonian. In Fig. 7 we show the bare level crossing diagram for the ordinary 3+1 scheme (left panel) and for the 3+1 framework with the new matter potential (central and right panel), where we have taken a large value $|f| \gg 1$, which is positive in the central panel and negative in the right panel. In all panels we have considered the case of NO, which implies that the 1-2 (solar) and 1-3 (atmospheric) crossings occur for the neutrino channel. The vertical axis corresponds to zero potential/energy.[20] The right part

[20] When studying the resonant behavior in a constant density medium as in the present work, in which case the potential is constant, the horizontal axis is proportional to the neutrino energy (positive for neutrinos, negative for antineutrinos). In the context of flavor conversion of a neutrino with definite energy in an environment with varying density, the horizontal axis is proportional to the matter potential which we will be a function of the time/position coordinate.

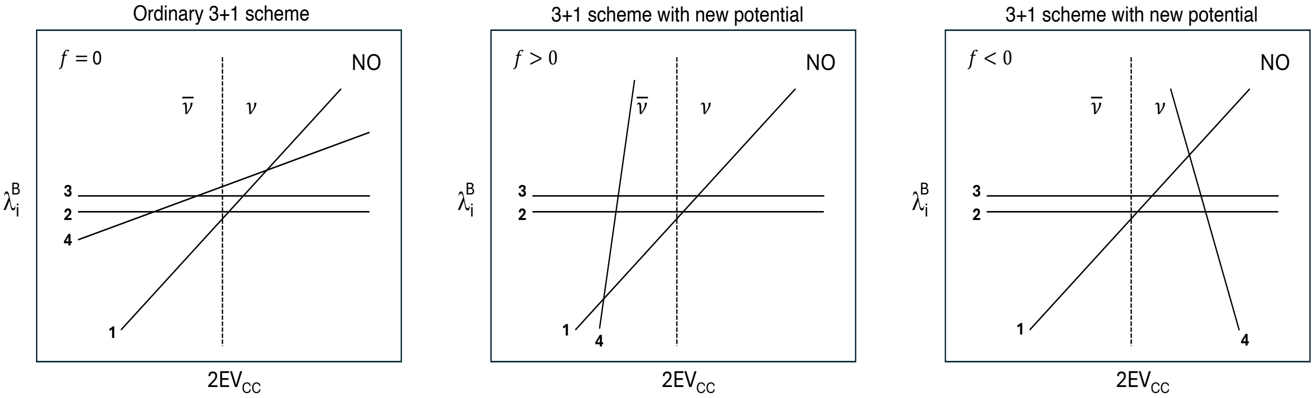

FIG. 7: The three panels represent the "bare level crossing diagram" obtained by setting to zero all the six mixing angles. The left panel refers to the 3+1 ordinary scheme. The central (right) panel refers to the 3+1 scheme with the new potential for a positive (negative) value of f much larger than one. In all cases we assume NO for the three light states. The energy scale of the diagrams is qualitative as they are envisaged to illustrate a topological structure.

of the plane refers to neutrinos, while the left one corresponds to antineutrinos. The scales are qualitative, as this diagram has the sole purpose to identify the topological structure of the crossings among the four different energy levels. When the mixing angles are switched on to form the complete or "dressed" Hamiltonian, the crossing points will become avoided crossings regions, where the phenomenon of eigenvalue repulsion [127, 128] occurs mediated by the off-diagonal entries which act as effective couplings among the different levels.

In the left panel we observe that in the ordinary 3+1 scheme, in addition to the standard 3-flavor 1-2 and 1-3 crossings, one expects three crossings involving the fourth state, a 1-4 crossing occurring in the neutrino channel and two crossings (2-4 and 3-4) in the antineutrino channel. This crossing scheme is related to the slope of the fourth state determined by the potential $0.5V_{CC}$ appearing in the (4,4) entry of the bare Hamiltonian. From the phenomenological point of view only the 2-4 crossing in the antineutrino channel is relevant because it induces $\bar{\nu}_\mu \to \bar{\nu}_s$ conversion observable in IceCube. The 1-4 and 3-4 crossings are less relevant since IceCube is not sensitive to $\nu_e \to \nu_s$ and $\bar{\nu}_\tau \to \bar{\nu}_s$ transitions due to the flavor composition of the atmospheric neutrinos. The central panel depicts the situation for a large positive value of the f parameter, which regulates the strength of the new potential. In this case the new potential in the (4,4) entry $\bar{f}V_{CC}$ is positive as in the ordinary 3+1 scheme but the slope of the fourth state is much larger. This implies that all the three crossings 1-4, 2-4, 3-4 occur in the antineutrino channel. Conversely, for a negative value of f, as apparent in the right panel, all such three level crossings occur in the neutrino channel.

One advantage of the bare level crsossing diagram is its role in identifying the mixing angles in matter which regulate a given resonance [124]. Once the sterile vacuum mixing angles (θ_{14}, θ_{24}, θ_{34}) are included to obtain the full Hamiltonian, three avoided crossings will emerge. These level repulsions will correspond to resonances[21] originating respectively from the [1-4, 2-4, 3-4] crossings, whose amplitude will be regulated by the corresponding mixing angles in matter [θ^m_{14}, θ^m_{24}, θ^m_{34}], which will be amplified with respect to their values in vacuum.[22] We will see that although these expectations will be fulfilled by the numerical simulations, in addition to such conventional resonances involving one of the three active species and the sterile one, we will encounter new unconventional resonances occurring among the active flavors (ν_e, ν_μ, ν_τ). The existence of such a kind of resonances is unexpected as it cannot be deduced from the bare level crossing diagram. We will see that they are generated by amplified second-order effects mediated by the sterile neutrino mixing and become appreciable only if f is sufficiently large. In the following we will expound and explain this new amplification mechanism.

---

[21] The resonant enhancement in a constant density medium will appear as a peak/dip when plotting the transition probability as a function of the energy. In the context of flavor conversion in a medium with varying density, the phenomenon of adiabatic conversion (possibly corrected by non-adiabatic transitions) will occur when the neutrino traverses the resonance region.

[22] It should be underlined that for the realization of a resonant phenomenon, an enhanced mixing angle in matter is a necessary but not sufficient condition. In fact, one also needs a sufficiently large oscillating factor in the conversion probability, which depends both on the dynamics (through the differences of the eigenvalues of the full Hamiltonian) and a phenomenological parameter, which is the baseline traveled by neutrinos. It is a very lucky circumstance that the dimension of our planet allows the developments of oscillating phases large enough to make such phenomena observable.

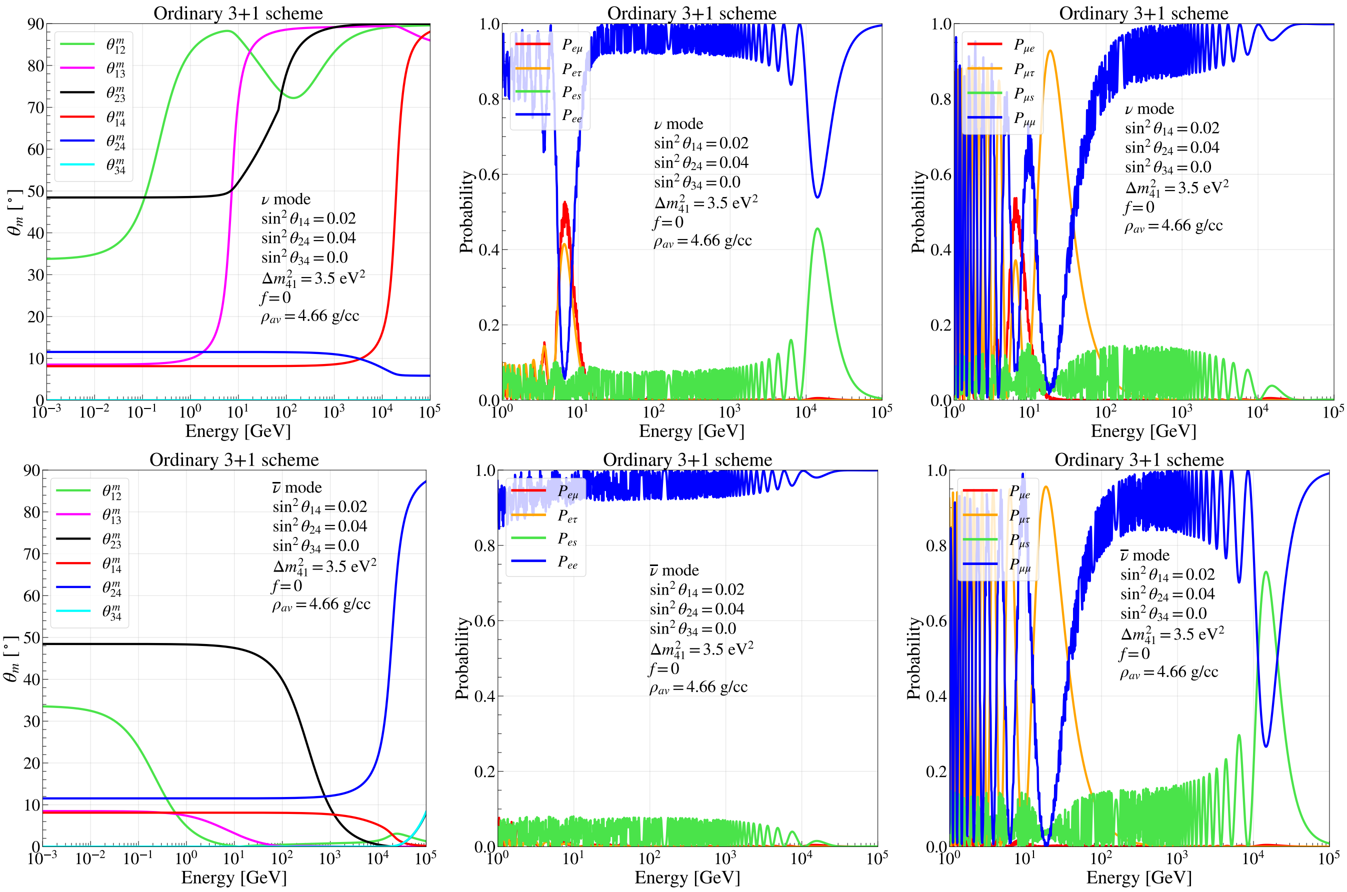

FIG. 8: The six panels summarize the properties of the ordinary 3+1 scheme for constant density equal to Earth mantle value. The upper (lower) panels refer to neutrinos (antineutrinos). The left panels represent the mixing angles in matter while the central and right ones depict the oscillation probabilities involving the electron and muon neutrino channel respectively.

B. Numerical diagonalization of the Hamiltonian in the case of constant density

As a second step towards the understanding the properties of the resonant behavior we perform a numerical study considering a constant density profile with density equal to that of the Earth mantle. For the ordinary 3+1 scheme we assume $\Delta m^2_{41} = 3.5$ eV^2 and $s^2_{24} = 0.04$, corresponding the IceCube best fit point. For the new scenario we take $f = -20$, $s^2_{24} = 0.001$ and $\delta_{14} = 0$, which is our benchmark point. In both the ordinary and new 3+1 scenarios we adopt the same value of $s^2_{14} = 0.02$ and set to zero θ_{34}. In the new scenario we rescale the value of the mass-squared difference by approximately the same factor $|f| \simeq 20$ so as to maintain the resonance energy fixed at $\simeq 10$ TeV as indicated by IceCube. We find numerically that the best matching of the resonance energy is obtained for $\Delta m^2 = 60$ eV^2, which we adopt as the benchmark value.

Figure 8 refers to the ordinary 3+1 scheme, in which case the new matter potential is absent. The upper (lower) panels refer to neutrino (antineutrino) channel. The left panels report the six mixing angles in matter (three active and three sterile) as a function of the neutrino energy.[23] The central panels depict the probabilities involving the electron neutrino channel, while the right panels report the probabilities entailing the muon neutrino channel. In the left-upper panel we recognize that around $E \simeq 15$ TeV there is a 1-4 resonance corresponding to a maximal value of the mixing angle θ^m_{14} in matter. This resonance gives rise to enhanced conversion in the (ν_e, ν_s) sub-system, which reveals in the upper-central panel. Such a conversion is of scarse phenomenological relevance because the flux of atmospheric electron neutrinos is very low, being one order of magnitude smaller than that of muon neutrinos. We

---

[23] Our findings on the behavior of the elements of the mixing matrix in matter as a function of the energy are in agreement with those obtained in [129] for the 3-flavor case and in [130] for the ordinary 3+1 framework.

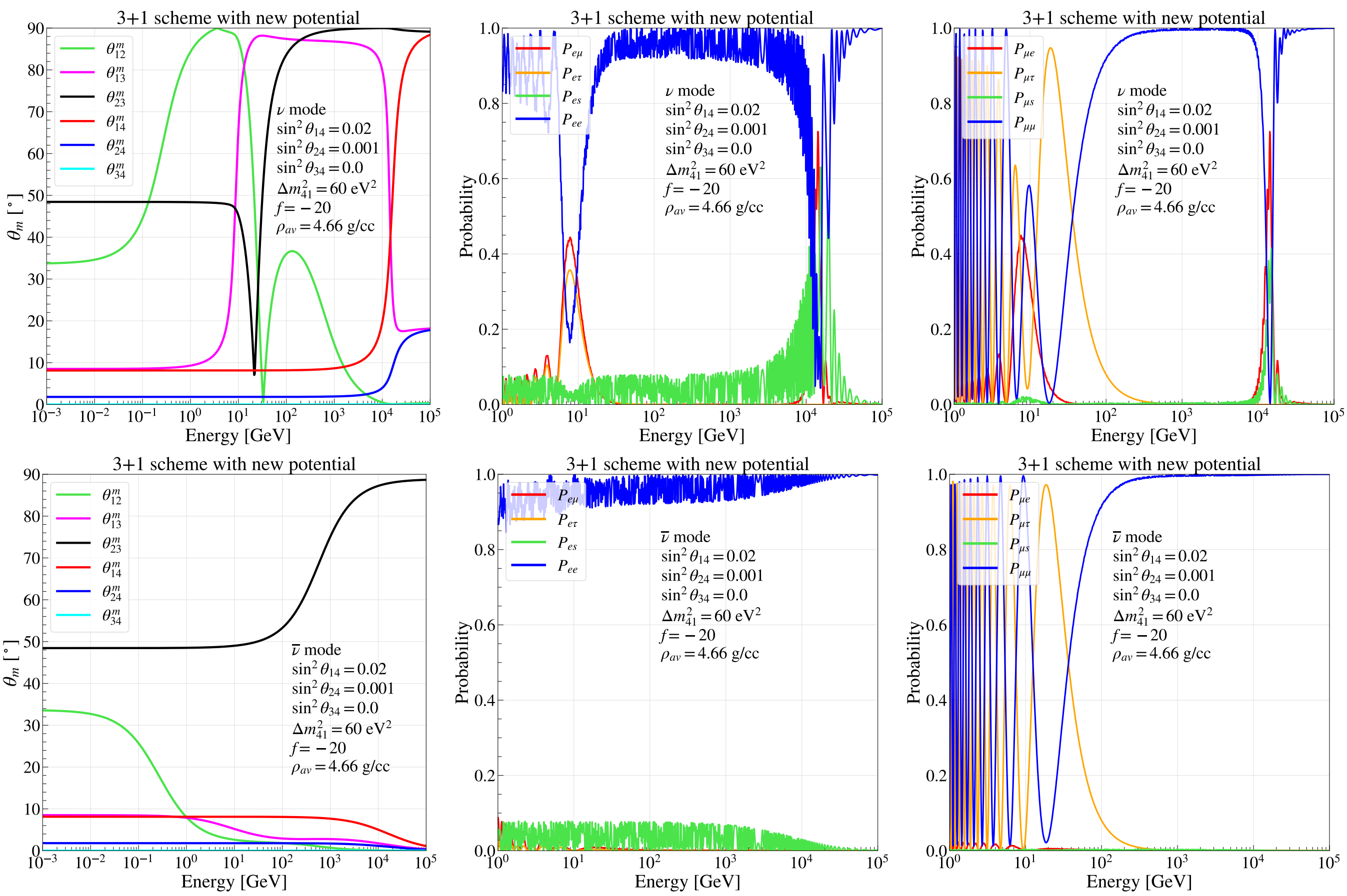

FIG. 9: The six panels summarize the results obtained in the 3+1 scheme with the new potential for the benchmark case $f = -20$ for constant density equal to Earth mantle value. The upper (lower) panels refer to neutrinos (antineutrinos). The left panels represents the mixing angles in matter while the central and right ones depict the oscillation probabilities involving the electron and muon neutrino channel respectively.

observe that in the range [0.1 TeV - 10 TeV] there are fast oscillations, which in average lead to an almost energy-independent suppression of the survival probability. This suppression is regulated by the amplitude of the θ_{14} mixing angle in vacuum ($s_{14}^2 = 0.02$). The right-upper panel shows the probabilities involving muon neutrinos, which, as expected do not present any resonant behavior. Also for muon neutrinos, in the range [0.1 TeV - 10 TeV] there are fast oscillations regulated by the amplitude of the θ_{24} mixing angle in vacuum, which in the ordinary 3+1 scheme is appreciably large ($s_{24}^2 = 0.04$). In the left-lower panel, corresponding to the antineutrino case, in the region around $E \simeq 15$ TeV there is a 2-4 resonance, corresponding to a maximal value of the mixing angle θ_{24}^m in matter. In this case, as confirmed by the lower-central panel, there is no resonance in the (ν_e, ν_s) sub-system, which is regulated by vacuum-like oscillations related to $s_{14}^2 = 0.02$. In the right-lower panel we can observe the resonant conversion in the (ν_μ, ν_s) sub-system, which is of phenomenological interest because the flux of atmospheric neutrinos is mostly of the muon type. We notice that in the ordinary 3+1 scheme everything goes as expected from the bare level crossing diagram (left panel of Fig. 7), with a 1-4 resonance in the neutrino channel and a 2-4 resonance in the antineutrino channel. The 3-4 resonance expected in the antineutrino channel is not there simply because we have adopted a zero value for the mixing angle θ_{34}. This picture confirms the usefulness of the bare diagram as a powerful guide in identifying the relevant resonances.

Figure 9 shows analogous plots to Fig. 8 but refers to the 3+1 model with pseudo-sterile neutrinos. The upper (lower) panels refer to the neutrino (antineutrino) channel. We use the benchmark parameters $f = -20$, $\Delta m_{41}^2 = 60$ eV^2 and the mixing angles $s_{14}^2 = 0.02$, $s_{24}^2 = 0.001$ and $\delta_{14} = 0$. Looking at the mixing angles in matter in the left-upper panel, we observe that around $E \simeq 15$ TeV there is a 1-4 resonance similarly to the ordinary 3+1 case and a 2-4 resonance (θ_{24}^m enhanced albeit not maximal). This pattern is expected based on the bare crossing diagram. What is less expected is the 1-3 resonance (θ_{13}^m maximal), which, as seen in both the upper-central and upper-right panels, drives amplified (ν_e, ν_μ) conversion. We notice that such a resonance is not predicted on the basis of the bare crossing diagram, where the only 1-3 crossing intervenes at low energies and it is the well-known standard 3-flavor resonance occurring at few GeV. This circumstance suggests that the (ν_e, ν_μ) resonance is not the result of a usual two-level avoided crossing. In fact, as we will discuss in the next subsection, this resonance is related to a three-level behavior mediated by the pseudo-sterile neutrinos. We observe that $P_{e\mu} = P_{\mu e}$ as can be checked confronting the upper-central and upper-right panels, as expected for the symmetric matter profile inside the Earth. In the central-upper and right-upper panels we can also observe the conventional resonances in the (ν_e, ν_s) and (ν_μ, ν_s) channels. In the right-upper panel we observe that in the energy range around 1 TeV, differently from the ordinary 3+1 scheme, the muon neutrino survival probability is basically equal to one because the fast oscillations induced by the vacuum mixing angle θ_{24} are suppressed by the very small value of this parameter ($s^2_{24} = 0.001$). In the lower panels, representing the antineutrino channel, we see that there is no resonance and that the behavior of the probabilities is similar to the 3-flavor scheme apart from the fast oscillating flat suppression of the electron survival probability in the lower central panel, which is a vacuum effect driven by the relatively large $s^2_{14} = 0.02$.

C. Three-level dynamics as the origin of the resonance in the (ν_e, ν_μ) sub-system

In the previous subsection we have seen that in the presence of the new potential a resonance in the (ν_e, ν_μ) sub-system takes place. Here, we try to gain some insight in this unexpected phenomenon. With this purpose, we set $\theta_{34} = 0$ as in the previous subsection. In the high-energy limit the 3-flavor parameters become irrelevant and it is easy to check that the Hamiltonian has the third row and third column exactly equal to zero. This means that the ν_τ state is unaffected by flavor conversion phenomena and remains unaltered during the evolution. Hence, we can extract from the four-flavor Hamiltonian the 3×3 sub-matrix with $(1, 2, 4)$ indexes, which regulates the dynamics of the 3-flavor sub-system (ν_e, ν_μ, ν_s). Neglecting the CP phase δ_{14}, we obtain the effective 3-flavor Hamiltonian

$$H^{(e\mu s)}_{3\nu} = R_{24} R_{14} K' R^T_{14} R^T_{24} + V' \simeq \begin{bmatrix} V_{\rm CC} + k s^2_{14} & k s_{14} s_{24} & k s_{14} \\ \dagger & k s^2_{24} & k s_{24} \\ \dagger & \dagger & \bar{f} V_{CC} + k \end{bmatrix}, \tag{49}$$

where $K' = {\rm diag}(0, 0, k \equiv k_{41})$ and $V' = {\rm diag}(V_{CC}, 0, \bar{f} V_{CC} = V_S - V_{NC})$ are the 3-dimensional diagonal matrixes corresponding to the 4-dimensional matrixes K and V from where we have omitted the third (equal to zero) entry. In the second equality in Eq. (49) we have taken the limit of small mixing angles which is of phenomenological interest. The diagonalization of such an Hamiltonian in general will require the product of three orthogonal rotations defining the three mixing angles in matter θ^m_{24}, θ^m_{14}, θ^m_{12}, and can be cast in the form

$$U^m_{3\nu} = R^m_{24} R^m_{14} R^m_{12}\,, \tag{50}$$

where we have respected the same order of the three rotations in vacuum. Now, we observe that if the mixing angle $\theta_{14} = 0$, the Hamiltonian in Eq. (49) has a block-diagonal form and is diagonalized by a simple rotation in the 2-4 plane, with $U^m_{3\nu} = R^m_{24}$ involving only the mixing angle θ^m_{24}. Physically, it happens that the ν_e flavor state evolves independently of the (ν_μ, ν_s) sub-system. This system presents a resonance for $[H(4,4) - H(2,2)] = 0$, i.e. $k \simeq -\bar{f} V_{CC} \simeq -0.5 f V_{CC}$, which occurs in the neutrino (antineutrino) channel for $f < 0$ ($f > 0$). Similarly, if the mixing angle $\theta_{24} = 0$, the Hamiltonian has again a block-diagonal form and is diagonalized by a simple rotation in the 1-4 plane with $U^m_{3\nu} = R^m_{14}$ depending on the mixing angle θ^m_{14}. In this case, the evolution of the ν_μ flavor state is decoupled from the (ν_e, ν_s) sub-system, which presents a resonance for $[H(4,4) - H(1,1)] = 0$, i.e. $k(1 - s^2_{14}) \simeq (1 - \bar{f}) V_{CC}$, which for the values of the parameters we are considering (small s^2_{14} and large $\bar{f}$), presents only a minor shift with respect to the resonance in the (ν_μ, ν_s) sub-system.

In the most general case in which both mixing angles θ_{14} and θ_{24} are non-zero, the Hamiltonian in Eq. (49) has not a block-diagonal structure anymore. It is clear that, in order to obtain its diagonalization, one would need all the three mixing angles in matter, and in particular a non-zero 1-2 mixing angle θ^m_{12} will emerge. What is less immediate to understand is that the 1-2 system may resonate, with θ^m_{12} becoming maximal. With the purpose of shedding light on this point, it is useful to come back to the rotated NSI-like Hamiltonian. Also in this case, taking the case $\theta_{34} = 0$, we can extract the 3×3 submatrix,

$$\bar{H}^{(e\mu s)}_{3\nu} = V_{\rm CC} \begin{bmatrix} 1 + \bar{f}_\oplus s^2_{14} & \bar{f}_\oplus \tilde{s}_{14} s_{24} & (1 - \bar{f}_\oplus) \tilde{s}_{14} \\ \dagger & \bar{f}_\oplus s^2_{24} & -\bar{f}_\oplus s_{24} \\ \dagger & \dagger & \bar{f}_\oplus + \frac{k_{41}}{V_{\rm CC}} \end{bmatrix} = V_{\rm CC} \begin{bmatrix} 1 + \varepsilon_{ee} & \varepsilon_{e\mu} & \varepsilon_{es} \\ \dagger & \varepsilon_{\mu\mu} & \varepsilon_{\mu s} \\ \dagger & \dagger & \delta(E) \end{bmatrix} \tag{51}$$

where for compactness we have introduced $\delta(E) = \bar{f}_\oplus + \frac{k_{41}}{V_{\rm CC}}$. We see that in the 4-flavor dynamics the off-diagonal NSI-like couplings ε_{es} and $\varepsilon_{\mu s}$ appear which involve one active state and the sterile one. Now, we can note that the

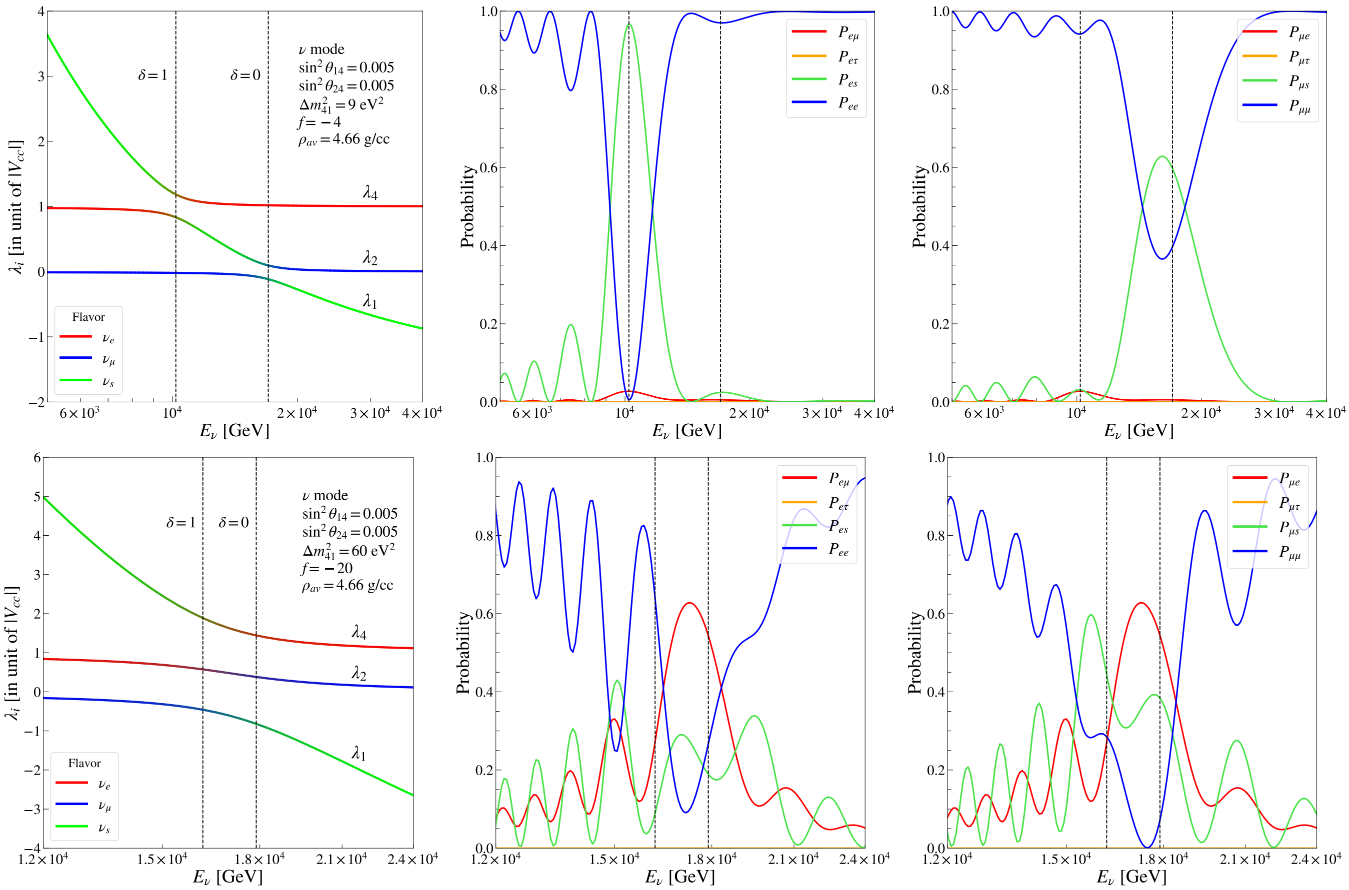

FIG. 10: The six panels summarize the behavior of the model in the resonance region highlighting the transition of the system from a two-level regime to a three-level one. In the upper (lower) panels we have taken two different values of the f parameter (respectively $f = -4$ and $f = -20$). The left panels report the behavior of the eigenvalues. The central (right) panels represent the oscillation probabilities relevant for the electron (muon) neutrino channel.

$\nu_\mu \to \nu_e$ transitions can be mediated by the coupling $\varepsilon_{e\mu}$ or via the product $\varepsilon_{es}\varepsilon_{\mu s}$. In the first case the coupling appears directly in the Hamiltonian, while in the second case it represents a second-order effect. In general, in the model we are considering, both direct and indirect couplings are different from zero, and the first order and second order mechanisms will act simultaneously and interfere. However, one can note that the the second order effects are amplified by the new potential being $\varepsilon_{es}\varepsilon_{\mu s} = \bar{f}^2_\oplus s_{14}s_{24}$, and dominate over the first order effects. These observations allow us to enucleate the core dynamics of the resonant (ν_e, ν_μ) conversion, which is captured by the simplified Hamiltonian

$$\bar{H}'^{(e\mu s)}_{3\nu} = V_{\rm CC}\begin{bmatrix} 1 & 0 & \varepsilon_{es} \\ 0 & 0 & \varepsilon_{\mu s} \\ \dagger & \dagger & \delta(E) \end{bmatrix} \tag{52}$$

where we have set to zero all the other couplings and for simplicity we consider real couplings (neglecting the CP-phases). Of course the missing couplings will modify the picture but are less fundamental. The system has two natural resonances corresponding to $\delta = 0$ and $\delta = 1$. When $\varepsilon_{es} = 0$ the (ν_μ, ν_s) sub-system resonates for $\delta = 0$, while when $\varepsilon_{\mu s} = 0$ the (ν_e, ν_s) sub-system resonates for $\delta = 1$. When both couplings are non-zero as implied in our model, the second order effects, far from the regions of the two well localized resonances [$(0 \lesssim \delta \lesssim 1)$ for the internal region and $(\delta \lesssim 0,\ \delta \gtrsim 1)$ for the external region], are expected to provide an effective NSI-like coupling $\propto \varepsilon_{es}\varepsilon_{\mu s}/\delta$. This perturbative approach, for small values of the couplings is expected to hold also in between the two resonances, where $\delta \simeq 1/2$, which remain well separated. For increasing value of the couplings these corrections will blow up in the region between the resonances making necessary a full 3-level treatment. One expects that the two resonances will get coupled for increasing values of the off-diagonal couplings giving rise to a more complex resonant behavior. In order to illustrate this point, in our full model we fix $s^2_{14} = s^2_{24} = 0.005$ and consider the two values of $f = -4$

and $f = -20$. These two choices make our full model very close to the toy model described by the Hamiltionian in Eq. (52) and correspond to two values of $\varepsilon_{es}\varepsilon_{\mu s} \simeq 0.07$ and 0.45 respectively. In the first (second) case, one expects a small (large) perturbation of the unperturbed Hamiltonian.

Figure 10 summarizes the behavior of the model in the resonance region highlighting the transition of the system from a regime in which the two resonances are decoupled to one in which they get coupled. In the upper (lower) panels we have taken two different values of the f parameter (respectively $f = -4$ and $f = -20$). The left panels report the energy eigenvalues in units of $|V_{CC}|$. The varying color along the curves represents the flavor composition of the eigenvectors in matter ν_i^m $(i = 1, 2, 4)$. Thanks to such colors we can clearly visualize the relevant flavor transitions occurring in the resonance region. For the smaller value of $f = -4$ (left-upper panel) we observe the presence of two distinct resonances corresponding to two separate avoided crossings, the first one involving the (ν_e, ν_s) system at $\delta = 1$ and the second one involving the (ν_μ, ν_s) system at $\delta = 0$. The central and right panels represent the oscillation probabilities relevant for the electron and muon neutrino channels respectively. The upper-central panel and the upper-right panels confirm that in the case of $f = -4$ there are only two resonances involving (ν_e, ν_s) and (ν_μ, ν_s) transitions. For large values of $f = -20$ (left-lower panel) the two avoided crossings merge to form a single triple-avoided crossing involving the full (ν_e, ν_μ, ν_s) system. From the colors of the curves, we see that in the region between $\delta = 1$ and $\delta = 0$, each eigenvector in matter is a superposition of at least two flavors, and we can deduce that the transitions will involve all the three sub-systems, and in particular the (ν_e, ν_μ) one. This is confirmed by the lower-central and lower-right panels, where we see that a resonance in the (ν_e, ν_μ) channel coexists with the two resonances in the (ν_e, ν_s) and (ν_μ, ν_s) systems. Therefore, for increasing values of the off-diagonal couplings ε_{es} and $\varepsilon_{\mu s}$, the system undergoes a transition from a regime where it is possible to describe it in terms of two separate 2-level systems to a regime where a genuine 3-level dynamics is at play. Finally, we note that the differences between the eigenvalues are related to the scale of the matter potential V_{CC}. Such large differences correspond to large phase factors $\phi_{ij} = (\lambda_i - \lambda_j)L \equiv \tilde{\Delta}m^2_{ij}L/2E$ (L being the baseline and with $\tilde{\Delta}m^2_{ij}$ we have indicated the mass-squared differences in matter) in the transition probabilities, which reveal as a fast oscillating behavior evidenced in the central and right panels of Fig. 10. The full analytical treatment of the 3-level system is beyond the scope of the present work and can be performed using for example the method recently introduced in [131]. However, the resulting formulas are not transparent since one cannot avoid to resolve a cubic secular equation in order to calculate the analytical expressions of the eigenvalues.

A closing technical remark is in order. In the simplified 3-flavor framework we have considered in this sub-section, we have seen that a matter 1-2 mixing angle θ_{12}^m emerges naturally. In the 4-flavor results presented in sub-section VIII B a non-zero 1-3 mixing appears (see Fig. 9). The explanation for this apparent inconsistency is the following. In the full 4-flavor system the ν_τ flavor is present, although at high energies, for $\theta_{34} = 0$ it does not participate to the flavor conversion. If one considers the flavor composition of the eigenvectors in matter ν_i^m, one would find that at energies below the resonance, at around $E \simeq 1$ TeV, one has that the second eigenstate coincides with the τ flavor state ($\nu_2^m \simeq \nu_\tau$). This can be checked by considering the expressions of the elements of the mixing matrix in matter U^m and is related to the fact that neutrinos (not antineutrinos) undergo the two standard resonances (solar and atmospheric) at low energies. This implies that the dynamics of the (ν_e, ν_μ) system involved in the new resonance is regulated by the (ν_1^m, ν_3^m) eigenvectors in matter. At the algebraic level this is achieved by replacing a rotation in the 1-2 plane (related to θ_{12}^m), with the product of a rotation in the 1-3 plane (related to θ_{13}^m) and a rotation in the 2-3 plane with $\theta_{23}^m = \pi/2$. In fact, from the left-upper panel in Fig. 9 it can be seen that for energies $E \gtrsim 1$ TeV, the mixing angle θ_{23}^m assumes a value equal to $\pi/2$. More precisely, one must note that in the full diagonalization, the 3-flavor mixing matrix $U_{3\nu}^m = R_{23}^m R_{13}^m R_{12}^m$ in matter lies at the external position, so this matrix performs the last step in the diagonalization process, after which the Hamiltonian acquires the diagonal form $H^{4nu}_{\rm diag} = {\rm diag}(\lambda_1, \lambda_2, \lambda_3, \lambda_4)$. One can check that the action of $U_{3\nu}^m = R_{23}(\pi/2)R_{13}(\theta_{13}^m)R_{12}(0)$ would produce the swapping of $\lambda_2 \leftrightarrow \lambda_3$. We have also checked that in the high-energy regime, the value of θ_{12}^m obtained in the simplified 3-flavor system is identical to the value of θ_{13}^m obtained in the 4-flavor case. Basically, this is an algebraic subtlety needed to ensure that the relevant dynamics intervenes between the two physical states involved in the level repulsion. We have also checked that in the antineutrino channel, where the (ν_e, ν_μ) resonant amplification occurs for positive values of f, one has $\nu_3^m \simeq \nu_\tau$, and in that case no 2-3 level swapping is needed and one simply has a rotation in the 1-2 plane with $U_{3\nu}^m = R_{23}(0)R_{13}(0)R_{12}(\theta_{12}^m) \equiv R_{12}(\theta_{12}^m)$.

D. Impact of non-zero θ_{34} and factorization of the 4-level dynamics

Until now, for definiteness, we have restricted our study to $\theta_{34} = 0$, in which case the ν_τ is not involved in the flavor transitions at high energies. However, in general, when such a mixing angle is non-zero, the resonant flavor conversion phenomena are expected to involve also the ν_τ flavor. When considering a non-zero θ_{34} one has to respect the low-energy constraints on the NSI-like couplings $\varepsilon_{e\tau}$, $\varepsilon_{\mu\tau}$ and $\varepsilon_{\tau\tau}$ which are related to such an angle. In particular,

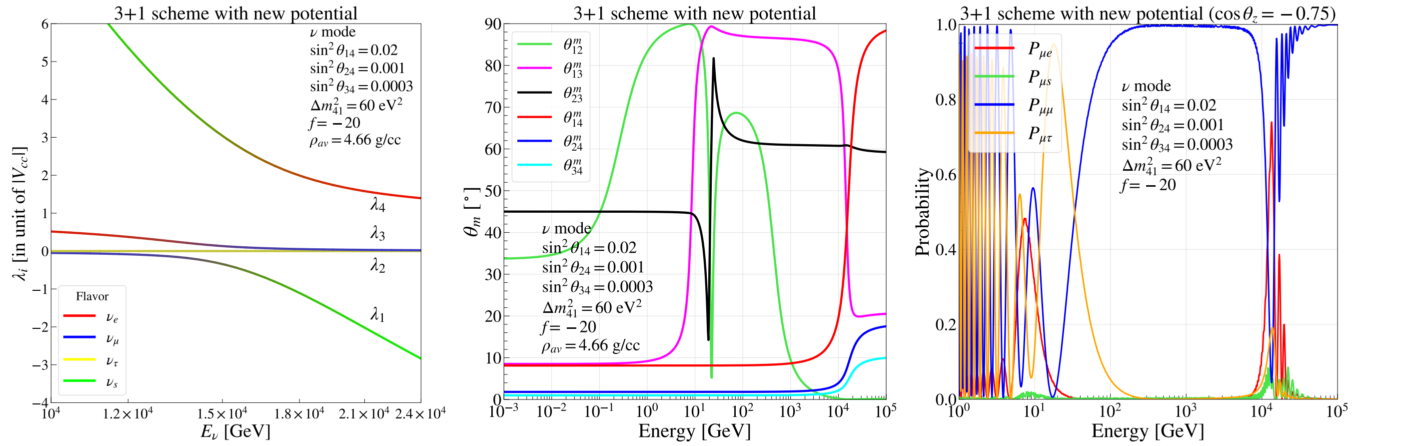

FIG. 11: The three panels summarize the results obtained in the 3+1 scheme with the new potential for a non-zero value of θ_{34}. The left panel represents the behavior of the eigenvalues in the high-energy resonance region. The central panel displays the mixing angles in matter for constant density equal to the average mantle value. The right panel reports the oscillation probabilities relevant for the muon neutrino channel for a mantle-crossing trajectory using the PREM profile.

one has to respect the bound on the coupling $\varepsilon_{\mu\tau} = \bar{f} s_{24}\tilde{s}^*_{34}$, which is the most stringent one being $|\varepsilon_{\mu\tau}| \lesssim 3\times10^{-3}$. For our benchmark values $f=-20$, $s^2_{24}=0.001$, one has $s^2_{34}\lesssim 3\times10^{-4}$. Even for such a low values we find observable effects at the level of the oscillation probabilities. In Fig. 11 we show the plots corresponding to $s^2_{34}=3\times10^{-4}$. The left panel represents the four eigenvalues in the resonance region. We note that in our previous eigenvalues plots, only three eigenvalues where shown since we illustrated the effective 3-flavor Hamiltonian. In such a context the fourth eigenvalue was zero by construction and was not shown. However, we can observe that in the more general case with non-zero θ_{34} the situation is very similar to the case of zero θ_{34}. In fact, one of the eigenvalues (λ_2) is constant and equal to zero. In order to understand this feature, let's consider the full rotated Hamiltonian for small values of the mixing-angles

$$\bar{H}_{4\nu} \approx V_{\rm CC}\begin{bmatrix} 1+\bar{f}_\oplus s^2_{14} & \bar{f}_\oplus \tilde{s}_{14}s_{24} & \bar{f}_\oplus \tilde{s}_{14}\tilde{s}^*_{34} & (1-\bar{f}_\oplus)\tilde{s}_{14} \\ \dagger & \bar{f}_\oplus s^2_{24} & \bar{f}_\oplus s_{24}\tilde{s}^*_{34} & -\bar{f}_\oplus s_{24} \\ \dagger & \dagger & \bar{f}_\oplus s^2_{34} & -\bar{f}_\oplus \tilde{s}_{34} \\ \dagger & \dagger & \dagger & \bar{f}_\oplus + \frac{k_{41}}{V_{\rm CC}} \end{bmatrix}. \tag{53}$$

In order to simplify the treatment, it is useful to extend our effective 3-flavor toy Hamiltonian in Eq. (52) to the 4-flavor case, defining

$$\bar{H}^{(e\mu\tau s)}_{4\nu} = V_{\rm CC}\begin{bmatrix} 1 & 0 & 0 & \varepsilon_{es} \\ 0 & 0 & 0 & \varepsilon_{\mu s} \\ 0 & 0 & 0 & \varepsilon_{\tau s} \\ \dagger & \dagger & \dagger & \delta(E)\,. \end{bmatrix} \tag{54}$$

where we consider the real NSI-couplings $\varepsilon_{es}, \varepsilon_{\mu s}, \varepsilon_{\tau s}$ setting to zero the CP-phases and neglect all the other couplings. In the limit in which the three off-diagonal couplings $\varepsilon_{es}, \varepsilon_{\mu s}, \varepsilon_{\tau s}$ are equal to zero, the system presents one 1-4 crossing for $\delta=1$, and two coinciding crossings at $\delta=0$ involving the 2-4 and 3-4 states. The structure of the Hamiltonian implies that in the (ν_μ,ν_τ) sub-space only a linear combination will be coupled to the sterile state. In fact, defining $\varepsilon_{as}=\sqrt{(\varepsilon^2_{\mu s}+\varepsilon^2_{\tau s})}$ and introducing the orthogonal normalized states

$$|\nu_+\rangle = \frac{\varepsilon_{\mu s}|\nu_\mu\rangle + \varepsilon_{\tau s}|\nu_\tau\rangle}{\varepsilon_{as}} = \frac{s_{24}|\nu_\mu\rangle + s_{34}|\nu_\tau\rangle}{\sqrt{s^2_{24}+s^2_{34}}}\,, \tag{55}$$

$$|\nu_-\rangle = \frac{-\varepsilon_{\tau s}|\nu_\mu\rangle + \varepsilon_{\mu s}|\nu_\tau\rangle}{\varepsilon_{as}} = \frac{-s_{34}|\nu_\mu\rangle + s_{24}|\nu_\tau\rangle}{\sqrt{s^2_{24}+s^2_{34}}}\,, \tag{56}$$

in the new basis $(\nu_e, \nu_+, \nu_-, \nu_s)$ the Hamiltonian takes the form[24]

$$\bar{H}_{4\nu}^{(e+-s)} = V_{\rm CC} \begin{bmatrix} 1 & 0 & 0 & \varepsilon_{es} \\ 0 & 0 & 0 & \varepsilon_{as} \\ 0 & 0 & 0 & 0 \\ \dagger & \dagger & 0 & \delta(E) \end{bmatrix} . \tag{57}$$

Therefore, the 4-level system is factorized in a non-trivial part involving the three-level system (ν_e, ν_+, ν_s) regulated by the Hamiltonian

$$\bar{H}_{3\nu}^{(e+s)} = V_{\rm CC} \begin{bmatrix} 1 & 0 & \varepsilon_{es} \\ 0 & 0 & \varepsilon_{as} \\ \dagger & \dagger & \delta(E) \end{bmatrix} , \tag{58}$$

and a trivial part involving the "spectator" state ν_-, which has constant zero energy.[25] This toy model provides a very good description of the real 4-flavor system because all the couplings involving directly the ν_τ flavor (for example $\varepsilon_{\mu\tau}$) are very small. It can be shown that the full 4-flavor model, because of the particular structure of the Hamiltonian, preserves exactly the basic properties of the toy model. In fact, it can be checked that in the full Hamiltonian (53) the second and third columns (or rows) are linearly dependent and therefore it has rank 3. It happens that the state ν_- defined in Eq. (56) is an exact eigenvector of the Hamiltonian (53) with zero eigenvalue. Therefore, the system can be factorized with the same rotation used for the toy model. The effective 3-flavor Hamiltonian in Eq. (58) will induce (possibly resonant) transitions within the (ν_e, ν_μ) and (ν_e, ν_τ) sub-systems mediated by the second-order coupling $\varepsilon_{es}\varepsilon_{as}$ of the ν_e with the ν_+ state. It is important to notice that the 4-dimensional Hamiltonian Eq. (57) will also induce (ν_μ, ν_τ) transitions mediated by the interference of the survival amplitudes of the spectator state ν_- (which has trivial dynamics) and of the state ν_+ (which has non-trivial dynamics). Hence, we can conclude that in the presence of a non-zero θ_{34}, the core dynamics of the 4-flavor system remains that of a 3-level system, allowing at the same time the ν_τ flavor to fully participate to the resonant conversion phenomena.

The central panel in Fig. 11 representing the running of the mixing angles in matter shows that in the high-energy resonant region, the mixing angle θ_{34}^m becomes appreciable and has a similar behavior to θ_{24}^m. In fact, we have checked that these two angles are identical if their vacuum value is the same, as expected from the $\mu - \tau$ symmetry of the Hamiltonian. Also we observe that the mixing angle θ_{23}^m assumes values different from $\pi/2$ and that it does not have a resonant like behavior. This angle basically regulates the relative amplitude of the 2-4 and 3-4 resonances. The right panel represents the transition probabilities involving the muon neutrino channel. We can observe that, albeit not very pronounced, there is a resonance involving the (ν_μ, ν_τ) sector. Similarly, we find (not shown) that there is a comparable resonance in the (ν_e, ν_τ) sector. Both such resonances can become more pronounced for values of θ_{34} larger than our benchmark choice. Hence, we see that in the most general case, all the active flavors are involved in the resonant conversion mediated by the sterile neutrino potential, as expected on the basis of our analytical treatment.

E. Full numerical results with the PREM density model and parametric enhancement

As a final step in our exploration of the resonant phenomenon, we consider some numerical results using the realistic PREM model of the Earth density. Figure 12 displays a few representative examples of the oscillation probabilities focusing on the muon neutrino channel, which is phenomenologically relevant. The left panels refers to the ordinary 3+1 scheme ($f = 0$) while the right panels represent the 3+1 scheme with the new potential for the benchmark value $f = -20$. All the parameters are fixed at the benchmark values adopted in the previous subsection. We stress that the left (right) panels represent antineutrino (neutrino) oscillations probabilities. The upper panels refer to a radial core-crossing trajectory with $\cos\theta_z = -1.0$ where θ_z is the zenith angle, while the lower panels refer to a mantle-crossing trajectory with $\cos\theta_z = -0.75$. The right plots confirm that in the presence of the new potential there is a strong resonance in the $\nu_\mu \to \nu_e$ channel (red color) as expected from the results obtained for the constant density case. However, while for the mantle-crossing trajectory the probabilities are very similar to the case of constant density (compare the right-lower panel to the right-upper panel in Fig. 9), for the core-crossing trajectory the probabilities

[24] The 4-flavor Hamiltonian is factorized by an orthogonal rotation in the (ν_μ, ν_τ) plane with an angle defined by $\cos\alpha = \varepsilon_{\mu s}/\varepsilon_{ea}$ and $\sin\alpha = \varepsilon_{\tau s}/\varepsilon_{ea}$.

[25] In the language of multi-level systems, in particular in atomic physics and quantum optics, the spectator state is dubbed as a "dark state" (see [132]).

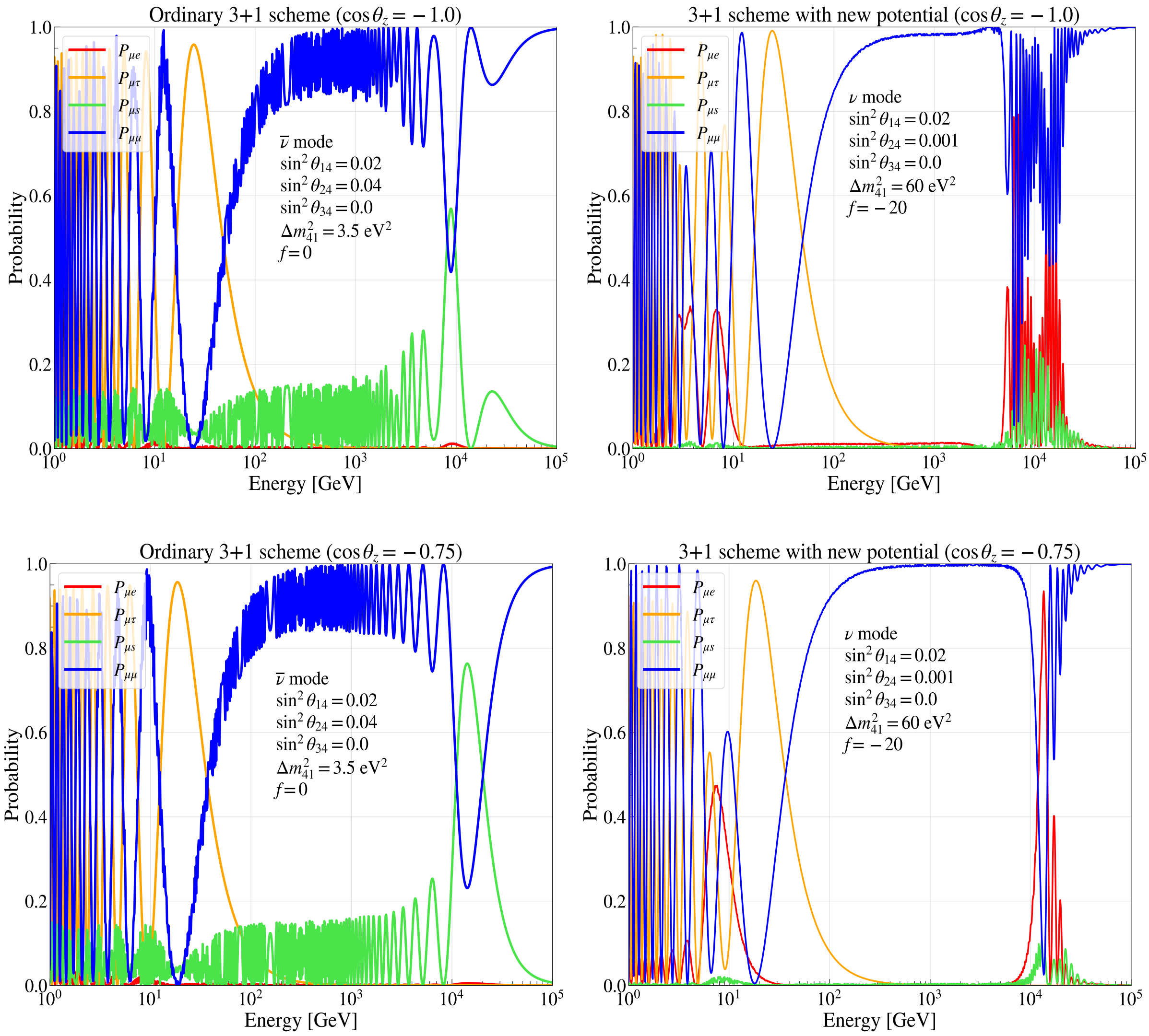

FIG. 12: Oscillation probabilities for the ordinary 3+1 scheme (left panels) and the 3+1 scheme with new potential (right panels). The left panels represent antineutrino oscillations probabilities, while the right panels represent neutrino oscillation probabilities. The upper panels refer to a radial core-crossing trajectory with $\cos\theta_z = -1.0$, while the lower panels refer to a mantle-crossing trajectory with $\cos\theta_z = -0.75$. In the left panel we assume $\Delta m^2_{41} = 3.5$ eV^2 and $s^2_{24} = 0.04$, $s^2_{14} = 0.02$. corresponding the IceCube best fit point in the ordinary 3+1 scheme. In the right panel we take $f = -20$, $\Delta m^2_{41} = 60$ eV^2, $s^2_{14} = 0.02$, $s^2_{24} = 0.001$ and $\delta_{14} = 0$, which is our benchmark point in the scenario with the new potential.

have a radically different behavior, presenting a very large width with fast oscillations. In addition, the muon survival probability presents two distinct dips. This behavior is the sign that huge parametric effects are at play induced by the layered structure of the Earth density. While IceCube cannot resolve the detail of the fast oscillations because of the limited energy resolution of the detector, it may be able to observe the large width of the resonance and possibly identify the two dips.

The resonant behavior can be further illustrated with the help of the so-called oscillograms, which are 2-dimensional iso-contour plots of the muon neutrino disappearance probability as a function of neutrino energy E and cosine of the zenith angle $\cos(\theta_z)$. In the left panel of Fig. 13 we show the oscillogram for the ordinary 3+1 case, with the same parameters used in Fig. 12. The plot refers to antineutrinos, for which one expects the resonance to occur in the ordinary 3+1 scheme and the oscillation pattern is well understood. The resonance enhancement of the $\bar{\nu}_\mu \to \bar{\nu}_s$ oscillation manifests as antineutrinos pass through the Earth's core and/or mantle. For trajectories crossing the core, that is $\cos\theta_z \lesssim -0.8$, the enhancement is described by a parametric resonance [114, 119] at the energy $\simeq$ (9 TeV) $(\Delta m^2_{41}/3.5\text{ eV}^2)$. For the mantle-crossing trajectories ($\cos\theta_z \gtrsim -0.8$) the enhancement is a MSW resonance at the energy $\simeq$ (14 TeV) $(\Delta m^2_{41}/3.5\text{ eV}^2)$. The right panel displays the oscillogram that we obtain for

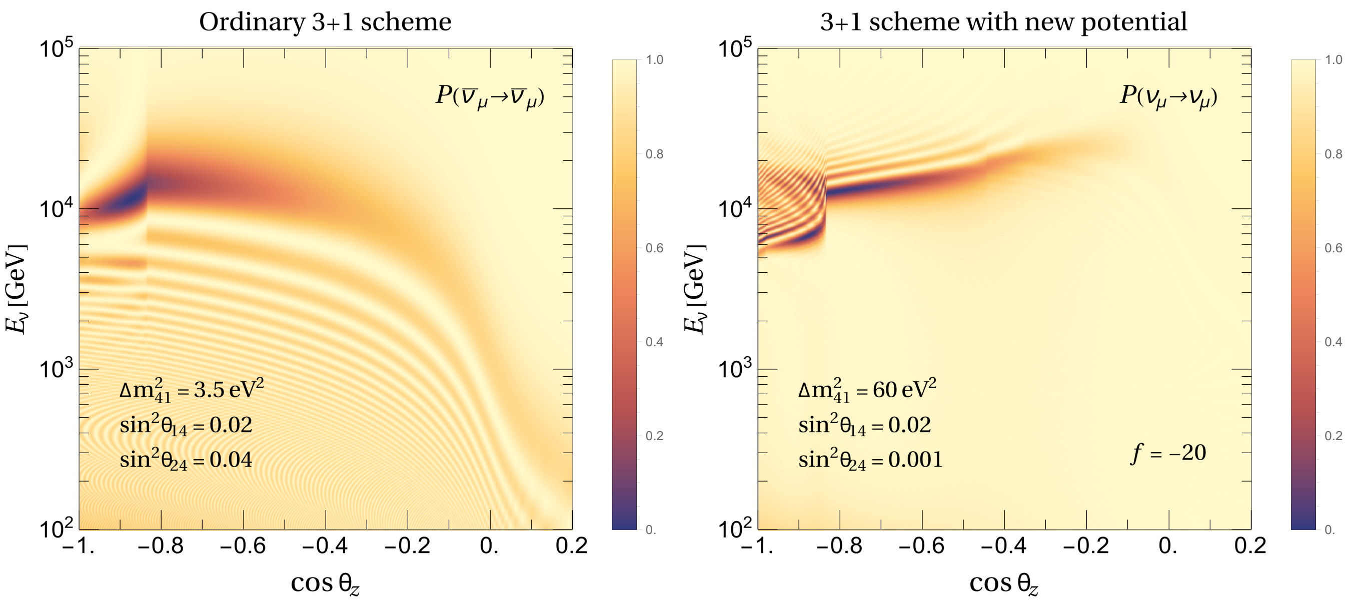

FIG. 13: Oscillograms for the ordinary 3+1 scheme (left panel) and the 3+1 scheme with new potential (right panel). The left panel refers to muon antineutrinos, while the right panel refers to muon neutrinos.

the 3+1 scenario with the novel potential, where the resonance occurs in the neutrino channel. From this plot we see that, as expected, there is a resonant behavior at the same energies involved in the ordinary 3+1 scheme. We still observe a well defined separation indicative of the transition between core-crossing and mantle-crossing trajectories. We find that the depth and the width of the resonance (both for core and mantle-crossing trajectories) depends on the value of s^2_{24} and the width can be noticeably influenced by s^2_{14}, becoming larger (smaller) for higher (lower) values of this parameter. The oscillogram confirms the presence of fast oscillations for core-crossing trajectories, which are imputable to parametric effects.

We could not perform a numerical study of the IceCube resonance beyond the level of probability plots and oscillograms because reproducing the IceCube analysis is prohibitive from outside the collaboration. Hence, it remains to be seen if the quality of the fit of the IceCube data to the new resonance is similar to that of the usual one. We note that the reconstruction of the neutrino energy is subject to a substantial degradation due to the limited energy resolution of the detector and what appears as a clear resonance at $E_\nu = 10$ TeV in the oscillogram, looking by eye at the IceCube 2D-histograms of events, is translated into a deficit of events around the muon energy of $E_\mu \sim 1$ TeV and to an arch-like pattern. So, it is plausible that the distinction between the ordinary resonance and the one predicted in the model under investigation should be difficult. However, an accurate official simulation performed by the IceCube collaboration is needed to clarify the issue. We also notice that IceCube could distinguish the new resonance from the ordinary one looking at the appearance of electron neutrinos, which should manifest as cascade events. However, according to a recent study [133] (see also the early study [134]) performed in the 3+1 scheme with a large non-zero θ_{34}, where ν_τ appearance is strongly enhanced giving rise to ν_τ events (indistinguishable from the ν_e ones), the sensitivity of IceCube to cascades is currently limited, albeit it could improve in the future by considering an expanded data sample larger (up to ten-years) than the one-year sample presently used in the analysis. Therefore, cascade events are a signature of the model under consideration provided that there is enough sensitivity to detect them.

An important remark is in order concerning the compatibility of the benchmark parameters of the model with the existing data. In Sec. VI we have seen that with the choice of a non-negligible value $s^2_{14} = 0.02$, solar and LBL data indicates $O(10)$ values for the f parameter regulating the strength of the new potential. In the present section, we have also seen that in order to maintain fixed the energy of the resonance at the value hinted at by IceCube ($E \simeq 10$ TeV), the new mass-squared must be rescaled by the factor $|f|$ with respect to the best fit value obtained in the ordinary 3+1 scheme, leading to the choice $\Delta m^2_{41} = 60\,\mathrm{eV}^2$. Here, one must notice that for such large values of the mass-squared splitting there are strong constraints on s^2_{14} established by KATRIN [103]. Looking at the exclusion regions in [103] (see Fig. 3), one can observe that in the window $\Delta m^2_{41} \simeq [30, 80]$ eV^2, the constraints are less restrictive compared with those provided for lower/higher values. This is confirmed by a very recent analysis combining KATRIN with SBL disappearance data [135]. In particular, for $\Delta m^2_{41} = 60\,\mathrm{eV}^2$ KATRIN allows values of $s^2_{14} \lesssim 0.025$. Therefore, our benchmark parameters are fully compatible with KATRIN. We observe that values of Δm^2_{41} (and consequently of f) a factor of two smaller or larger than our benchmark choice would be disfavored by KATRIN since the bound on s_{14}^2 becomes stronger. It is interesting to observe that because of the connection between f and Δm_{41}^2, KATRIN indirectly constrains the new potential and it provides an independent indication that f should be $O(10)$. New data with increased statistics expected to come from KATRIN should be able to push the sensitivity around the benchmark value of our model possibly confirming/disconfirming it.

As a closing observation, we stress that the estimated $O(10)$ value for the parameter f is strictly related to our assumption to fix an appreciable value of $s_{14}^2 \simeq 0.01 - 0.03$. We have checked that basically all manifestations of the model where matter effects are crucial, such as the explanation of the LBL discrepancy between NOvA and T2K, the production of an excess of ν_e-like events in Super-Kamiokande multi-GeV atmospheric neutrinos and the multi-TeV resonance in IceCube, are intact also for very small values of s_{14}^2 provided that the parameters f and s_{24}^2 are appropriately rescaled (considering much larger values for f and much smaller values for s_{24}^2), in order to keep fixed the $\varepsilon_{ee}^{\oplus}$ and $\varepsilon_{e\mu}^{\oplus}$ couplings at their benchmark values identified in Sec. VI [see Eqs. (44)-(45)]. However, one must notice that a realization of the scenario with a very small value of $s_{14}^2 \ll 0.01$ would be of no relevance for the explanation of the SBL electron neutrino disappearance findings such as the Gallium and Reactor anomalies.

IX. NEW RESONANCE IN ICECUBE FOR θ_{12} IN THE DARK OCTANT

Until now we have assumed that the solar mixing angle lies in the lower octant ($\sin^2\theta_{12} < 0.5$). In fact, we have seen that if the new potential is proportional to the neutron number density, the combination of solar neutrino data with NOvA and T2K, excludes the higher (or dark) octant ($\sin^2\theta_{12} > 0.5$) solution. However, if the new potential is proportional to the electron or proton number density, the degeneracy persists in the combination of solar and LBL experiments. This is a consequence of the so-called generalized mass-ordering degeneracy [81], which implies that the oscillation physics is invariant under the combined transformation[26] $\varepsilon_{ee} \to -2-\varepsilon_{ee}$, $\theta_{12} \to \pi/2-\theta_{12}$, $\Delta m_{31}^2 \to -\Delta m_{32}^2$ (i.e. NO $\to$ IO), $\delta_{13} \to \pi - \delta_{13}$. Therefore, in this case the dark degenerate solution cannot be discarded. According to the degeneracy theorem, the 3-flavor phenomenology will not allow the distinction between the two neutrino mass orderings. For example, in the dark octant solution, the 6 GeV resonance in Super-Kamionande in the neutrino channel will occur in IO instead of NO. Also, the current preference for NO of reactor experiments when combined with LBL experiments, would become a preference for IO. All in all, in the 3-flavor framework, in the presence of large NSI-like couplings (possibly close to $\varepsilon_{ee} \simeq -2$), there is no way to determine the NMO if the NSI are proportional to the electron or proton number density.

It is natural to ask if in the 3+1 scheme with the new matter potential, it is possible to distinguish between the two degenerate solutions. The answer is positive essentially for a very simple reason. Differently from what happens for the NMO in the 3-flavor scheme, the sign of Δm_{41}^2 is fixed to be positive. The case of a negative Δm_{41}^2 is excluded because the light neutrino states would have a mass incompatible with cosmology, especially in our scenario where Δm_{41}^2 can be much bigger than the usual $\sim 1\,\mathrm{eV}^2$ scale more often considered in the literature. This renders less dangerous a possible 4-flavor generalization of the 3-flavor degeneracy theorem. If we consider the IceCube resonance at 10 TeV, the 3-flavor parameters are irrelevant, so apparently it is blind to the octant of θ_{12} and to the NMO. On the other hand, one must observe that the coupling $\varepsilon_{ee}^{\oplus} = \bar{f}_{\oplus} s_{14}^2$ is relatively small in the lower-octant solution (since $f \simeq -20$), while it becomes close to -2 in the dark-octant solution for which one needs much larger (negative) values of f. Since the value of f is different and much larger in the dark-octant solution, one may expect a different behavior in the two degenerate solutions. This means, that the study of the IceCube resonance, breaking the generalized 3-flavor degeneracy, can allow us to pin down indirectly the correct octant of the solar mixing angle and the NMO. In fact, we find that the degeneracy is maximally broken since for the dark-octant solution there exists a (ν_e, ν_μ) resonance in the antineutrino channel, which has no counterparts for the ordinary solution. In oder to understand this behavior we report below the expression of the Hamiltonian regulating the (ν_e, ν_μ, ν_s) oscillations already introduced in Eq. (49),

$$H_{3\nu}^{(e\mu s)} = \begin{bmatrix} V_{\rm CC}+ks_{14}^2 & ks_{14}s_{24} & ks_{14} \\ \dagger & ks_{24}^2 & ks_{24} \\ \dagger & \dagger & \bar{f}V_{CC}+k \end{bmatrix}. \tag{59}$$

We first notice that for antineutrinos one has $V_{CC} < 0$, and for a very large negative values of $\bar{f}$, the $(4,4)$ entry in the Hamiltonian is positive-definite and can be much larger than the $(1,4)$ and $(2,4)$ entries. In this limit the sterile

[26] In the presence of off-diagonal NSI-like couplings the symmetry requires $\varepsilon_{\alpha\beta} \to \varepsilon_{\alpha\beta}^*$, which in our model is obtained by the replacement of the CP-phases $\delta_{14} \to 2\pi - \delta_{14}$ and $\delta_{34} \to 2\pi - \delta_{34}$.

state ν_s can be approximately integrated away, and the effective dynamics of the (ν_e, ν_μ) system is approximately that of a 2-flavor system. Second, we observe that for $V_{CC} < 0$, the condition $[H(2,2) - H(1,1)] = 0$ can be verified giving rise to a resonant enhancement regulated by a mixing angle θ^m_{12}.[27] In the limit of very large f, it is possible to provide an analytical expression for the 1-2 mixing angle in matter diagonalizing the (1,2) block of the Hamiltonian, obtaining

$$\sin 2\theta^m_{12} = \frac{2s_{14}s_{24}}{\sqrt{4s^2_{14}s^2_{24} + (\frac{V_{CC}}{k} + s^2_{14} - s^2_{24})^2}}\,, \tag{60}$$

and the conversion probability of muon to electron neutrinos can be expressed as

$$P_{\mu e} = \sin^2 2\theta^m_{12} \sin^2 2\phi^m_{12}\,, \tag{61}$$

where we have introduced the oscillation phase

$$\phi^m_{12} = \frac{kL}{2}\sqrt{4s^2_{14}s^2_{24} + \big(\frac{V_{CC}}{k} + s^2_{14} - s^2_{24}\big)^2}\,. \tag{62}$$

These expressions explicitly show that the origin of the mixing angle in matter θ^m_{12} and of the oscillation phase ϕ^m_{12} is purely dynamical and completely unrelated to their value in vacuum. The two-flavor (ν_e, ν_μ) conversion is an effective phenomenon mediated by the far pseudo-sterile state ν_s.

The resonance condition, given the hierarchical pattern $s^2_{24} \ll s^2_{14}$ is well approximated by $|V_{CC}| = ks^2_{14}$. This implies that, for a fixed resonance energy (determined by IceCube), we have $\Delta m^2 \simeq 2E_{\rm res}|V_{CC}|/s^2_{14}$, which is independent of $\bar{f}$. We have verified that this equality is a good approximation provided that $|\bar{f}|$ is sufficiently large ($|\bar{f}| \gtrsim 10^3$). Considering our dark NSI-like solution, for which $\varepsilon^{\oplus}_{ee} = \bar{f}s^2_{14} \simeq -2$ and $|\bar{f}| \simeq 2/s^2_{14}$, we see that for sufficiently small values of s^2_{14}, the parameter $\bar{f}$ can be very large. Therefore, one may expect a nearly 2-flavor behavior in the dark resonance. We observe that such a kind of resonance cannot occur in the neutrino channel because it requires $V_{CC} < 0$. Hence, for the dark solar octant solution ($s^2_{12} \simeq 0.7$ and $\varepsilon_{ee} = \bar{f}s^2_{14} \simeq -2$), we have a (ν_e, ν_μ) resonance in IceCube always in the antineutrino channel.[28]

We illustrate this (ν_e, ν_μ) resonant behavior for one selected choice of parameters. We find that $s^2_{14} = 0.02$ (adopted until now) and the value of $f \simeq -200$, which jointly provide $\varepsilon^{\oplus}_{ee} = \bar{f}_{\oplus}s^2_{14} \simeq -2$, are not phenomenologically interesting because such an electron neutrino mixing at the resulting rescaled value of $\Delta m^2_{41} \simeq 600$ eV^2 (needed to maintain fixed the resonance energy at ~ 10 TeV), is excluded by KATRIN, which imposes the upper bound $s^2_{14} \lesssim 0.005$ at 95% C.L. (see Fig. 3 in [103]). This leads us to move towards smaller (larger) values of s^2_{14} ($|f|$), and thus to larger values of Δm^2_{41}, where the bounds from KATRIN get relaxed. Our final choice is to adopt the values $s^2_{14} = 0.005$, $f = -800$ (which still provide $\varepsilon^{\oplus}_{ee} = \bar{f}_{\oplus}s^2_{14} = -2$) and $\Delta m^2_{41} = 3000$ eV^2. These parameters are compatible with KATRIN and also with Mainz [136] and Troitsk [137, 138], which are sensitive in the region of such very high values of Δm^2_{41} (see Fig. 1 in [139] for their combined fit). Note that the large value of f, leads us to select an extremely small value of $s^2_{24} \simeq 2 \times 10^{-5}$, which serves to respect the bounds on the $\varepsilon_{e\mu}$ and $\varepsilon_{\mu\mu}$ NSI-like couplings imposed by the low-energy ($E \lesssim 1$ TeV) phenomenology.

In Fig. 14 we illustrate the "dark resonance" of IceCube. The left-upper panel represents the behavior of the eigenvalues. The largest eigenvalue, which is positive and very large is not represented in the plot, where we report only the three smaller eigenvalues. Note that the order of the three eigenvalues is different with respect to the case considered in the previous section, because for consistency with the degeneracy theorem, in the dark solution we have fixed the NMO to be the IO. However, this is relevant only at low energies while it is completely irrelevant for the high-energy dynamics which is independent on the 3-flavor parameters. We can observe that one of the eigenvalues is constant and equal to zero because we have set $\theta_{34} = 0$ and the ν_τ is not involved in the flavor conversion. We can observe that the other two eigenvalues display a clear avoided crossing, which is induced by the off-diagonal 1-2 coupling which at the resonance takes the value $k_{\rm res}s_{14}s_{24} = |V_{CC}|s_{24}/s_{14} \simeq 0.22\,|V_{CC}|$. At the resonance, as confirmed by the varying color along the eigenvalues curves, there is maximal admixture of ν_e and ν_μ flavors. The right-upper panel reports the mixing angles in matter. For consistency we have fixed θ_{12} at the octant symmetric "dark" best fit value $\sin^2\theta_{12} = 0.69$, albeit this is irrelevant at high energies. We can see that, differently from the

[27] We underline that, as we have seen in the previous section, in the full 4-flavor scheme the mixing angle θ^m_{12} is replaced by θ^m_{13} in conjunction with $\theta_{23} \simeq \pi/2$.

[28] For completeness, we mention that there is also an observable dark conventional (ν_e, ν_s) resonance occurring in the neutrino channel, which however is of scarse phenomenological interest.

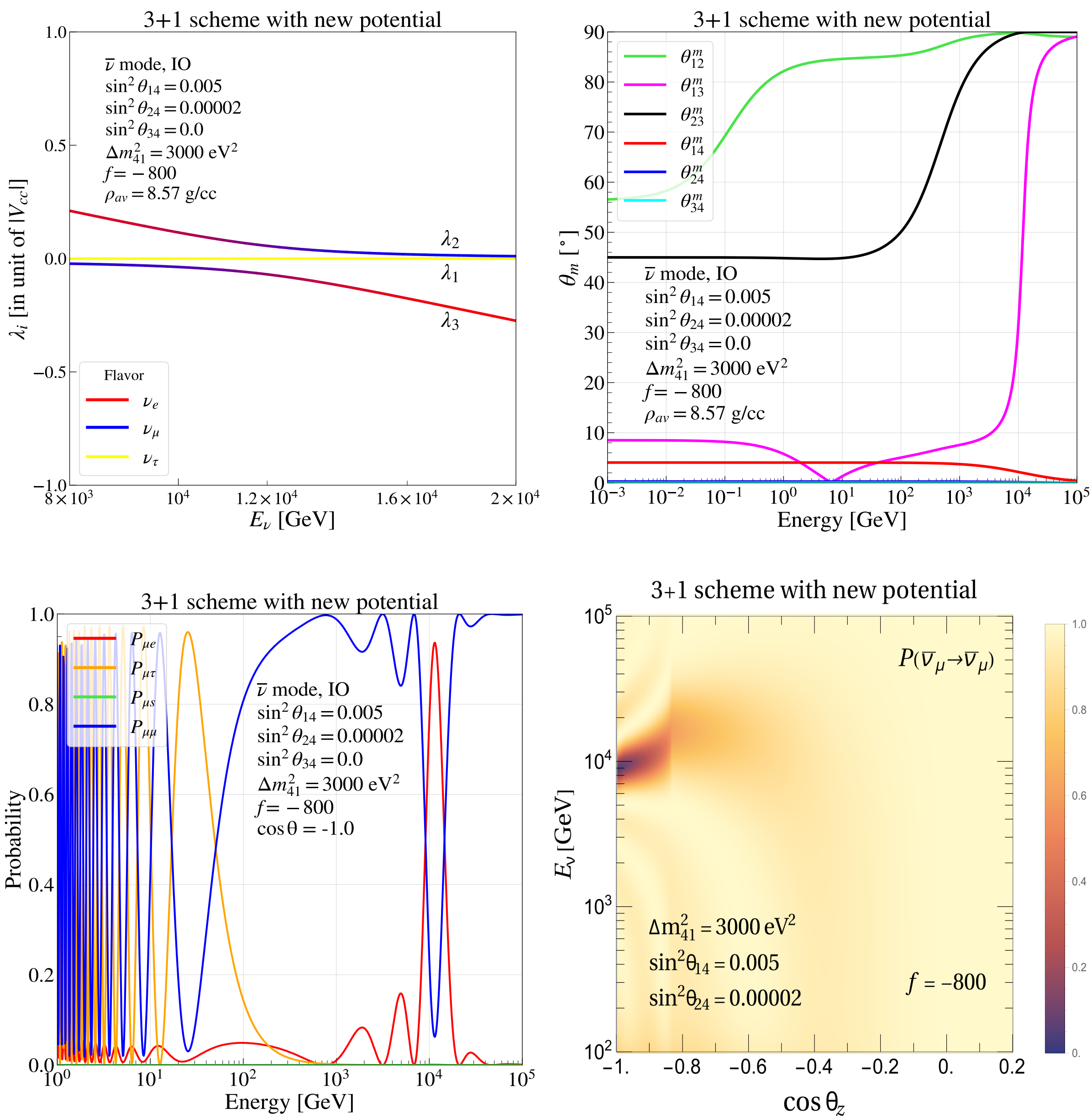

FIG. 14: Illustration of the IceCube resonance for parameters in the dark θ_{12} octant solution as indicated in the plots.

resonance encountered in the ordinary (non-dark) scenario, only the mixing angle θ^m_{13} becomes maximal, confirming that the effective dynamics is a 2-flavor one, albeit it is mediated by the far pseudo-sterile state. The left-lower panel depicting the muon channel probabilities shows that there is a pure (ν_e, ν_μ) resonance as expected. All these findings confirm our analytical description. For completeness, in the right-lower panel we report the oscillogram of the muon anti-neutrino disappearance probability, from which we can infer that the dark resonance is more pronounced for core-crossing trajectories.

We must observe that the dark solution would have little impact in the electron disappearance short-baseline anomalies since the implied θ_{14} mixing angle is very small. However, we think that the illustration of the resonance occurring for the dark octant solution is conceptually important independently of its possible phenomenological relevance, because of three different reasons. First, as already underlined, this resonance offers the possibility to determine indirectly the octant of θ_{12} and consequently distinguishing the NMO in the framework in which pseudo-sterile neutrinos oscillate with a potential proportional to electron or proton number density. In fact, confronting the oscillation probabilities and the oscillogram with those obtained for the benchmark parameters used for the lower-octant solution discussed in Sec. VIII (see the right panels in Figs. 12 and 13), we see that the behavior is quite different. Second, we realize that the unconventional dark (ν_e, ν_μ) resonance occurs in the absence of the conventional resonances in the (ν_e, ν_s) and (ν_μ, ν_s) sub-systems. Hence, we learn that the new resonant phenomenon mediated by the sterile neutrinos in the presence of the new potential can manifest independently of the coexistence of conventional resonances. Third, it must be noted that the dark resonance cannot be predicted on the basis of the bare level crossing diagram, which shows no other 1-3 resonance apart from the standard 3-flavor one occurring at energies of few GeV. Finally, we remark that for a non-zero value of θ_{34} a companion dark resonance in the (ν_e, ν_τ) channel is present, as expected based on our discussion in the previous section. However, such a resonance is of less phenomenological interest given the involved flavors.

X. INTERACTION OF PSEUDO-STERILE NEUTRINOS WITH ASYMMETRIC DARK MATTER

In the treatment provided in the previous sections we have assumed that the sterile neutrino potential is produced by their interaction with ordinary matter. The question arises if the such an interaction can involve the background dark matter (DM) instead of the ordinary matter. This is possible only under very particular circumstances. First of all, one has to assume that the DM is asymmetric (see [140] for a review). In this case, as already investigated in various works, both active [141–150] and sterile neutrinos [89, 151–153] can entail MSW effects. In this scenario, the discrepancies recorded in LBL, low-energy and high-energy atmospheric neutrinos, should be interpreted as a hint of the refraction of the pseudo-sterile neutrinos on the DM particles encountered along the path traversed by neutrinos from source to detector. The explanation of the anomalies provides the strength of the needed potential, which should be fine-tuned to be approximately ten times larger than the standard potential in the Earth crust/mantle. This potential should be generated by an extremely low matter density equal to the density of the DM halo in the solar neighborhood $\rho_\chi(r_\odot) \simeq 0.4$ GeV/cm^3. This low density should be counterbalanced by an enormous strength of the new interaction $G_X = f_\chi G_F$, with $f_\chi \simeq n_e/n_\chi \sim 10^{24}$, pointing towards an ultralight vector mediator.

A potential issue arises concerning solar neutrinos since the DM can be accreted by the Sun and accumulated at its center. In general one may expect an over-density of DM inside the Sun with respect to its average Halo value felt by terrestrial neutrinos, which would imply big MSW effects in solar neutrinos, which however are not observed. In fact, we have seen that solar neutrinos can tolerate only the small effects considered in Sec. V. In order to circumvent this difficulty one has to avoid that the DM particles are accreted in the Sun, which can be obtained adopting a mass of the DM well below the evaporation threshold [154] ($m_\chi^{\rm evp} \simeq 4$ GeV) and/or supposing that the DM interaction with ordinary matter is negligibly small. In these conditions the Sun would be transparent to DM and, apart from small effects induced by gravitational focusing (see [155, 156]), no over-density with respect to the surrounding Halo would be present in its interior. Under this assumption, sterile neutrinos traveling from the Sun center to the Earth, would propagate in a medium of constant density with a potential similar in size (approximately ten times larger) to the standard potential in the Earth crust/mantle. This potential is too small to impact solar neutrino transitions, as we have explicitly checked with a numerical simulation. As a result, in this scenario solar neutrinos will behave as in the ordinary 3+1 scheme just providing the upper bound on θ_{14}.

It is important to note that atmospheric neutrinos are expected to distinguish between a potential related to ordinary matter from a potential due to dark matter. In fact, only in the first case, in which the density varies abruptly along the path due to the layered structure of the Earth (in particular due to mantle-core-mantle transition), one has parametric effects. We have seen that the parametric enhancement has a huge impact on the IceCube resonance for core-crossing trajectories, providing the resonance with distinctive features (see the right-upper panel of Fig. 12). In the case of MSW on a dark matter background this structure would be absent. In order to be more quantitative, we show in Fig. 15 the behavior of the IceCube resonance assuming a new potential having a (negative) constant value in all points of the Earth equal to twenty times the value of the standard neutral current potential in the mantle $V_S = 20 V_{NC}^{\rm mantle}$. The left plot shows the probabilities relevant for the muon neutrino channel for a core crossing trajectory. A comparison with the similar plot obtained for a potential proportional to the (layered) neutron number density presented in the right-upper panel of Fig. 12, shows a drastic reduction of the parametric effects. This is confirmed by the oscillogram displayed in the right panel. A comparison with the results obtained in the ordinary case (see right panel in Fig. 13), shows also a different shape of the oscillograms, in particular the slope in the $[\cos(\theta_z), E]$ plane. Therefore, in principle, a spectroscopic study of the high-energy resonance would allow the distinction between the two cases. Similarly, a precision study of the parametric resonances in multi-GeV atmospheric neutrinos could help in distinguishing between the two possibilities.

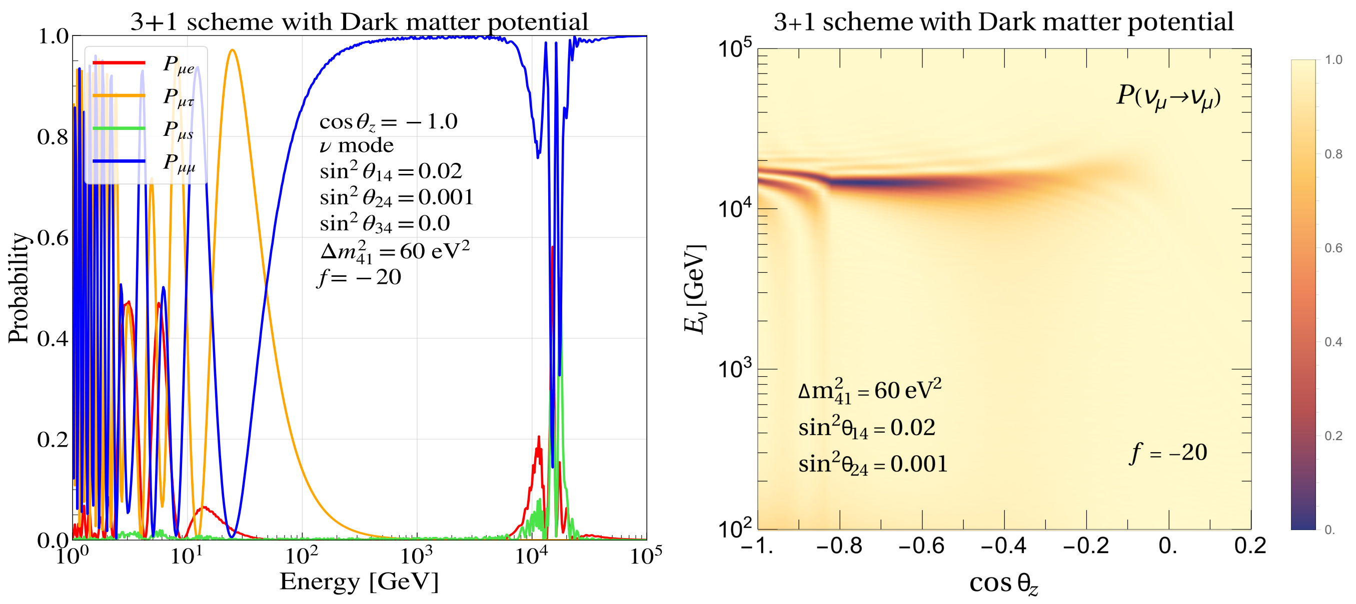

FIG. 15: The figure illustrates the IceCube resonance assuming that the new matter potential is proportional to a constant density of dark matter particles. The left panel represents the oscillation probabilities in the muon neutrino channel for a core-crossing trajectory. The right panel represents the oscillogram for the muon neutrino survival probability.

XI. DISCUSSION AND FUTURE PERSPECTIVES

A. Possible origin of the new matter potential

Although we remain agnostic on the nature of the interaction leading to the new matter potential, here we comment about its possible origin. The simplest scenario entails a hidden $U(1)$ gauge group involving a new vector boson Z'. In this model, in the case in which the potential is related to ordinary baryonic matter, one expects a possible signal in coherent scattering experiments. However, these constraints can be evaded by choosing a sufficiently small value of the mediator mass $m_{Z'}$. This is possible because the matter potential represents a process with zero-momentum exchange, while in the scattering experiments the exchanged momentum is finite. Of course, it remains to be understood how the pseudo-sterile neutrinos impact astrophysics and cosmology, which is a highly non-trivial question. While the ordinary sterile neutrinos are severely constrained by cosmology, the situation is less obvious if they interact with ordinary or dark matter. A common mechanism invoked to render sterile neutrinos compatible with cosmology are self-interactions [39–50], which seem capable to suppress their mixing. Sterile neutrinos with a new potential have been recently investigated in [60], where it has been shown that they are compatible with a series of bounds from laboratory and cosmology provided that the mass of the vector mediator is extremely light (~ 10 eV). According to the same work, self interactions of sterile neutrinos suppress active-sterile mixing and their production before neutrino decoupling and BBN era, provided that sterile neutrinos have contact NSI-like interactions with dark matter particle with an asymmetric dark matter particle. Considered the highly involved situation of the status of pseudo-sterile neutrinos in cosmology we think that the last word on these exotic neutrino states should be left to oscillations experiments.

B. Dirac vs Majorana nature of the pseudo-sterile neutrinos

We briefly comment on the nature (Dirac vs Majorana) of the sterile neutrino within the model under consideration. It is well known that light sterile neutrinos, if Majorana particles, may be observable in neutrinoless double beta decay [157–166]. In fact, sterile neutrino mass contributes to the effective Majorana mass $m_{\beta\beta}$ with a complex term proportional to $|U_{e4}^2| m_4 e^{i\alpha_4}$, where α_4 is a CP-phase related to Dirac and Majorana phases. The recent study [166] takes into account the most restrictive bounds coming from KamLAND-Zen, $m_{\beta\beta} < (28 - 122)\,$meV at the 90% C.L., where the interval corresponds to the uncertainty in the nuclear matrix element. According to this work, a Majorana sterile neutrinos with $|U_{e4}|^2 \simeq 0.01 - 0.03$ and mass-squared $\Delta m^2_{41} \simeq 60\,\mathrm{eV}^2$, as that considered in the present work, is excluded or at least strongly disfavored by data, especially for the case of normal neutrino mass ordering. We stress that if θ_{12} lies in the dark octant it is expected to have a substantial impact (in particular for the NO case) in neutrinoless double beta decay as shown in [167, 168], but this is true only in the 3-flavor framework with large ordinary NSI. Within the 3+1 framework, where the effective Majorana mass $m_{\beta\beta}$ is dominated by the sterile contribution, the octant of θ_{12} is expected to have a minor impact on the limits. Therefore, the pseudo-sterile neutrinos we are considering, if s^2_{14} is appreciable, are most probably of the Dirac type. This conclusion can be evaded if $s^2_{14} \ll 0.01$, or within 3+2 and 3+3 schemes where the contribution to the effective Majorana mass of the additional mass eigenstates ν_5 and ν_6 can in principle lead to cancellations. However, for this scenario to work, one needs fine tuning or an underlying symmetry forcing the effective Majorana towards values close to zero.

C. Possible manifestations of pseudo-sterile neutrinos in MiniBooNE

In the study of the oscillation phenomenology of the pseudo-sterile neutrinos we have considered basically all kinds of anomalies, with the exception of the SBL accelerator anomalies such as LSND and MiniBooNE. Regarding this last one, it must be noted that MicroBooNE has recently excluded the electron neutrino appearance [12] as a possible explanation of the excess. We observe that our model produces a negligible signal since the transition probability is proportional to the effective appearance mixing angle $\sin^2 2\theta_{\mu e} = 4U^2_{e4}U^2_{\mu 4} \simeq 10^{-4}$, and therefore it has no role in the appearance of electron neutrinos. However, pseudo-sterile neutrinos may manifest in MiniBooNE in different ways. Here we will mention two (possibly intertwined) options.

i) *Neutral current interactions of pseudo-sterile neutrinos with emission of photons.* The existence of a new matter potential giving rise to the coherent forward scattering, a process involving zero exchanged momentum $q^2 = 0$, strongly suggests that the pseudo-sterile states may also interact in neutral-current scattering processes where a finite q^2 exchange is involved. An obvious candidate to mediate such an interaction is a new vector Z' boson related to a symmetry group $U(1)$. The explanation of MiniBooNE excess may require a non-trivial coupling of the Z' with baryons and photons. In our model, one has a guaranteed flux of pseudo-sterile neutrinos at the detector proportional to $P(\nu_\mu \to \nu_s) \simeq 2U^2_{\mu 4}$, where we have assumed averaged oscillations. In this condition a minimal dark sector containing a vector Z' and a scalar ϕ can produce a neutral current scattering with emission of photons. A similar process has been recently proposed in [169], where the active neutrinos have been supposed to be coupled to the new mediators. We believe that the same model could work even more naturally by replacing the active neutrinos with the pseudo-sterile ones.

ii) *Visible decay of pseudo-sterile neutrinos.* We have already underlined that the small values of $|U_{\mu 4}|^2 \simeq 0.001$ preferred by the data would eliminate the tension between IceCube and the most stringent negative ν_μ disappearance searches of MINOS/MINOS+ [65] and NOvA [66]. Such low values of $|U_{\mu 4}|^2$, in principle, present another advantage, having been invoked to explain the LSND and MiniBooNE excesses in models in which the sterile neutrino is endowed with visible decay [34–38]. However, to this regard, it must be noted that a recent study [38] has shown that MicroBooNE results are in tension with the visible decay explanation of MiniBooNE. We note that the visible decay scenario may coexist with the neutral current scattering with emission of photons since the same vector and/or scalar particles can mediate both processes.

D. Implications for flavor conversion in a medium with varying density

In our present study of the resonant behavior focused on matter effects in the Earth, along the neutrino trajectory the density is constant or presents layers of constant density. In this case, the dynamics of the resonance is determined by the mixing angles in matter and by the oscillating phases. The situation would be different in the case of neutrinos traversing a matter profile with varying density. In this case, one may interpret the eigenvalues as the energies of the instantaneous mass eigenstates in matter as a function of the density. Looking from this perspective at the eigenvalues plots, one expects that for large values of f a strong adiabatic conversion between the flavors ν_μ and ν_e will occur traversing the resonance region. As a consequence, a muon neutrino produced at high density (above the resonance condition) would be transformed in an electron-neutrino at lower density (below the resonance condition). Therefore, one expects that the model will have implications for neutrinos propagating in dense environments. As a matter of fact, the recent work [170] has shown that even in the standard 3-flavor scheme there is an observable impact of matter effects in high-energy neutrinos produced in dense environments, leading to observable deviations of the flavor composition detected on the Earth, with respect to the case of pure vacuum oscillations. In the presence of pseudo-sterile neutrinos the situation is expected to change appreciably. We think that this can be a potential signature of our model, which can be investigated with future upgraded versions of the Neutrino telescopes such as IceCube-Gen2 [171].

E. Signatures of the model

The proposed scenario has several signatures in planned neutrino experiments. In case of appreciable values of $|U_{e4}|^2 \simeq \sin^2\theta_{14} \sim 0.01-0.03$, the pseudo-sterile neutrinos should show up with a distinctive kink in the β-decay energy spectrum measured by KATRIN [103]. Hence, one of the most effective smoking guns of the model is non-oscillatory. We notice that KATRIN in [103] has presented the analysis of five measurement campaigns. The collaboration has already collected data in other eleven campaigns [172], which cumulatively contain a statistics four times larger than the first five ones. Hence, we can expect a noticeable improvement of the sensitivity in the near future.

Considering the most obvious oscillation feature, which is the L/E dependency of oscillations in vacuum, we must notice that it is difficult to be observed. In fact, the high indicated value of $\Delta m^2_{41} \sim 60$ eV^2 would give rise to a mere energy-independent deficit in all existing short-baseline oscillation experiments. The observation of the oscillation pattern at energies of a few MeV would require a baseline of few centimeters. In principle one could circumvent this obstacle by considering a movable finely segmented detector with an exceptional spatial resolution. Indeed, some of the existing experiments are already using this kind of approach. However, from the contour plots of the exclusion regions [22], it seems that all the current experiments loose sensitivity for $\Delta m^2_{41} \gtrsim 10$ eV^2. Perhaps an upgraded version of the existing detectors may be able to improve the sensitivity. Considering larger GeV energies obtained in accelerators, the new SBL project nuSCOPE [173] has an impressive sensitivity in the range of high Δm^2_{41}, and would provide the possibility to probe directly the tiny values of the sterile mixing angles implied by the new scenario by measuring the electron and muon disappearance as well as the muon appearance channels (see [174]).

Considering signatures involving the presence of matter effects, we highlight what we have called the matter-vacuum synergy. In fact, this concept applied to T2K (quasi-vacuum) and NOvA (matter-dominated) has been an important guide for us to build the model and will have an even more important role in the future. In fact, having at our disposal two new experiments, Hyper-Kamiokande [175], and DUNE [176], which will substantially upgrade the existing ones would allow us to maximally exploit the matter-vacuum interplay. The first experiment would work as as a solid (quasi-vacuum) anchor for the second (matter-dominated) one, making it possible to better identify the new matter effects. In addition, it is worthwhile to mention that DUNE, with a broad band spectrum, would be particularly sensitive to the spectral energy distortions induced by the NSI-like couplings and together with Hyper-Kamiokande and ESSνSB [177] will constitute the ideal setup for exploring the NSI-like Hamiltonian shown in Eq. (24) and Eq. (53), which is another very distinctive signature of the model. We have shown that the model predicts an excess of electron-like events due to the modification of the standard 3-flavor resonance occurring at few GeV in atmospheric neutrinos. Dedicated analyses performed by Super-Kamiokande and IceCube DeepCore may provide interesting indications about this feature. The future detectors Hyper-Kamiokande, DUNE and KM3NeT-ORCA [178] are expected to be extremely sensitive to the behavior of multi-GeV atmospheric neutrinos, and will be able to perform a precision spectroscopy of the resonance. However, one should keep in mind that in LBL and low-energy atmospheric neutrinos, the effects of the 3+1 model with the new matter potential are indistinguishable from those induced by NSI couplings, albeit such couplings have a well definite pattern in our model. Ultimately, the 4-flavor origin of the observed effects can be proved only by looking at high-energy multi-TeV atmospheric neutrinos or by exploiting kinematical methods outlined above (SBL oscillations and β-decay). On the other hand, we underline that purely kinematical experiments cannot reveal the new matter potential, whose identification makes necessary the explorations performed with LBL, atmospheric neutrino experiments and with neutrinos of astrophysical origin.

Concerning the resonance at around 10 TeV, we have already underlined the limits of our work, in which we could not perform a full data analysis. An accurate official analysis would be indispensable to establish the quality of the fit, which is of the foremost importance to confirm the existence of the new matter potential. Strictly speaking, a good quality of the fit would not provide per se a distinctive signature of the model but only a sort of degenerate solution with the ordinary 3+1 scheme. In principle, one should be able to distinguish sufficiently well the new resonance from the usual one, which is probably a much more difficult task. However, taking the IceCube fit together with other pieces of evidence would strongly support the model. We note that a precision study of the resonance would be possible with an experiment of new conception such as the Neutrino Kaleidoscope recently proposed in [179], where a collimated beam of TeV neutrinos [180] produced in a muon collider [181] would be detected in one of the existing or planned Neutrino Telescopes such as IceCube, KM3NeT and P-ONE. The realization of such an ambitious experiment would enable us to explore the amplification phenomenon for mantle and core-crossing trajectories, using our planet with its layered structure as the ultimate neutrino oscilloscope. Moving to the sky, the scenario is expected to impact the flavor composition of astrophysical neutrinos produced in dense environments. In particular, a substantial conversion of muon into electron neutrinos is expected. All in all, we think that our model is highly predictive and can be efficiently tested by the current and future experiments.

XII. CONCLUSIONS

We have considered a 3+1 scenario in which sterile neutrinos feel a new matter potential proportional to background density. We have called such states as *pseudo-sterile neutrinos*. We have shown that the model behaves as an effective NSI-like scenario at low energies ($E \lesssim 1$ TeV) and presents a very distinctive Hamiltonian. In such a regime the model is able to provide an explanation of the discrepancy observed between NOvA and T2K and predicts an excess of ν_e-like events in multi-GeV atmospheric neutrinos as hinted at by Super-Kamiokande. At higher energies ($E \simeq 10$ TeV) the new scenario reveals its full 4-flavor nature producing a resonance as suggested by IceCube. We have shown that the structure of the amplification phenomenon is much more complex with respect to the ordinary 3+1 framework. Specifically, we have demonstrated that a genuine three-level dynamics emerges different from the usual two-level avoided crossing mechanism.

In order to be phenomenologically relevant, the new scenario requires that the new potential is approximately twenty times larger than the standard neutral-current potential and has negative sign $f = V_S/|V_{NC}| \simeq -20$. The preferred value of the mass-squared splitting lies around $\Delta m^2_{41} = 60$ eV^2. Both $|f|$ and Δm^2_{41} are roughly uncertain by a factor of a two and are positively correlated since their ratio is required to be approximately constant in order to fix the IceCube resonance energy at ~ 10 TeV. The data also indicate that the admixture of the muon neutrinos with the fourth sterile neutrino mass eigenstate is one order of magnitude smaller than the mixing of the electron neutrinos ($|U_{e4}|^2 \simeq 0.01 - 0.03$, $|U_{\mu4}|^2 \simeq 0.001$). The small values of $|U_{\mu4}|^2$ eliminate the tension between IceCube and the other negative ν_μ disappearance searches. Also the values of $|U_{\tau4}|^2$ are limited to be at least one order of magnitude smaller than $|U_{e4}|^2$. The predictions for Δm^2_{41} and $|U_{e4}|^2$ will be directly tested in the near future by KATRIN, in which one expects a characteristic kink in the β-decay energy spectrum.

We have shown that in the case in which the new matter potential is proportional to the electron or proton number density, a degenerate solution exists for the solar mixing angle in the dark octant. This solution seems phenomenologically less interesting as it involves very small values of θ_{14}, which are not relevant for the short-baseline anomalies. We have also demonstrated that the study of the resonant behavior at high-energies can distinguish between the ordinary and the dark solution. Finally, we have discussed the possibility that the new potential is generated by the interaction of the pseudo-sterile states with a background of asymmetric dark matter particles pointing out the role of parametric enhancement in the Earth in discriminating such a scenario.

The pseudo-sterile neutrino scenario presents an extremely rich phenomenology, involving baselines from the centimeter scale to the Earth-Sun distance, passing through the hundreds/thousands kilometers traveled by LBL and atmospheric neutrinos. Also the interested energies span from a fraction of MeV of *pp* solar neutrinos, to hundreds of TeV of atmospheric neutrinos. It is plausible to expect further signatures at even larger baselines and higher energies in neutrinos of astrophysical origin. Also, additional pseudo-sterile species are naturally expected to exist, making the picture even more complex and intriguing. Given such a rich landscape, if the proposed scenario were to be confirmed, a strenuous effort would be required to the neutrino community to shape the model and identify the nature of the new fundamental interaction involving the pseudo-sterile states. We would like to conclude by recalling that the neutrino index of refraction in matter has led to the resolution of the longstanding solar neutrino problem, and likewise we hope that it can shed light on the modern puzzle of the terrestrial neutrino oscillation anomalies in an even more spectacular way.

Acknowledgments

The work of S.S.C. is funded by the Deutsche Forschungsgemeinschaft (DFG, German Research Foundation) – project number 510963981. A.P. acknowledges partial support by the research grant number 2022E2J4RK "PANTHEON: Perspectives in Astroparticle and Neutrino THEory with Old and New messengers" under the program PRIN 2022 funded by the Italian Ministero dell'Università e della Ricerca (MUR) and by the European Union – Next Generation EU as well as partial support by the research project *TAsP* funded by the Instituto Nazionale di Fisica Nucleare (INFN).

[1] **LSND** Collaboration, A. Aguilar *et al.*, "Evidence for neutrino oscillations from the observation of $\bar{\nu}_e$ appearance in a $\bar{\nu}_\mu$ beam," *Phys. Rev. D* **64** (2001) 112007, `arXiv:hep-ex/0104049`.

[2] G. Mention, M. Fechner, T. Lasserre, T. A. Mueller, D. Lhuillier, M. Cribier, and A. Letourneau, "The Reactor Antineutrino Anomaly," *Phys. Rev. D* **83** (2011) 073006, `arXiv:1101.2755 [hep-ex]`.

[3] **GALLEX** Collaboration, P. Anselmann *et al.*, "First results from the Cr-51 neutrino source experiment with the GALLEX detector," *Phys. Lett. B* **342** (1995) 440–450.
[4] **GALLEX** Collaboration, W. Hampel *et al.*, "Final results of the Cr-51 neutrino source experiments in GALLEX," *Phys. Lett. B* **420** (1998) 114–126.
[5] F. Kaether, W. Hampel, G. Heusser, J. Kiko, and T. Kirsten, "Reanalysis of the GALLEX solar neutrino flux and source experiments," *Phys. Lett. B* **685** (2010) 47–54, `arXiv:1001.2731 [hep-ex]`.
[6] D. N. Abdurashitov *et al.*, "The Russian-American gallium experiment (SAGE) Cr neutrino source measurement," *Phys. Rev. Lett.* **77** (1996) 4708–4711.
[7] **SAGE** Collaboration, J. N. Abdurashitov *et al.*, "Measurement of the solar neutrino capture rate with gallium metal. III: Results for the 2002–2007 data-taking period," *Phys. Rev. C* **80** (2009) 015807, `arXiv:0901.2200 [nucl-ex]`.
[8] V. V. Barinov *et al.*, "Results from the Baksan Experiment on Sterile Transitions (BEST)," *Phys. Rev. Lett.* **128** no. 23, (2022) 232501, `arXiv:2109.11482 [nucl-ex]`.
[9] V. V. Barinov *et al.*, "Search for electron-neutrino transitions to sterile states in the BEST experiment," *Phys. Rev. C* **105** no. 6, (2022) 065502, `arXiv:2201.07364 [nucl-ex]`.
[10] **NEUTRINO-4** Collaboration, A. P. Serebrov *et al.*, "First Observation of the Oscillation Effect in the Neutrino-4 Experiment on the Search for the Sterile Neutrino," *Pisma Zh. Eksp. Teor. Fiz.* **109** no. 4, (2019) 209–218, `arXiv:1809.10561 [hep-ex]`.
[11] **MiniBooNE** Collaboration, A. A. Aguilar-Arevalo *et al.*, "Updated MiniBooNE neutrino oscillation results with increased data and new background studies," *Phys. Rev. D* **103** no. 5, (2021) 052002, `arXiv:2006.16883 [hep-ex]`.
[12] **MicroBooNE** Collaboration, P. Abratenko *et al.*, "Search for an Anomalous Production of Charged-Current νe Interactions without Visible Pions across Multiple Kinematic Observables in MicroBooNE," *Phys. Rev. Lett.* **135** no. 8, (2025) 081802, `arXiv:2412.14407 [hep-ex]`.
[13] **(IceCube Collaboration)‖, IceCube** Collaboration, R. Abbasi *et al.*, "Search for an eV-Scale Sterile Neutrino Using Improved High-Energy $\nu\mu$ Event Reconstruction in IceCube," *Phys. Rev. Lett.* **133** no. 20, (2024) 201804, `arXiv:2405.08070 [hep-ex]`.
[14] **IceCube** Collaboration, R. Abbasi *et al.*, "Exploration of mass splitting and muon/tau mixing parameters for an eV-scale sterile neutrino with IceCube," *Phys. Lett. B* **858** (2024) 139077, `arXiv:2406.00905 [hep-ex]`.
[15] J. Wolcott, "New Neutrino Oscillations Results from NOνA with 10 years of Data," *Talk presented at Neutrino 2024, 16-22 Jun 2024* (2024) . `https://indico.fnal.gov/event/43209/timetable/#20200622.detailed`.
[16] C. Giganti, "T2K Experiments Status and Plan," *Talk presented at Neutrino 2024, 16-22 Jun 2024* (2024) . `https://agenda.infn.it/event/37867/contributions/233954/attachments/121809/177671/Neutrino2024_T2K_Claudio.pdf`.
[17] P. B. Denton, J. Gehrlein, and R. Pestes, "CP -Violating Neutrino Nonstandard Interactions in Long-Baseline-Accelerator Data," *Phys. Rev. Lett.* **126** no. 5, (2021) 051801, `arXiv:2008.01110 [hep-ph]`.
[18] S. S. Chatterjee and A. Palazzo, "Nonstandard Neutrino Interactions as a Solution to the $NO\nu A$ and T2K Discrepancy," *Phys. Rev. Lett.* **126** no. 5, (2021) 051802, `arXiv:2008.04161 [hep-ph]`.
[19] S. S. Chatterjee and A. Palazzo, "Status of tension between NOvA and T2K after Neutrino 2024 and possible role of nonstandard neutrino interactions," *Phys. Rev. D* **110** no. 11, (2024) 113002, `arXiv:2409.10599 [hep-ph]`.
[20] **Super-Kamiokande** Collaboration, T. Wester *et al.*, "Atmospheric neutrino oscillation analysis with neutron tagging and an expanded fiducial volume in Super-Kamiokande I–V," *Phys. Rev. D* **109** no. 7, (2024) 072014, `arXiv:2311.05105 [hep-ex]`.
[21] B. Dasgupta and J. Kopp, "Sterile Neutrinos," *Phys. Rept.* **928** (2021) 1–63, `arXiv:2106.05913 [hep-ph]`.
[22] M. A. Acero *et al.*, "White paper on light sterile neutrino searches and related phenomenology," *J. Phys. G* **51** no. 12, (2024) 120501, `arXiv:2203.07323 [hep-ex]`.
[23] S. Gariazzo, C. Giunti, M. Laveder, Y. F. Li, and E. M. Zavanin, "Light sterile neutrinos," *J. Phys. G* **43** (2016) 033001, `arXiv:1507.08204 [hep-ph]`.
[24] M. Dentler, Á. Hernández-Cabezudo, J. Kopp, P. A. N. Machado, M. Maltoni, I. Martinez-Soler, and T. Schwetz, "Updated Global Analysis of Neutrino Oscillations in the Presence of eV-Scale Sterile Neutrinos," *JHEP* **08** (2018) 010, `arXiv:1803.10661 [hep-ph]`.
[25] A. Diaz, C. A. Argüelles, G. H. Collin, J. M. Conrad, and M. H. Shaevitz, "Where Are We With Light Sterile Neutrinos?," *Phys. Rept.* **884** (2020) 1–59, `arXiv:1906.00045 [hep-ex]`.
[26] J. Villarreal, J. Woodward, J. Hardin, and J. Conrad, "A Frequentist Simulation-Based Inference Treatment of Sterile Neutrino Global Fits," *Mach. Learn. Sci. Tech.* **6** (2025) 035053, `arXiv:2507.01153 [hep-ph]`.
[27] **MicroBooNE** Collaboration, P. Abratenko *et al.*, "Search for light sterile neutrinos with two neutrino beams at MicroBooNE," *Nature* **648** no. 8092, (2025) 64–69, `arXiv:2512.07159 [hep-ex]`.
[28] J. M. Berryman, "Constraining Sterile Neutrino Cosmology with Terrestrial Oscillation Experiments," *Phys. Rev. D* **100** no. 2, (2019) 023540, `arXiv:1905.03254 [hep-ph]`.
[29] S. Hagstotz, P. F. de Salas, S. Gariazzo, M. Gerbino, M. Lattanzi, S. Vagnozzi, K. Freese, and S. Pastor, "Bounds on light sterile neutrino mass and mixing from cosmology and laboratory searches," *Phys. Rev. D* **104** no. 12, (2021) 123524, `arXiv:2003.02289 [astro-ph.CO]`.
[30] M. Archidiacono and S. Gariazzo, "Two Sides of the Same Coin: Sterile Neutrinos and Dark Radiation, Status and Perspectives," *Universe* **8** no. 3, (2022) 175, `arXiv:2201.10319 [hep-ph]`.
[31] H. Minakata, "eV-scale sterile neutrino: A window open to non-unitarity?," `arXiv:2503.09280 [hep-ph]`.
[32] M. H. Moulai, C. A. Argüelles, G. H. Collin, J. M. Conrad, A. Diaz, and M. H. Shaevitz, "Combining Sterile Neutrino

Fits to Short Baseline Data with IceCube Data," *Phys. Rev. D* **101** no. 5, (2020) 055020, arXiv:1910.13456 [hep-ph].
[33] J. M. Hardin, I. Martinez-Soler, A. Diaz, M. Jin, N. W. Kamp, C. A. Argüelles, J. M. Conrad, and M. H. Shaevitz, "New Clues about light sterile neutrinos: preference for models with damping effects in global fits," *JHEP* **09** (2023) 058, arXiv:2211.02610 [hep-ph].
[34] S. Palomares-Ruiz, S. Pascoli, and T. Schwetz, "Explaining LSND by a decaying sterile neutrino," *JHEP* **09** (2005) 048, arXiv:hep-ph/0505216.
[35] Y. Bai, R. Lu, S. Lu, J. Salvado, and B. A. Stefanek, "Three Twin Neutrinos: Evidence from LSND and MiniBooNE," *Phys. Rev. D* **93** no. 7, (2016) 073004, arXiv:1512.05357 [hep-ph].
[36] M. Dentler, I. Esteban, J. Kopp, and P. Machado, "Decaying Sterile Neutrinos and the Short Baseline Oscillation Anomalies," *Phys. Rev. D* **101** no. 11, (2020) 115013, arXiv:1911.01427 [hep-ph].
[37] A. de Gouvêa, O. L. G. Peres, S. Prakash, and G. V. Stenico, "On The Decaying-Sterile Neutrino Solution to the Electron (Anti)Neutrino Appearance Anomalies," *JHEP* **07** (2020) 141, arXiv:1911.01447 [hep-ph].
[38] M. Hostert, K. J. Kelly, and T. Zhou, "Decaying sterile neutrinos at short baselines," *Phys. Rev. D* **110** no. 7, (2024) 075002, arXiv:2406.04401 [hep-ph].
[39] S. Hannestad, R. S. Hansen, and T. Tram, "How Self-Interactions can Reconcile Sterile Neutrinos with Cosmology," *Phys. Rev. Lett.* **112** no. 3, (2014) 031802, arXiv:1310.5926 [astro-ph.CO].
[40] B. Dasgupta and J. Kopp, "Cosmologically Safe eV-Scale Sterile Neutrinos and Improved Dark Matter Structure," *Phys. Rev. Lett.* **112** no. 3, (2014) 031803, arXiv:1310.6337 [hep-ph].
[41] M. Archidiacono, S. Hannestad, R. S. Hansen, and T. Tram, "Cosmology with self-interacting sterile neutrinos and dark matter - A pseudoscalar model," *Phys. Rev. D* **91** no. 6, (2015) 065021, arXiv:1404.5915 [astro-ph.CO].
[42] N. Saviano, O. Pisanti, G. Mangano, and A. Mirizzi, "Unveiling secret interactions among sterile neutrinos with big-bang nucleosynthesis," *Phys. Rev. D* **90** no. 11, (2014) 113009, arXiv:1409.1680 [astro-ph.CO].
[43] A. Mirizzi, G. Mangano, O. Pisanti, and N. Saviano, "Collisional production of sterile neutrinos via secret interactions and cosmological implications," *Phys. Rev. D* **91** no. 2, (2015) 025019, arXiv:1410.1385 [hep-ph].
[44] X. Chu, B. Dasgupta, and J. Kopp, "Sterile neutrinos with secret interactions—lasting friendship with cosmology," *JCAP* **10** (2015) 011, arXiv:1505.02795 [hep-ph].
[45] J. F. Cherry, A. Friedland, and I. M. Shoemaker, "Short-baseline neutrino oscillations, Planck, and IceCube," arXiv:1605.06506 [hep-ph].
[46] M. Archidiacono, S. Gariazzo, C. Giunti, S. Hannestad, R. Hansen, M. Laveder, and T. Tram, "Pseudoscalar—sterile neutrino interactions: reconciling the cosmos with neutrino oscillations," *JCAP* **08** (2016) 067, arXiv:1606.07673 [astro-ph.CO].
[47] X. Chu, B. Dasgupta, M. Dentler, J. Kopp, and N. Saviano, "Sterile neutrinos with secret interactions—cosmological discord?," *JCAP* **11** (2018) 049, arXiv:1806.10629 [hep-ph].
[48] Y. Farzan, "Ultra-light scalar saving the 3 + 1 neutrino scheme from the cosmological bounds," *Phys. Lett. B* **797** (2019) 134911, arXiv:1907.04271 [hep-ph].
[49] J. M. Cline, "Viable secret neutrino interactions with ultralight dark matter," *Phys. Lett. B* **802** (2020) 135182, arXiv:1908.02278 [hep-ph].
[50] M. Archidiacono, S. Gariazzo, C. Giunti, S. Hannestad, and T. Tram, "Sterile neutrino self-interactions: H_0 tension and short-baseline anomalies," *JCAP* **12** (2020) 029, arXiv:2006.12885 [astro-ph.CO].
[51] K. M. Belotsky, A. L. Sudarikov, and M. Y. Khlopov, "Constraint on anomalous 4nu interaction," *Phys. Atom. Nucl.* **64** (2001) 1637–1642.
[52] A. E. Nelson and J. Walsh, "Short Baseline Neutrino Oscillations and a New Light Gauge Boson," *Phys. Rev. D* **77** (2008) 033001, arXiv:0711.1363 [hep-ph].
[53] N. Engelhardt, A. E. Nelson, and J. R. Walsh, "Apparent CPT Violation in Neutrino Oscillation Experiments," *Phys. Rev. D* **81** (2010) 113001, arXiv:1002.4452 [hep-ph].
[54] M. Pospelov, "Neutrino Physics with Dark Matter Experiments and the Signature of New Baryonic Neutral Currents," *Phys. Rev. D* **84** (2011) 085008, arXiv:1103.3261 [hep-ph].
[55] G. Karagiorgi, M. H. Shaevitz, and J. M. Conrad, "Confronting the Short-Baseline Oscillation Anomalies with a Single Sterile Neutrino and Non-Standard Matter Effects," arXiv:1202.1024 [hep-ph].
[56] J. Kopp and J. Welter, "The Not-So-Sterile 4th Neutrino: Constraints on New Gauge Interactions from Neutrino Oscillation Experiments," *JHEP* **12** (2014) 104, arXiv:1408.0289 [hep-ph].
[57] J. M. Berryman, V. Brdar, and P. Huber, "Particle physics origin of the 5 MeV bump in the reactor antineutrino spectrum?," *Phys. Rev. D* **99** no. 5, (2019) 055045, arXiv:1803.08506 [hep-ph].
[58] J. Liao, D. Marfatia, and K. Whisnant, "MiniBooNE, MINOS+ and IceCube data imply a baroque neutrino sector," *Phys. Rev. D* **99** no. 1, (2019) 015016, arXiv:1810.01000 [hep-ph].
[59] A. Esmaili and H. Nunokawa, "On the robustness of IceCube's bound on sterile neutrinos in the presence of non-standard interactions," *Eur. Phys. J. C* **79** no. 1, (2019) 70, arXiv:1810.11940 [hep-ph].
[60] P. B. Denton, Y. Farzan, and I. M. Shoemaker, "Activating the fourth neutrino of the 3+1 scheme," *Phys. Rev. D* **99** no. 3, (2019) 035003, arXiv:1811.01310 [hep-ph].
[61] D. S. M. Alves, W. C. Louis, and P. G. deNiverville, "Quasi-sterile neutrinos from dark sectors. Part I. BSM matter effects in neutrino oscillations and the short-baseline anomalies.," *JHEP* **08** (2022) 034, arXiv:2201.00876 [hep-ph].
[62] C. Sponsler, M. Hostert, I. Martinez-Soler, and C. A. Argüelles, "Resonant Neutrino Flavor Conversion in the Atmosphere," arXiv:2405.12140 [hep-ph].
[63] V. Brdar and D. S. Chattopadhyay, "Does the 220 PeV Event at KM3NeT Point to New Physics?," arXiv:2502.21299

[hep-ph].
[64] T.-K. Kuo and J. T. Pantaleone, "Three Neutrino Oscillations and the Solar Neutrino Experiments," *Phys. Rev. D* **35** (1987) 3432.
[65] **MINOS+** Collaboration, P. Adamson *et al.*, "Search for sterile neutrinos in MINOS and MINOS+ using a two-detector fit," *Phys. Rev. Lett.* **122** no. 9, (2019) 091803, arXiv:1710.06488 [hep-ex].
[66] **NOvA** Collaboration, M. A. Acero *et al.*, "Dual-Baseline Search for Active-to-Sterile Neutrino Oscillations in NOvA," *Phys. Rev. Lett.* **134** no. 8, (2025) 081804, arXiv:2409.04553 [hep-ex].
[67] N. Klop and A. Palazzo, "Imprints of CP violation induced by sterile neutrinos in T2K data," *Phys. Rev. D* **91** no. 7, (2015) 073017, arXiv:1412.7524 [hep-ph].
[68] S. Parveen, K. Sharma, S. Patra, and P. Mehta, "Signals of eV-scale sterile neutrino at long baseline neutrino experiments," *Eur. Phys. J. C* **85** no. 2, (2025) 181, arXiv:2305.16824 [hep-ph].
[69] S. K. Agarwalla, S. S. Chatterjee, and A. Palazzo, "Physics Reach of DUNE with a Light Sterile Neutrino," arXiv:1603.03759 [hep-ph].
[70] S. S. Chatterjee and A. Palazzo, "Interpretation of NOνA and T2K data in the presence of a light sterile neutrino," arXiv:2005.10338 [hep-ph].
[71] G. L. Fogli, E. Lisi, A. Marrone, and A. Palazzo, "Evidence for Mikheyev-Smirnov-Wolfenstein effects in solar neutrino flavor transitions," *Phys. Lett. B* **583** (2004) 149–156, arXiv:hep-ph/0309100.
[72] F. Capozzi, E. Lisi, F. Marcone, A. Marrone, and A. Palazzo, "Updated bounds on the (1,2) neutrino oscillation parameters after first JUNO results," arXiv:2511.21650 [hep-ph].
[73] I. Esteban, M. C. Gonzalez-Garcia, M. Maltoni, I. Martinez-Soler, J. P. Pinheiro, and T. Schwetz, "Lessons from the first JUNO results," arXiv:2601.09791 [hep-ph].
[74] F. Capozzi, W. Giarè, E. Lisi, A. Marrone, A. Melchiorri, and A. Palazzo, "Neutrino masses and mixing: Entering the era of subpercent precision," *Phys. Rev. D* **111** no. 9, (2025) 093006, arXiv:2503.07752 [hep-ph].
[75] I. Esteban, M. C. Gonzalez-Garcia, M. Maltoni, I. Martinez-Soler, J. P. Pinheiro, and T. Schwetz, "NuFit-6.0: updated global analysis of three-flavor neutrino oscillations," *JHEP* **12** (2024) 216, arXiv:2410.05380 [hep-ph].
[76] P. F. de Salas, D. V. Forero, S. Gariazzo, P. Martínez-Miravé, O. Mena, C. A. Ternes, M. Tórtola, and J. W. F. Valle, "2020 global reassessment of the neutrino oscillation picture," *JHEP* **02** (2021) 071, arXiv:2006.11237 [hep-ph].
[77] P. Huber, M. Lindner, and W. Winter, "Simulation of long-baseline neutrino oscillation experiments with GLoBES (General Long Baseline Experiment Simulator)," *Comput.Phys.Commun.* **167** (2005) 195, arXiv:hep-ph/0407333 [hep-ph].
[78] P. Huber, J. Kopp, M. Lindner, M. Rolinec, and W. Winter, "New features in the simulation of neutrino oscillation experiments with GLoBES 3.0: General Long Baseline Experiment Simulator," *Comput.Phys.Commun.* **177** (2007) 432–438, arXiv:hep-ph/0701187 [hep-ph].
[79] J. Kopp *Sterile neutrinos and non-standard neutrino interactions in GLoBES* (2019) . https://www.mpi-hd.mpg.de/personalhomes/globes/tools/snu-1.0.pdf.
[80] O. G. Miranda, M. A. Tortola, and J. W. F. Valle, "Are solar neutrino oscillations robust?," *JHEP* **10** (2006) 008, arXiv:hep-ph/0406280 [hep-ph].
[81] P. Coloma and T. Schwetz, "Generalized mass ordering degeneracy in neutrino oscillation experiments," arXiv:1604.05772 [hep-ph].
[82] L. Wolfenstein, "Neutrino Oscillations in Matter," *Phys.Rev.* **D17** (1978) 2369–2374.
[83] **ANTARES** Collaboration, A. Albert *et al.*, "Search for non-standard neutrino interactions with 10 years of ANTARES data," *JHEP* **07** (2022) 048, arXiv:2112.14517 [hep-ex].
[84] **(IceCube Collaboration)*, IceCube** Collaboration, R. Abbasi *et al.*, "All-flavor constraints on nonstandard neutrino interactions and generalized matter potential with three years of IceCube DeepCore data," *Phys. Rev. D* **104** no. 7, (2021) 072006.
[85] **KM3NeT** Collaboration, S. Aiello *et al.*, "Search for non-standard neutrino interactions with the first six detection units of KM3NeT/ORCA," *JCAP* **02** (2025) 073, arXiv:2411.19078 [hep-ex].
[86] **Super-Kamiokande** Collaboration, G. Mitsuka *et al.*, "Study of Non-Standard Neutrino Interactions with Atmospheric Neutrino Data in Super-Kamiokande I and II," *Phys. Rev. D* **84** (2011) 113008, arXiv:1109.1889 [hep-ex].
[87] A. Palazzo, "Testing the very-short-baseline neutrino anomalies at the solar sector," *Phys. Rev. D* **83** (2011) 113013, arXiv:1105.1705 [hep-ph].
[88] C. Giunti and Y. F. Li, "Matter Effects in Active-Sterile Solar Neutrino Oscillations," *Phys. Rev. D* **80** (2009) 113007, arXiv:0910.5856 [hep-ph].
[89] F. Capozzi, I. M. Shoemaker, and L. Vecchi, "Solar Neutrinos as a Probe of Dark Matter-Neutrino Interactions," *JCAP* **07** (2017) 021, arXiv:1702.08464 [hep-ph].
[90] T.-K. Kuo and J. T. Pantaleone, "Neutrino Oscillations in Matter," *Rev. Mod. Phys.* **61** (1989) 937.
[91] A. Palazzo, "An estimate of θ_{14} independent of the reactor antineutrino flux determinations," *Phys. Rev. D* **85** (2012) 077301, arXiv:1201.4280 [hep-ph].
[92] K. Goldhagen, M. Maltoni, S. E. Reichard, and T. Schwetz, "Testing sterile neutrino mixing with present and future solar neutrino data," *Eur. Phys. J. C* **82** no. 2, (2022) 116, arXiv:2109.14898 [hep-ph].
[93] M. C. Gonzalez-Garcia, M. Maltoni, and J. P. Pinheiro, "Solar model independent constraints on the sterile neutrino interpretation of the Gallium Anomaly," *Phys. Lett. B* **862** (2025) 139297, arXiv:2411.16840 [hep-ph].
[94] B. T. Cleveland, T. Daily, R. Davis, Jr., J. R. Distel, K. Lande, C. K. Lee, P. S. Wildenhain, and J. Ullman, "Measurement of the solar electron neutrino flux with the Homestake chlorine detector," *Astrophys. J.* **496** (1998)

505–526.
[95] **SNO** Collaboration, B. Aharmim *et al.*, “Combined Analysis of all Three Phases of Solar Neutrino Data from the Sudbury Neutrino Observatory,” *Phys. Rev. C* **88** (2013) 025501, arXiv:1109.0763 [nucl-ex].
[96] **Super-Kamiokande** Collaboration, K. Abe *et al.*, “Solar neutrino measurements using the full data period of Super-Kamiokande-IV,” *Phys. Rev. D* **109** no. 9, (2024) 092001, arXiv:2312.12907 [hep-ex].
[97] G. Bellini *et al.*, “Precision measurement of the 7Be solar neutrino interaction rate in Borexino,” *Phys. Rev. Lett.* **107** (2011) 141302, arXiv:1104.1816 [hep-ex].
[98] **BOREXINO** Collaboration, G. Bellini *et al.*, “Neutrinos from the primary proton–proton fusion process in the Sun,” *Nature* **512** no. 7515, (2014) 383–386.
[99] **Borexino** Collaboration, M. Agostini *et al.*, “First Simultaneous Precision Spectroscopy of *pp*, ^{7}Be, and *pep* Solar Neutrinos with Borexino Phase-II,” *Phys. Rev. D* **100** no. 8, (2019) 082004, arXiv:1707.09279 [hep-ex].
[100] Y. Herrera and A. Serenelli, “Standard Solar Models B23/SF-III,”. https://doi.org/10.5281/zenodo.10174170.
[101] **JUNO** Collaboration, A. Abusleme *et al.*, “First measurement of reactor neutrino oscillations at JUNO,” arXiv:2511.14593 [hep-ex].
[102] P. Coloma, M. C. Gonzalez-Garcia, M. Maltoni, J. a. P. Pinheiro, and S. Urrea, “Global constraints on non-standard neutrino interactions with quarks and electrons,” *JHEP* **08** (2023) 032, arXiv:2305.07698 [hep-ph].
[103] **KATRIN** Collaboration, H. Acharya *et al.*, “Sterile-neutrino search based on 259 days of KATRIN data,” arXiv:2503.18667 [hep-ex].
[104] **IceCube** Collaboration, R. Abbasi *et al.*, “Strong Constraints on Neutrino Nonstandard Interactions from TeV-Scale ν_u Disappearance at IceCube,” *Phys. Rev. Lett.* **129** no. 1, (2022) 011804, arXiv:2201.03566 [hep-ex].
[105] **(IceCube Collaboration)‖, IceCube** Collaboration, R. Abbasi *et al.*, “Measurement of Atmospheric Neutrino Oscillation Parameters Using Convolutional Neural Networks with 9.3 Years of Data in IceCube DeepCore,” *Phys. Rev. Lett.* **134** no. 9, (2025) 091801, arXiv:2405.02163 [hep-ex].
[106] M. P. Rodriguez, *Measurement of the Neutrino Mass Ordering with 9.28 Years of IceCube DeepCore Data*. PhD thesis, Wisconsins-Madison U., 2024. https://digital.library.wisc.edu/1711.dl/24CPK3B2BJYH586.
[107] E. K. Akhmedov, M. Maltoni, and A. Y. Smirnov, “1-3 leptonic mixing and the neutrino oscillograms of the Earth,” *JHEP* **05** (2007) 077, arXiv:hep-ph/0612285.
[108] G. L. Fogli, E. Lisi, and A. Palazzo, “Quasi energy independent solar neutrino transitions,” *Phys. Rev. D* **65** (2002) 073019, arXiv:hep-ph/0105080.
[109] S. Mikheev and A. Y. Smirnov, “Resonance Amplification of Oscillations in Matter and Spectroscopy of Solar Neutrinos,” *Sov.J.Nucl.Phys.* **42** (1985) 913–917.
[110] S. Mikheev and A. Y. Smirnov, “Resonant amplification of neutrino oscillations in matter and solar neutrino spectroscopy,” *Nuovo Cim.* **C9** (1986) 17–26.
[111] O. Yasuda, “Neutrino oscillations with four generations,” in *Joint U.S. / Japan Workshop on New Initiatives in Muon Lepton Flavor Violation and Neutrino Oscillation with High Intense Muon and Neutrino Sources*, pp. 151–163. 10, 2000. arXiv:hep-ph/0102166.
[112] H. Nunokawa, O. L. G. Peres, and R. Zukanovich Funchal, “Probing the LSND mass scale and four neutrino scenarios with a neutrino telescope,” *Phys. Lett. B* **562** (2003) 279–290, arXiv:hep-ph/0302039.
[113] S. Choubey, “Signature of sterile species in atmospheric neutrino data at neutrino telescopes,” *JHEP* **12** (2007) 014, arXiv:0709.1937 [hep-ph].
[114] S. Razzaque and A. Y. Smirnov, “Searching for sterile neutrinos in ice,” *JHEP* **07** (2011) 084, arXiv:1104.1390 [hep-ph].
[115] V. Barger, Y. Gao, and D. Marfatia, “Is there evidence for sterile neutrinos in IceCube data?,” *Phys. Rev. D* **85** (2012) 011302, arXiv:1109.5748 [hep-ph].
[116] S. Razzaque and A. Y. Smirnov, “Searches for sterile neutrinos with IceCube DeepCore,” *Phys. Rev. D* **85** (2012) 093010, arXiv:1203.5406 [hep-ph].
[117] A. Esmaili, F. Halzen, and O. L. G. Peres, “Constraining Sterile Neutrinos with AMANDA and IceCube Atmospheric Neutrino Data,” *JCAP* **11** (2012) 041, arXiv:1206.6903 [hep-ph].
[118] S. K. Agarwalla, T. Li, O. Mena, and S. Palomares-Ruiz, “Exploring the Earth matter effect with atmospheric neutrinos in ice,” arXiv:1212.2238 [hep-ph].
[119] A. Esmaili and A. Y. Smirnov, “Restricting the LSND and MiniBooNE sterile neutrinos with the IceCube atmospheric neutrino data,” *JHEP* **12** (2013) 014, arXiv:1307.6824 [hep-ph].
[120] M. Lindner, W. Rodejohann, and X.-J. Xu, “Sterile neutrinos in the light of IceCube,” *JHEP* **01** (2016) 124, arXiv:1510.00666 [hep-ph].
[121] S. T. Petcov, “On the IceCube Result on $\bar{\nu}_\mu \to \bar{\nu}_s$ oscillations,” *Int. J. Mod. Phys. A* **32** no. 04, (2017) 1750018, arXiv:1611.09247 [hep-ph].
[122] L. S. Miranda and S. Razzaque, “Revisiting constraints on 3 + 1 active-sterile neutrino mixing using IceCube data,” *JHEP* **03** (2019) 203, arXiv:1812.00831 [hep-ph].
[123] E. Cabrera, A. Esmaili, and A. A. Quiroga, “Limits on the parameter space of (3+2) sterile neutrino scenario by IceCube data,” *JCAP* **11** (2024) 059, arXiv:2405.10419 [hep-ph].
[124] M. Brettell, I. Martinez-Soler, and H. Minakata, “Sterile-active resonance: A global qualitative picture,” *JHEP* **04** (2025) 011, arXiv:2411.19022 [hep-ph].
[125] **IceCube** Collaboration, M. G. Aartsen *et al.*, “Searching for eV-scale sterile neutrinos with eight years of atmospheric neutrinos at the IceCube Neutrino Telescope,” *Phys. Rev. D* **102** no. 5, (2020) 052009, arXiv:2005.12943 [hep-ex].

[126] **(IceCube Collaboration)‖, IceCube** Collaboration, R. Abbasi *et al.*, "Methods and stability tests associated with the sterile neutrino search using improved high-energy $\nu\mu$ event reconstruction in IceCube," *Phys. Rev. D* **110** no. 9, (2024) 092009, arXiv:2405.08077 [hep-ex].
[127] F. Hund, "Zur Deutung der Molekelspektren I," *Zeitschrift fur Physik* **40** (1927) 742.
[128] J. von Neumann and E. Wigner, "Über merkwürdige diskrete Eigenwerte. Uber das Verhalten von Eigenwerten bei adiabatischen Prozessen," *Physikalische Zeitschrift* **30** (1929) 467.
[129] Z.-z. Xing, S. Zhou, and Y.-L. Zhou, "Renormalization-Group Equations of Neutrino Masses and Flavor Mixing Parameters in Matter," *JHEP* **05** (2018) 015, arXiv:1802.00990 [hep-ph].
[130] S. Zeng and F. Xu, "Matter effects of sterile neutrino in light of renormalization-group equations," *JHEP* **09** (2022) 029, arXiv:2202.09851 [hep-ph].
[131] P. B. Denton, S. J. Parke, and X. Zhang, "Neutrino oscillations in matter via eigenvalues," *Phys. Rev. D* **101** no. 9, (2020) 093001, arXiv:1907.02534 [hep-ph].
[132] X. Zhao, L.-M. Kuang, and J.-Q. Liao, "General dark-state theory for arbitrary multilevel quantum systems," *Phys. Rev. A* **113** no. 1, (2026) 013723, arXiv:2510.05561 [quant-ph].
[133] B. R. Smithers, B. J. P. Jones, C. A. Argüelles, J. M. Conrad, and A. Diaz, "Cascade appearance signatures of sterile neutrinos at 1–100 TeV," *Phys. Rev. D* **105** no. 5, (2022) 052001, arXiv:2111.08722 [hep-ph].
[134] A. Esmaili, F. Halzen, and O. L. G. Peres, "Exploring $\nu_\tau - \nu_s$ mixing with cascade events in DeepCore," *JCAP* **07** (2013) 048, arXiv:1303.3294 [hep-ph].
[135] C. Giunti, Y. F. Li, and R. P. Zhang, "Revival of the Reactor Antineutrino Anomaly," arXiv:2605.10353 [hep-ph].
[136] C. Kraus, A. Singer, K. Valerius, and C. Weinheimer, "Limit on sterile neutrino contribution from the Mainz Neutrino Mass Experiment," *Eur. Phys. J. C* **73** no. 2, (2013) 2323, arXiv:1210.4194 [hep-ex].
[137] A. I. Belesev, A. I. Berlev, E. V. Geraskin, A. A. Golubev, N. A. Likhovid, A. A. Nozik, V. S. Pantuev, V. I. Parfenov, and A. K. Skasyrskaya, "An upper limit on additional neutrino mass eigenstate in 2 to 100 eV region from 'Troitsk nu-mass' data," *JETP Lett.* **97** (2013) 67–69, arXiv:1211.7193 [hep-ex].
[138] A. I. Belesev, A. I. Berlev, E. V. Geraskin, A. A. Golubev, N. A. Likhovid, A. A. Nozik, V. S. Pantuev, V. I. Parfenov, and A. K. Skasyrskaya, "The search for an additional neutrino mass eigenstate in the 2–100 eV region from 'Troitsk nu-mass' data: a detailed analysis," *J. Phys. G* **41** (2014) 015001, arXiv:1307.5687 [hep-ex].
[139] C. Giunti, Y. F. Li, and Y. Y. Zhang, "KATRIN bound on 3+1 active-sterile neutrino mixing and the reactor antineutrino anomaly," *JHEP* **05** (2020) 061, arXiv:1912.12956 [hep-ph].
[140] K. M. Zurek, "Asymmetric Dark Matter: Theories, Signatures, and Constraints," *Phys. Rept.* **537** (2014) 91–121, arXiv:1308.0338 [hep-ph].
[141] R. Horvat, "Resonant conversions of extremely high-energy neutrinos in dark matter halos," *Phys. Rev. D* **59** (1999) 123003, arXiv:hep-ph/9812228.
[142] P. F. de Salas, R. A. Lineros, and M. Tórtola, "Neutrino propagation in the galactic dark matter halo," *Phys. Rev. D* **94** no. 12, (2016) 123001, arXiv:1601.05798 [astro-ph.HE].
[143] K.-Y. Choi, E. J. Chun, and J. Kim, "Neutrino Oscillations in Dark Matter," *Phys. Dark Univ.* **30** (2020) 100606, arXiv:1909.10478 [hep-ph].
[144] A. V. Penacchioni, O. Civitarese, and C. R. Argüelles, "Testing dark matter distributions by neutrino–dark matter interactions," *Eur. Phys. J. C* **80** no. 3, (2020) 183.
[145] A. Y. Smirnov and V. B. Valera, "Resonance refraction and neutrino oscillations," *JHEP* **09** (2021) 177, arXiv:2106.13829 [hep-ph].
[146] G.-y. Huang and W. Rodejohann, "Tritium beta decay with modified neutrino dispersion relations: KATRIN in the dark sea," *Nucl. Phys. B* **993** (2023) 116262, arXiv:2110.03718 [hep-ph].
[147] G. M. Salla, "Characterising dark matter-induced neutrino potentials," *Eur. Phys. J. C* **83** no. 3, (2023) 204, arXiv:2209.00442 [hep-ph].
[148] H.-X. Lin, J. Tang, and S. Vihonen, "Ultralight dark matter in neutrino oscillations to accommodate T2K and NOνA tension," arXiv:2312.11704 [hep-ph].
[149] T. Gherghetta and A. Shkerin, "Probing a local dark matter halo with neutrino oscillations," *Phys. Rev. D* **108** no. 9, (2023) 095009, arXiv:2305.06441 [hep-ph].
[150] G. Chauhan, R. A. Gustafson, G. Herrera, T. Johnson, and I. M. Shoemaker, "The dark matter diffused supernova neutrino background," *JCAP* **10** (2025) 020, arXiv:2505.03882 [hep-ph].
[151] O. G. Miranda, C. A. Moura, and A. Parada, "Sterile neutrinos, dark matter, and resonant effects in ultra high energy regimes," *Phys. Lett. B* **744** (2015) 55–58, arXiv:1308.1408 [hep-ph].
[152] I. Lopes, "The Sun: Light Dark Matter and Sterile Neutrinos," *Astrophys. J.* **905** no. 1, (2020) 22, arXiv:2101.00210 [hep-ph].
[153] S. Chattopadhyay and A. Dighe, "Refractive neutrino masses in the solar DM halo: Can the dark-LMA solution be revived?," arXiv:2511.19420 [hep-ph].
[154] A. Gould, "WIMP Distribution in and Evaporation From the Sun," *Astrophys. J.* **321** (1987) 560.
[155] S. K. Lee, M. Lisanti, A. H. G. Peter, and B. R. Safdi, "Effect of Gravitational Focusing on Annual Modulation in Dark-Matter Direct-Detection Experiments," *Phys. Rev. Lett.* **112** no. 1, (2014) 011301, arXiv:1308.1953 [astro-ph.CO].
[156] H. Kim and A. Lenoci, "Gravitational focusing of wave dark matter," *Phys. Rev. D* **105** no. 6, (2022) 063032, arXiv:2112.05718 [hep-ph].

[157] S. Goswami and W. Rodejohann, "Constraining mass spectra with sterile neutrinos from neutrinoless double beta decay, tritium beta decay and cosmology," *Phys. Rev. D* **73** (2006) 113003, arXiv:hep-ph/0512234.
[158] S. Goswami and W. Rodejohann, "MiniBooNE results and neutrino schemes with 2 sterile neutrinos: Possible mass orderings and observables related to neutrino masses," *JHEP* **10** (2007) 073, arXiv:0706.1462 [hep-ph].
[159] J. Barry, W. Rodejohann, and H. Zhang, "Light Sterile Neutrinos: Models and Phenomenology," *JHEP* **07** (2011) 091, arXiv:1105.3911 [hep-ph].
[160] Y. F. Li and S.-s. Liu, "Vanishing effective mass of the neutrinoless double beta decay including light sterile neutrinos," *Phys. Lett. B* **706** (2012) 406–411, arXiv:1110.5795 [hep-ph].
[161] W. Rodejohann, "Neutrinoless double beta decay and neutrino physics," *J. Phys. G* **39** (2012) 124008, arXiv:1206.2560 [hep-ph].
[162] I. Girardi, A. Meroni, and S. T. Petcov, "Neutrinoless Double Beta Decay in the Presence of Light Sterile Neutrinos," *JHEP* **11** (2013) 146, arXiv:1308.5802 [hep-ph].
[163] C. Giunti and E. M. Zavanin, "Predictions for Neutrinoless Double-Beta Decay in the 3+1 Sterile Neutrino Scenario," *JHEP* **07** (2015) 171, arXiv:1505.00978 [hep-ph].
[164] J.-H. Liu and S. Zhou, "Another look at the impact of an eV-mass sterile neutrino on the effective neutrino mass of neutrinoless double-beta decays," *Int. J. Mod. Phys. A* **33** no. 02, (2018) 1850014, arXiv:1710.10359 [hep-ph].
[165] K. N. Deepthi, S. Goswami, V. K. N., and T. K. Poddar, "Implications of the dark large mixing angle solution and a fourth sterile neutrino for neutrinoless double beta decay," *Phys. Rev. D* **102** no. 1, (2020) 015020, arXiv:1909.09434 [hep-ph].
[166] S. Jana, L. Puetter, and A. Y. Smirnov, "Restricting sterile neutrinos by neutrinoless double beta decay," *Phys. Rev. D* **111** no. 1, (2025) 015011, arXiv:2408.01488 [hep-ph].
[167] K. N. Vishnudath, S. Choubey, and S. Goswami, "New sensitivity goal for neutrinoless double beta decay experiments," *Phys. Rev. D* **99** no. 9, (2019) 095038, arXiv:1901.04313 [hep-ph].
[168] S.-F. Ge and J.-y. Zhu, "Phenomenological Advantages of the Normal Neutrino Mass Ordering," *Chin. Phys. C* **44** no. 8, (2020) 083103, arXiv:1910.02666 [hep-ph].
[169] B. Dutta, A. Karthikeyan, D. Kim, A. Thompson, and R. G. Van de Water, "Photon excess from dark matter and neutrino scattering at MiniBooNE and MicroBooNE," *Phys. Rev. D* **113** no. 1, (2026) 015029, arXiv:2504.08071 [hep-ph].
[170] P. S. B. Dev, S. Jana, and Y. Porto, "Matter effects on flavor composition of astrophysical neutrinos," *Phys. Rev. D* **112** no. 9, (2025) 093003, arXiv:2312.17315 [hep-ph].
[171] **IceCube-Gen2** Collaboration, A. Omeliukh *et al.*, "Optimization of the optical array geometry for IceCube-Gen2," *PoS* **ICRC2021** (2021) 1184, arXiv:2107.08527 [astro-ph.HE].
[172] K. Valerius, "Latest results from KATRIN: Neutrino Mass and Beyond," *Talk presented at CERN EP Seminar, 6 May 2025* (2025) . https://indico.cern.ch/event/1500288/attachments/3061689/5414279/CERN-EP_KATRIN_2025-05-06.pdf.
[173] F. Acerbi *et al.*, "nuSCOPE: A short-baseline neutrino beam at CERN for high-precision cross-section measurements," arXiv:2503.21589 [hep-ex].
[174] A. B. et al., "nuSCOPE sensitivity studies for sterile neutrino mixing with beam neutrinos," *Talk presented at EP-nu Group Meeting, 25 Sep 2025* (2025) . https://indico.cern.ch/event/1592586/contributions/6711151/attachments/3142944/5578746/20250925_EPNU_nuSCOPE.pdf.
[175] **Hyper-Kamiokande** Collaboration, K. Abe *et al.*, "Hyper-Kamiokande Design Report," arXiv:1805.04163 [physics.ins-det].
[176] **DUNE** Collaboration, R. Acciarri *et al.*, "Long-Baseline Neutrino Facility (LBNF) and Deep Underground Neutrino Experiment (DUNE): Conceptual Design Report, Volume 2: The Physics Program for DUNE at LBNF," arXiv:1512.06148 [physics.ins-det].
[177] **ESSnuSB** Collaboration, A. Alekou *et al.*, "Updated physics performance of the ESSnuSB experiment: ESSnuSB collaboration," *Eur. Phys. J. C* **81** no. 12, (2021) 1130, arXiv:2107.07585 [hep-ex].
[178] **KM3Net** Collaboration, S. Adrian-Martinez *et al.*, "Letter of intent for KM3NeT 2.0" *J. Phys. G* **43** no. 8, (2016) 084001, arXiv:1601.07459 [astro-ph.IM].
[179] N. W. Kamp and G. Putnam, "The Neutrino Kaleidoscope: Searches for Non-Standard Neutrino Oscillations at Neutrino Telescopes with a TeV Muon Accelerator Source," arXiv:2508.09249 [hep-ph].
[180] L. Bojorquez-Lopez, M. Hostert, C. A. Argüelles, and Z. Liu, "Muon Colliders and the Neutrino Slice," *Phys. Rev. Lett.* **135** no. 9, (2025) 091803, arXiv:2412.14115 [hep-ph].
[181] **International Muon Collider** Collaboration, C. Accettura *et al.*, "The Muon Collider," arXiv:2504.21417 [physics.acc-ph].